Response to Reviewers

We would like to thank the reviewers for their helpful comments. We would like to point out to the reviewers that for consistency and accuracy across all acoustic resonators, we have switched to using the electromechanical coupling K^2, which is equal to C_x/C_0 for most of this paper. We have also added the relationship between K^2 and the effective piezoelectric coupling k_{eff}^2 and the piezoelectric coupling coefficient, k_t^2, for completeness and to allow comparisons across the literature as all of these parameters are currently being used.

In addition to the specific issues raised by the reviewers, other minor changes to improve readability and correct errors have been made throughout the document.

Reviewer 1:

This is a great article, providing a very inclusive summary on various types of MEMS devices. The field of RF-MEMS can really use an article of such to educate outside readers about the progress and state-of-the-art in RF-MEMS. The authors have done a great job in categorizing different type of MEMS devices for RF applications. The review believes that it should be published with the following suggestion minor revisions.

1. Table 1, Could authors put relevant references behind each materials in the table?

References have been added to the table. Note that the reference numbers match the reference numbers for the final version rather than the ones in the marked-up version.

2. Table 2, the mathematical expressions for force scaling need to be properly typeset without star signs. The actuation Voltage for Piezoelectric devices can be lower, 7V in this reference: Chung, D.J.; Polcawich, R.G.; Judy, Daniel; Pulskamp, Jeffrey; Papapolymerou, J., "A SP2T and a SP4T switch using low loss piezoelectric MEMS," *Microwave Symposium Digest, 2008 IEEE MTT-S International* , vol., no., pp.21,24, 15-20 June 2008

The minimum piezoelectric actuation value in the table was lowered to 5V in consideration of the referenced work and similar work to lower actuation voltages in piezoelectric actuators.

3. Actuation current (0A for both electrostatic and piezoelectric) is misleading. There is a transient current charging the capacitor to transduce electrostatically or piezoelectrically. It is a very small value in comparison to thermal. It depends on device size, but authors should list a non-zero range.

A paragraph discussing dynamic power dissipation was added to the text, and the table was modified to reflect that the current is a static current, with a very small but non-zero value.

4. Can the authors add references to individual approach listed in the mitigation approaches in table 3 and 4?

References have been added to the table. Note that the reference numbers match the reference numbers for the final version rather than the ones in the marked-up version.

5. There are four classes mentioned in the text, but only three classes are illustrated in the picture.

Class IV is missing in Fig 2. The classifications, although highly appreciated by the reviewer, are confusing. In class I, by electromagnetic devices, the reviewer believes that authors mean passive RF components fabricated with micromachining techniques but without mechanical displacements in device operation. If so, wouldn't it be better if they were lumped into their own class as opposed to combined together with MEMS/acoustic resonator? If they are either lumped elements (such tunable inductors with mechanical displacement) or waveguide/transmission lines with MEMS integrated (including cavity resonators, phase shifters, tunable filters), they probably should also be grouped into their own class. The latter is definitely RF-MEMS technology, but more so as demonstrations on a sub-system level using either the devices in class II or III. Just like for electromechanical resonators, oscillators and sensors are also subsystem demo. The review suggests that the author can create another level on the tree map to classify subsystems using various types of MEMS.

The purpose of the chart is to introduce the various types of MEMS devices. Class IV was originally excluded from the table because it is not very relevant to RF MEMS (but is very relevant to gears and other devices), and has been added into the figure for completeness. Because the 4 classes of devices are defined by the cited references, it would be inappropriate to create a new class by separating electromechanical and electromagnetic Class I devices into separate classes, so they are left in the same class. A comment intended to clarify the definition of Class I has been added to the text.

The four classes are intended to focus on mechanical attributes of the devices, rather than on specific applications, and the authors feel that adding an additional layer of applications would make the chart and discussion overly complicated. However, a comment about applications for each type of device was added to the paragraph describing them. In the chart, filters and high-Q resonators were removed from the electromagnetic category because they are realized using the other two types of devices (transmission lines and passives).

6. Page 16. The authors should consider commenting on some of the newer research trends in lamb wave resonators, including using piezoelectric materials on low loss acoustic materials to form composite structures:
For example, on Si:
Piazza, Gianluca, Reza Abdolvand, and Farrokh Ayazi. "Voltage-tunable piezoelectricallytransduced single-crystal silicon resonators on SOI substrate." In *Micro Electro Mechanical Systems, 2003. MEMS-03 Kyoto. IEEE The Sixteenth Annual International Conference on*, pp. 149-152. IEEE, 2003.
On diamond:
Hediyeh Fatemi, Hongjun Zeng, John Carlisle; Reza Abdolvand; "High-Frequency Thin-Film AlN-on-Diamond Lateral–Extensional Resonators," *Journal of Microelectromechanical Systems*, vol.PP, no.99, pp.1-9.
On SiC:
Gong, Songbin, Nai-Kuei Kuo, and Gianluca Piazza. "GHz high-lateral overmoded bulk acoustic-wave resonators using epitaxial SiC thin film." *Microelectromechanical Systems, Journal of* 21, no. 2 (2012): 253-255.
On Sapphire:
Kuo, Nai-Kuei, Songbin Gong, J. Hartman, J. Kelliher, W. Miller, J. Parke, S. V. Krishaswamy, John D. Adam, and G. Piazza. "Micromachined sapphire GHz lateral overtone bulk acoustic resonators transduced by aluminum nitride." In *Micro Electro Mechanical Systems (MEMS), 2012 IEEE 25th International Conference on*, pp. 27-30. IEEE, 2012.
Capacitively transduced piezoelectric resonators:
Hung, Li-Wen, and Clark T-C. Nguyen. "Capacitive-piezo transducers for higher Q contourmode

AlN resonators at 1.2 GHz." In *Solid-State Sensor Actuator Workshop*, pp. 463-466. 2010.

Response: A short section on this topic including the references above has been added on page 18.

7. Page 18, the highest FoM lamb wave LN resonators are reported in this recent publication: Songbin Gong; Piazza, G., "Figure-of-Merit Enhancement for Laterally Vibrating Lithium Niobate MEMS Resonators," *Electron Devices, IEEE Transactions on* , vol.60, no.11, pp.3888,3894, Nov. 2013.
The author should update the reported performance and cite this paper on LN Lamb resonators. The author should also comment on LN Lamb resonators, as they have been demonstrated to achieve high k_eff^2 and Q simultaneously. The k_t^2 (defined differently from k_eff^2) reported in the reference translate to a k_eff^2 of 16.7%.

Response: The state-of-the-art in Lithium Niobate Lamb wave resonator performance has been added to the paper including the reference above.

8. Page 30, one of tunable MEMS capacitors' important application, besides the mentioned tuned voltage-controlled oscillators, tunable filters, switching networks, and matching networks, is phase shifters, the distributed phase shifters or switched line phase shifters. Some representative references on MEMS-enable phase shifters:
Barker, N. Scott, and Gabriel M. Rebeiz. "Distributed MEMS true-time delay phase shifters and wide-band switches." *Microwave Theory and Techniques, IEEE Transactions on* 46.11 (1998): 1881-1890.
Gong, Songbin, Hui Shen, and N. Scott Barker. "A 60-GHz 2-bit switched-line phase shifter using SP4T RF-MEMS switches." *Microwave Theory and Techniques, IEEE Transactions on* 59, no. 4 (2011): 894-900.

Response: Distributed time delays and phase shifters were added, along with the Barker reference mentioned and an additional reference. The Gong reference falls in the category of switched line devices that are covered in the Rebeiz review.

9. page 40. The authors should comment on the recent development of temperature insensitive RF-MEMS metal switches, and the temperature range of operation.
Temperature insensitive designs:
For cantilevers:
Gong, Songbin, Theodore Reck, and N. Scott Barker. "A temperature insensitive DC-contact RF-MEMS switch." In *Microwave Conference (EuMC), 2010 European*, pp. 1114-1117. IEEE, 2010.
For fixed-fixed beams:
Patel, Chirag D., and Gabriel M. Rebeiz. "A high power (> 5 W) temperature stable RF MEMS metal-contact switch with orthogonal anchors and force-enhancing stoppers." In *Microwave Symposium Digest (MTT), 2011 IEEE MTT-S International*, pp. 1-4. IEEE, 2011.
Low temperature and cryogenic switches:
Gong, Songbin, Hui Shen, and N. Scott Barker. "Study of broadband cryogenic DC-contact RF MEMS switches." *Microwave Theory and Techniques, IEEE Transactions on* 57.12 (2009): 3442-3449.
Brown, Chris, Arthur S. Morris, Angus I. Kingon, and Jacqueline Krim. "Cryogenic performance of RF MEMS switch contacts." *Microelectromechanical Systems, Journal of* 17, no. 6 (2008): 1460-1467.

A brief comment about temperature sensitivity and mitigation through design has been added to the reliability section, with the two Gong references added. A journal article on the Patel work was already included elsewhere and the citation added, and the Reines paper on temperature insensitivity in the context of capacitive switches has been added. The Brown paper is already included in the review paper by Toler that has been cited, and has not been added.

10. In the "further reading" section, the reviewer suggests to include the book "RF bulk acoustic wave filters for communication" from Hashimoto. There is a lot of good information on BAW resonators and filters.

Response: This reference has been added at the end of the BAW resonator section, and is cited in the "further reading" section.

Reviewer 2:

Comments to the Author
The article is very clear and well-organized. It is definitely worth publishing after some minor revisions. More references on AlN lamb-wave resonators/oscillators should be added.

Response: The additional references suggested by Reviewer 1 have been added.

Please provide at least brief captions for all figures for clarity. A glossary of abbreviations could be included at the beginning or end to provide an easy reference for the reader.

Response: Captions for all of the figures and tables are included at the end of the document, before the references (p 61-62). A glossary of abbreviations and nomenclature has been added at the end of the document.

Pg 4, line 30: It is mentioned that components with high-Q are desirable, but an explanation of the meaning of Q is not presented before this point.

Response: The definition of Q was added to the introduction in section 1.1.

Pg 15, line 6: Phrase "may also be used if there transduction is supported" seems to be a typo.

Response: This has been changed to "Vibrations in a longitudinal thickness mode are the most common form of BAW resonator but thickness shear modes may also be used if direct transduction of shear modes is supported by the piezoelectric material."

Pg 17, line 6: "acoustic velocity is equal to effective Young's modulus and effective mass density" – confusing phrasing – either spell out equation (square root effective Young's modulus divided by effective mass density) or replace "is equal to" with "is related to".

Response: Agreed. This has been changed to "The acoustic velocity is related to the effective Young's modulus, E_{eff}, and effective mass density, ρ_{eff}, of the membrane." Equation 16 with the exact relation is directly above.

Pg 17: The authors should add more references to thin film AlN lamb-wave resonators operating in the super high frequency band: "5-10 GHz AlN Contour-Mode Nanoelectromechanical Resonators"; "Ultra-Thin Super High Frequency two-port AlN Contour-Mode Resonators and Filters"; "AlN Contour-Mode Resonators for Narrow-Band Filters above 3 GHz"; "Super high frequency width extensional aluminum nitride (AlN) MEMS resonators"; "Super High Frequency Two-Port AlN Contour-Mode Resonators for RF Applications",

Response: Many references, including many of those suggested by the reviewer, have been included on page 18.

Pg. 22, lines 52-57: The authors should add references demonstrating that the higher power handling of piezoelectric resonators results in close to carrier oscillator phase noise on par with electrostatic resonators despite the lower Q: "Power Handling and Related Frequency Scaling Advantages in Piezoelectric AlN Contour-Mode MEMS Resonators"; "Effects of Volume and Frequency Scaling in AlN Contour Mode NEMS Resonators on Oscillator Phase Noise" ; "Reconfigurable CMOS Oscillator based on Multi-Frequency AlN Contour-Mode MEMS Resonators"

Response: We have added several references, including many of those recommended by the reviewer. We have included references to both electrostatic and piezoelectric oscillators, the piezoelectric resonator power handling and a previous article summarizing the state-of-the-art in MEMS oscillators. The prior article confirms the similar phase noise performance of electrostatic and piezoelectric MEMS oscillators.

Pg 32, line 23: should define VCO for those who are unfamiliar.

Response: The text has been changed to say "….voltage controlled oscillator (VCO)…"

Pg 67, Figure 1: Should be an explanation on the Figure about what the numbered components represent (just a brief description so that the figure is clearer).

Response: Text has been added to the figure with a brief description of each component type.

Pg 77-78, Figure 11, 12: The label for the thickness, t, is hard to distinguish. Change color of piezoelectric layer or move label outside diagram.

Response: These figures have been changed.

Pg 82, Figure 16: In the cross-section view – a – the left electrode is labelled as "Conductive Fixed Electrode (Port 1)." In the top down view – b – the left electrode is labelled as "Conductive Anchored Electrode." Are these labelled differently on purpose?

Response: These were not labelled differently on purpose. All labels in Figure 16 now use the term "Conductive Anchored Electrode".

Pg 88, Figure 22: It would be a bit clearer if the opening and closing curves were different colors.

Response: The closing curve was changed from a solid line to a dashed line.

1. INTRODUCTION

Radio Frequency Microelectromechanical System (RF MEMS) devices are microscale devices that achieve superior performance relative to other technologies by taking advantage of the accuracy, precision, materials, and miniaturization available through microfabrication. These devices utilize their mechanical and electrical properties to perform a specific RF electrical function such as switching, transmission, or filtering. RF MEMS has been a popular area of research since the early 1990's, and within the last several years the technology has matured sufficiently for commercialization and use in commercial market systems.

1.1 RF MEMS Applications

Potential applications for RF MEMS can be illustrated with the representative RF transceiver front end shown in Figure 1. This notional transceiver has two functions that share a common RF front end with a two-element antenna array with beam steering capability. Each function has its own digital signal processing and RF chain including I-Q modulators, power amplifier, low noise amplifier, local oscillator, and duplexer. The functions are connected to the antenna with a single-pole-double-throw (SPDT) switch that selects one function at a time. In reality, modern wireless systems are much more complicated, having over a dozen functions operating through multiple antennas, requiring SPnT switches, where n>10.

In a modern RF system, modern electronics allows many of the active functions to be implemented with a single integrated circuit, but many components such as filters and oscillators require a high quality factor, or "Q", which is defined as the ratio of energy stored to energy lost in a resonant device. Because this performance cannot be achieved using traditional electronics, these functions are realized with separate passive components that occupy a disproportionate share of system volume. In particular, RF MEMS technologies offer the possibility of reducing the overall

system size through miniaturization and component reuse. Along with adding functionality through tunable amplifiers and filters throughout the RF chain, specific opportunities for RF MEMS are denoted in Figure 1 by numbers, and are:

1. A reconfigurable antenna aperture that can adapt to different operating frequencies, functions and environments. This tuning may be achieved with RF MEMS devices such as switches or tunable capacitors.

2. An antenna matching network to allow for improved impedance matching at relevant frequencies. This matching network may be realized with tunable or switched components.

3. Tunable time delays and/or phase shifters for beam steering with multiple antennas. These are generally realized by using MEMS switches to select delay paths of varied lengths.[1]

4. A tunable RF filter to adapt to the desired function and reject undesired out-of-band signals. The high-Q and low loss of RF MEMS tunable components are ideal for realizing filters use tunable impedances or switched fixed filters to change properties.

5. A low-loss SPnT switch to connect the desired function to the antenna. A similar switch may also be used as a transmit/receive switch in place of a duplexer. RF MEMS switches allow for a large number of paths with low resistance and a minimum of parasitic capacitance.

6. A miniature duplexer to separate transmit and receive paths for each function. This duplexer must provide sufficient isolation between transmit and receive paths and have power handling and linearity sufficient for the transmit signal power. These duplexers can be based upon either acoustic or electromagnetic resonators.

7. A tunable oscillator that can be used to adapt to different operating frequencies or provide frequency hopping or spread spectrum capability. MEMS resonators can provide high-

Q, low noise, references for miniaturizing these synthesizers, and MEMS tunable capacitors may be used to tune voltage controlled oscillators.

8. RF filters are required throughout the signal path to select desired signals and eliminate spurious signals. These filters may be miniaturized through RF MEMS resonator technologies, and may be tunable through RF MEMS tuning elements.

9. IF filters are used to select specific channels within the signal band, and may be reconfigured to match specific frequency and bandwidth requirements. This reconfigurability may be achieved by switching between fixed acoustic resonator filters.

1.2 RF MEMS Taxonomy

RF MEMS covers a broad range of devices operating over numerous frequency bands. MEMS devices can be broken down into four classes of devices in the context of reliability[2,3], as shown in Figure 2. As the devices progress towards higher classes, additional failure mechanisms and reliability challenges are introduced. Static (Class I) devices use micromachined structures to provide an RF function but do not use significant mechanical motion to provide tuning or another active function during operation. Movable non-contacting (Class II) devices vary their structure mechanically without making contact to provide real-time tuning of impedance or another attribute. Moving and contacting (Class III) devices achieve dramatic impedance changes by moving two tuning or contact elements together. A fourth class (Class IV) of devices that utilize rubbing and sliding surfaces have not been applied to RF MEMS because of materials compatibility and reliability limitations, but have potential for sliding tuners and similar devices.

Class I RF MEMS devices support electromagnetic or mechanical modes that achieve a combination of lower loss, lower dispersion, higher Q, or smaller size when compared to traditional devices, but do not change structure substantially during operation. Devices that support mechanical

modes include resonators, filters, and time delays using either electrostatic or piezoelectric transducers to convert RF energy from an electrical to mechanical or acoustic mode. In spite of some motion in the form of mechanical vibration, these devices can be considered to fall into this category because the motion is small relative to the device size and the device dimensions are generally not tuned to change the response. Electromagnetic devices in this category include devices fabricated using micromachining approaches but not intended to move during operation, such as micromachined transmission lines and resonators, high-Q miniature capacitors and inductors, micromachined cavity resonators and waveguides, and micromachined antennas. The high performance of these types of Class I devices translate into improved performance at the next system level in devices such as oscillators, filters, time delays, and passive networks.

Class II RF MEMS add tuning capability by moving part of the mechanical structure, which in turn changes the impedance or some other attribute of the device. The most common example of this device is a tunable capacitor in which the device capacitance is changed by varying the distance between two parallel plates, but tunable inductance has also been achieved by varying the mutual coupling between two coils. Acoustic device tuning is less common, but can be achieved by artificially changing the stiffness of a structure by applying strain with an actuator. These devices may be used to realize tunable and reconfigurable circuits and RF systems such as tunable oscillators, tunable filters, and steerable antennas.

Class III devices use movement into contact to achieve the highest possible impedance change. Examples of these types of devices include metal contacting or capacitive switches fabricated from metal and silicon layers. Because of integration challenges, there have only been a few examples of this type of switching for acoustic devices. Common applications uses for these devices are switch networks for time delays, switched filters, and multi-function RF front ends.

Class IV devices that use lateral sliding or rubbing motions have very challenging reliability issues and have not been extensively explored for RF applications. However, if reliability problems associated with laterally sliding surfaces could be overcome, these devices have potential for tunable capacitors and sliding tuners.

1.3 Micromachining Techniques

RF MEMS technologies are enabled by micromachining, which takes advantage of modern semiconductor fabrication techniques to perform tasks such as metal and dielectric film deposition, high aspect ratio dry etching, and selective dry or wet etching to achieve specific mechanical device structures[4]. Generally, micromachining uses standard integrated circuit processes such as metallization and etching, but also utilizes additional processes such as selective etching to remove sacrificial films to create suspended and movable films, deep etching to remove large volumes of silicon, and wafer bonding for packaging or integration.

A simple surface micromachining process flow showing the essential steps for realizing suspended structures is shown in Figure 3. After any underlying structures are completed, a sacrificial layer on which to fabricate the MEMS device is deposited. Openings are etched into this sacrificial layer to define attachment points or anchors for the device layer, and then the device layers themselves are deposited and patterned to form the desired mechanical structure. Finally, the MEMS device is "released" to form a suspended structure that is attached to the substrate by the anchor points.

The materials and details of the full device process depend on the specific type of MEMS device desired and on the toolset and process capability of the fabrication facility. While silicon (Si) mechanical layers with silicon dioxide (SiO_2) release layers are commonly used in MEMS devices, they are not commonly used for RF MEMS devices because of the high processing temperatures and RF losses in the Si mechanical structure. Instead, RF MEMS devices typically use metallic or dielectric mechanical layers

with metal, dielectric, or organic sacrificial materials. In some cases, when the goal is minimizing substrate RF losses, part of the silicon substrate is removed to isolate the mechanical layer on a dielectric membrane.

2 MICROMACHINED RF ACOUSTIC RESONATORS

Direct conversion and super heterodyne radio architectures commonly use acoustic resonators for the RF filters and diplexers, intermediate frequency (IF) filters and frequency sources. Due to the speed of sound being roughly four orders of magnitude slower than the speed of light, acoustic resonators are orders of magnitude smaller than electromagnetic resonators for similar quality factors, *Q,* in the frequency bands most often utilized for RF communications (< 10 GHz). The high-Q, >1000, of the acoustic resonators ensures low oscillator phase noise and the steep filter skirts required for narrow diplexer, band, and channel frequency spacing. Such high performance frequency control components are required for efficient utilization of the RF spectrum. Traditionally, filters and oscillators based on quartz crystal or surface acoustic wave (SAW) resonators[5] were utilized for frequency control in RF communications systems. Micromachining of acoustic resonators offers tremendous advantages that lead to both performance improvements (coupling and Q) and miniaturization compared to these traditional solutions.

2.1 Acoustic Resonator Modeling and Figures of Merit

RF MEMS acoustic resonators transduce RF electrical signals into the acoustic domain where they are processed using highly frequency selective vibrating mechanical structures. The solution to the 2nd order differential equation that describes mechanical vibrations in beams, plates and other acoustic structures is identical in form to the equation describing electrical oscillations in a series RLC tank circuit,

$$H(s) = \frac{\frac{2\pi f_s}{Q}s}{s^2+\frac{2\pi f_s}{Q}s+(2\pi f_s)^2}, \qquad (1)$$

where f_s is the natural or series resonant frequency of the oscillating mechanical or electrical resonator and Q is the unloaded resonator quality factor. This allows the majority of micromachined RF acoustic resonators, including the most prevalent ones transduced by piezoelectric or electrostatic forces, to be

described by either the Butterworth-Van Dyke (BVD) electrical equivalent circuit model in Figure 4 or the stacked crystal electrical equivalent circuit model in Figure 5[6]. Using electrical equivalent circuits to model RF MEMS acoustic resonators allows for accurate simulation of the devices in an electronic RF circuit.

The series resonant frequency of an electronic or mechanical resonator, where the through impedance reaches a minimum, is equal to

$$f_s = \frac{1}{2\pi\sqrt{L_X C_X}} = \frac{1}{2\pi}\sqrt{\frac{k}{M}}, \quad (2)$$

where L_X is the motional inductance, C_X is the motional capacitance, M is the effective mass of a mechanical resonator and k is the effective mechanical resonator stiffness. In the electrical equivalent circuit models the effective mass of a mechanical resonator is captured by the motional inductance,

$$L_X = M, \quad (3)$$

while the motional capacitance models the effective mechanical resonator stiffness,

$$C_X = \frac{1}{k}. \quad (4)$$

The motional impedance, R_X, is the impedance through the motional branch of the resonator at series resonance. R_X models the acoustic damping of the resonator and the coupling between the electrical and acoustic domains. R_X is related to the other equivalent circuit parameters by

$$R_X = \frac{2\pi f_s L_X}{Q}. \quad (5)$$

Also shown in Figure 4 is the electrical shunt capacitance across the resonator, C_S. This capacitance is inherent to the piezoelectric or electrostatic transducer used to launch and detect the acoustic waves and defines the transmission of the resonator, or isolation, far from the acoustic

resonance. It is important to note that the discrete circuit elements in Figure 4 and Figure 5 cannot be adjusted individually. Instead, they are interrelated by the resonator electromechanical coupling, K^2, Q, f_s, and C_S. The electromechanical coupling is the ratio of the energy converted between the electrical and mechanical domains to the energy input to the electromechanical transducer. The electromechanical coupling fundamentally limits the maximum bandwidth of filters that can be achieved with a given insertion loss. The resonator Q determines the minimum bandwidth for a filter that can be realized for a given insertion loss as well as the phase noise of acoustic oscillators. The motional impedance, which to reiterate is the impedance seen looking through the motional branch of the resonator at series resonance, is equal to

$$R_X = \frac{1}{2\pi f_s K^2 Q C_S}. \quad (6)$$

In designing an acoustic resonator, generally a certain R_X is desired to meet a specific filter or oscillator requirement. Since the maximum K^2 and Q are set by the materials used and the type of transduction, and the frequency of operation is determined by the application, the R_X of the resonator is specified by designing the resonator to a specific area or value of C_S.

The impedance of C_S is equal to

$$Z_{C_S} = \frac{1}{j2\pi f_s C_S}. \quad (7)$$

The ratio of the impedance of the shunt capacitance (impedance far from resonance) to the motional resistance (impedance at series resonance), which defines the isolation of the resonator, is

$$\frac{Z_{C_S}}{R_X} = K^2 Q. \quad (8)$$

Hence, the isolation of the acoustic resonator is determined solely by the K^2Q product of the resonator, which is the resonator figure of merit, FOM_{filter}, discussed below.

To demonstrate the importance of K^2 and K^2Q product on the acoustic response, simulation results for the BVD equivalent circuit model of 900 MHz resonators with a C_S of 100 fF, a Q of 1000, and a K^2 of 0.01%, 0.1%, 1% and 10% are shown in Figure 6. When the K^2Q product is low, the acoustic response of the resonator is barely visible above the feed through response of C_S. The result of low K^2Q product is degradation of the insertion loss for a filter with a given out-of-band rejection. In oscillators, resonators with too low a K^2Q in a Butterworth-Van Dyke configuration cannot be oscillated because the phase response of the resonator does not pass through 0 degrees; a property necessary to meet the oscillation criteria, Figure 7. For resonators with a K^2Q barely large enough to sustain oscillation, the phase slope of the resonator is reduced at the 0 degree phase crossing, degrading the oscillator phase noise. In general, the K^2Q product will bound the minimum insertion loss of a filter and the minimum power consumption of an oscillator realized from an acoustic resonator.

Shown in Figure 6, for the resonator simulation with a *K^2 of 10%*, are both the series resonance and the parallel resonance, f_p, where the impedance through the resonator reaches a maximum. While f_s is ideally determined only by the mechanical resonance, f_p is a function of L_X, C_X and C_S,

$$f_p = f_s\sqrt{1+K^2} = f_s\sqrt{1+\frac{C_X}{C_S}}. \qquad (9)$$

This leads to another important parameter, the effective piezoelectric coupling coefficient, k_{eff}^2, which is defined[7] by the separation between series and parallel resonances

$$k_{eff}{}^2 = \frac{f_p{}^2 - f_s{}^2}{f_p{}^2} = \frac{K^2}{1+K^2}. \qquad (10)$$

When the electromechanical coupling is low, K^2 and k_{eff}^2 are equal. For a given filter topology and insertion loss, the resonator k_{eff}^2 will determine the maximum achievable filter bandwidth[8]. The resonator figure of merit, as it pertains to filters, is defined as[7]

$$FOM_{filter} = \frac{{k_{eff}}^2 Q}{1-{k_{eff}}^2} = K^2 Q \ . \qquad (11)$$

To reiterate, FOM_{filter} determines both the minimum filter insertion loss and the isolation of a single resonator. It is important to note that the acoustic resonator figure of merit as it pertains to oscillators is

$$FOM_{oscillator} = f_s Q \ . \qquad (12)$$

This is because the minimum oscillator phase noise that can be achieved at a given frequency, which can be different than f_s by means of dividers or frequency synthesizers, is directly related to $FOM_{oscillator}$.

In applications such as oscillators and intermediate frequency (IF) filters, where filter out-of-band rejection or oscillator phase noise is more important than insertion loss, acoustic resonators are often configured to provide the stacked crystal equivalent circuit model shown in Figure 5. Here C_S, which is across the resonator in the BVD equivalent circuit model, is instead shunted to ground. Further examination of Figure 5 reveals that although the stacked crystal configuration dramatically improves the isolation, it also doubles the impedance seen through the motional arm of the resonator, $2R_X$, at series resonance. Simulations of BVD and stacked crystal resonators with, $f_s = 900\ MHz$, $C_S = 100\ fF$, $Q = 1000$ and $K^2 = 0.1\%$ demonstrate this effect in Figure 8 and Figure 9. With such a low K^2Q product, the through response of the BVD resonator is barely visible above the feed through and the phase response of the BVD resonator makes it unusable for oscillator applications. The stacked crystal resonator, by contrast, is clearly distinguishable from any feed through despite the fact that the minimum through impedance is larger. In addition, the phase response of the stacked crystal resonator passes through 0 degrees, making the high-Q resonator highly applicable in oscillator applications despite the low K^2Q. The lower admittance for the stacked crystal resonator leads to higher insertion loss filters when compared to the minimum insertion loss achievable using resonators in a BVD configuration. In

addition, if too large a C_S is used to reduce R_X, additional loss and phase shift can be introduced in the stacked crystal model by the low pass filter formed from C_S and the $Port_1$ and $Port_2$ termination impedances.

Grounding $Port_2$ and looking into $Port_1$ in the circuit models also reveals that the K^2 of the stacked crystal resonator is reduced compared to that of the BVD resonator. This reduction is because the through capacitance has been cut in half, to $C_X/2$, while C_S has remained constant. The result is that the separation between f_p and f_s is reduced. This is shown in Figure 10 when comparing the Y_{11} for BVD and stacked crystal resonators with $f_s = 900\ MHz$, $C_S = 100\ fF$, $Q = 1000$ and $K^2 = C_X/C_S = 1\%$. The k_{eff}^2 has been reduced from 1.0% (BVD) to 0.53% (Stacked Crystal). While the ultimate stop-band rejection of a stacked crystal resonator filter is superior to that of a filter realized using BVD resonators, the minimum insertion loss and maximum achievable bandwidth of a stacked crystal resonator filter is degraded.

In this section we have reviewed the BVD and stacked crystal resonator equivalent circuits that can be used to describe the vast majority of RF MEMS acoustic resonators. Most importantly, we have discussed how the equivalent circuit values used to model MEMS acoustic resonators are intrinsically linked through the resonator geometry, K^2 and Q. A more thorough treatment of electromechanical transducers and acoustic resonator modeling, including more advanced devices such as transformers, can be found in Tilmans[9].

2.2 RF MEMS Resonator Transduction and Types of RF MEMS Resonators

2.2.1 Piezoelectric Bulk Acoustic Wave Resonators

To date, bulk acoustic wave (BAW) resonators have been the most successful and widely deployed RF MEMS acoustic resonator technology[10,11,12]. The success of BAW resonator technology is largely due to its high FOM_{filter}, high power handling, and high volume, low cost manufacturing. Filters based on BAW resonators are pervasive in wireless handsets, forming the front-end duplexers that

isolate the transmit and receive paths in full-duplex radios[13]. A cross-section diagram of a membrane type BAW, also commonly referred to as a film bulk acoustic resonator (FBAR)[12], is shown in Figure 11. A piezoelectric material is used to electrically excite an acoustic standing wave through the thickness of the membrane, which is formed by the piezoelectric layer itself along with the top and bottom metal electrodes. The membrane is suspended above the substrate using micromachining techniques and a sacrificial layer. The acoustic wave reflects off the interface between the membrane and the surrounding gas or vacuum, which presents a very large acoustic impedance mismatch. The fundamental resonant frequency occurs when the thickness of the membrane, *t*, is equal to half an acoustic wavelength, $\lambda/2$,

$$f_s = \frac{v}{\lambda} = \frac{v}{2t}, \qquad (13)$$

where *v* is the acoustic velocity of the piezoelectric layer and the metal electrodes. The acoustic velocity is equal to the effective Young's modulus, E_{eff}, and effective mass density, ρ_{eff}, of the membrane,

$$v = \sqrt{\frac{E_{eff}}{\rho_{eff}}}. \qquad (14)$$

In BAW resonators the most commonly used piezoelectric layer is aluminum nitride (AlN)[12]. Current research is investigating other piezoelectric layers that can be deposited in thin film format, such as zinc oxide (ZnO)[10,14] and lead zirconate titanate (PZT)[14,15]. AlN is generally preferred for BAW filter applications because of its high FOM_{filter}, compatibility with complementary metal oxide semiconductor (CMOS) transistor fabrication, low acoustic and dielectric loss, high acoustic velocity, and chemical inertness. The metal electrodes in BAW are most often formed from metals with high acoustic impedance such as tungsten (W) and molybdenum (Mo), which has been shown to improve the k_{eff}^2 by concentrating more of the stress field of the acoustic standing wave in the piezoelectric material[16]. It should be noted that single crystal quartz BAW resonators[17] may be preferred for oscillator applications

because of the inherent temperature compensation and low damping of the material. Vibrations in a longitudinal thickness mode are the most common form of BAW resonator but thickness shear modes may also be used if direct transduction of shear modes is supported by the piezoelectric material. A summary of RF MEMS acoustic resonator materials is presented in Table 1.

The BAW resonator shown in Figure 11 can be modeled by the BVD electrical equivalent circuit previously discussed. The electromechanical coupling for a BAW resonator neglecting the metal electrodes is given by

$$K^2 = \frac{8}{\pi^2}\frac{{d_{ij}}^2 \mathrm{E}}{\varepsilon_{ij}}, \qquad (15)$$

where d_{ij} is the piezoelectric coefficient for the mode being excited, E is the modulus and ε_{ij} is the dielectric constant. The subscripts ij refer to matrix indices for the piezoelectric coefficient and dielectric constant which are direction dependent, an effect which arises from the piezoelectric crystal structure. It should be noted that the electromechanical coupling K^2 is related to the commonly used coupling coefficient[8], k_t^2, by

$$K^2 = \frac{8}{\pi^2}{k_t}^2 = \frac{C_X}{C_S}. \qquad (16)$$

Typical measured K^2 and Q values for AlN membrane type BAW resonators are 6.5% and 2000-4000 respectfully. Much of the early and on-going work in BAW resonators focuses on solidly mounted resonators (SMR)[11], where instead of having an air or vacuum gap below the resonator, the resonator is fabricated on an acoustic Bragg mirror of alternating quarter wavelength layers of high and low acoustic impedance materials. While the SMR approach may result in simplified packaging and increased damping of unwanted vibrational modes, the micromachining of membrane type BAW resonators results in slightly higher $K^2$and 2-4 times higher Q and FOM_{filter}, because acoustic energy is neither lost

nor stored in the reflector. Both membrane and SMR type BAW resonators and filters are available commercially.

Shown in Figure 12 is the cross-section diagram of a stacked crystal BAW resonator which can be modeled using the stacked crystal equivalent circuit previously discussed. In the stacked crystal implementation, three electrodes and two piezoelectric layers are utilized. The middle electrode is grounded to ensure high isolation between the top (Port 1) and bottom (Port 2) electrodes. The membrane is designed to resonate at the 2nd harmonic of either the thickness extensional (most common) or thickness shear mode, with a total membrane thickness equal to a single acoustic wavelength, λ. The stacked crystal implementation is most often utilized in narrow bandwidth filters and oscillator references where isolation is more critical than insertion loss. A great deal of information about BAW resonators and acoustic resonator filters can be found in Aigner[18] and Hashimoto[19].

2.2.2 Piezoelectric Lamb Wave Resonators

The thickness mode BAW resonators discussed in the previous section have their resonant frequencies set by the total membrane thickness. This makes the realization of multiple resonant frequencies on a single substrate costly. In practice, multiple resonant frequency BAW resonators are realized on a single substrate by altering the top electrode thickness, with an additional mask level required for each frequency. The range of frequencies that can be practically realized using this method, however, is limited, because when the top electrode becomes too thick, the resonator coupling is significantly degraded.

The desire to include filters and resonators at vastly different frequencies on a single chip led to the development of the piezoelectric Lamb wave resonators[20,21], also commonly referred to as contour mode resonators, depicted in Figure 13, Figure 14 and Figure 15. Piezoelectric Lamb wave resonator technology has been utilized to demonstrate resonators and filters spanning the high frequency (HF = 3-

30 MHz) through the super high frequency (SHF = 3-30 GHz) band[22,23,24,25,26,27,28]. The cross-section diagram of the Lamb wave resonator in Figure 13 is very similar to that of the BAW resonator in Figure 11, with a piezoelectric layer sandwiched between two metal electrodes. In the Lamb wave resonator, however, the acoustic wave propagates laterally in the film, with the resonant frequency defined by the lateral dimension, $L = \lambda/2$,

$$f_s = \frac{v}{\lambda} = \frac{v}{2L} = \frac{\sqrt{\frac{E_{eff}}{\rho_{eff}}}}{2L}, \qquad (17)$$

where v is the acoustic velocity of the piezoelectric layer and the metal electrodes. The acoustic velocity is related to the effective Young's modulus, E_{eff}, and effective mass density, ρ_{eff}, of the membrane. The ability to set the resonant frequency using lateral dimensions defined by a single photolithographic mask enables resonators varying by 3-4 orders of magnitude in frequency to be realized on a single chip. In general, the membrane thickness must be less than half the acoustic wavelength in order to avoid significant dispersion that results in a greatly reduced sound velocity and coupling[29].

The diagram in Figure 13 uses thickness field excitation (TFE), where the RF electric field is applied vertically across the piezoelectric layer, while the acoustic wave propagates laterally in the membrane reflecting off of the etched sidewalls. Because this configuration decouples the shunt capacitance per unit area (i.e. the piezoelectric layer thickness) from the acoustic wavelength, large reductions in size, especially at lower frequencies, are achievable when compared to other resonator technologies[22]. It is also possible to utilize lateral field excitation (LFE), such as that shown in Figure 14, where only electrodes on top of the piezoelectric are used to excite the acoustic wave. With LFE, the electromechanical coupling can be highly dependent on the thickness to wavelength ratio[29], t/λ, limiting the range of frequencies that can be practically achieved on a single substrate. In all approaches, the key to achieving the highest possible electromechanical coupling is to have the electric field between

the exciting electrodes interacting strongly with the maximum of the stress field of the acoustic standing wave. One significant advantage of Lamb wave resonators, when compared to surface acoustic wave (SAW) resonators, is micromachining confines the acoustic wave more closely to the surface where it interacts more strongly with the RF electric field, resulting in significant increases in the electromechanical coupling for a given material[30].

As in BAW resonators, the most commonly used piezoelectric layer for Lamb wave resonators is AlN[13,20,21,22] while other piezoelectric layers that can be deposited in thin film format, such as ZnO[31] and PZT[32] are also common. Al, Pt, Au and Mo are common electrode materials utilized in Lamb wave resonators and tend to be selected based on process integration with the piezoelectric material. In some cases, a thick layer of Si[33] or another high-Q material such as diamond[34] is included under the piezoelectric resonator in order to increase the resonator Q factor at the expense of the electromechanical coupling. Another method to increase the Q factor of a piezoelectrically transduced Lamb wave resonator is to overtone many acoustic wavelengths in a delay line realized from a high-Q material such as silicon carbide[35] or sapphire[36]. This approach ideally directly trades K^2 for Q while holding a constant FOM_{filter}. Recently AlN Lamb wave resonators have also been fabricated with metal electrodes suspended above and below the resonator by narrow capacitive gaps[37]. Since the primary sources of damping in many piezoelectric Lamb wave resonators are either from the metal electrodes or from the interface between the metal electrodes and the piezoelectric material, suspending the electrodes can dramatically improve the Q factor while only slightly degrading the K^2.

The electromechanical coupling can be calculated using equation 15, where different piezoelectric coefficients are utilized for the transduction of Lamb and BAW resonators. For example, in AlN, the d_{33} piezoelectric coefficient is utilized to transduce the longitudinal BAW resonators in Figure 11 and Figure 12, while the d_{31} piezoelectric coefficient is utilized to transduce the symmetric (S0) Lamb

wave resonators in Figure 13, Figure 14 and Figure 15. Typical measured K^2 and Q values for AlN Lamb wave resonators are 1.5% and 2000. The reduction in K^2 and FOM_{filter} when compared to AlN BAW resonators is significant, because $d_{31}=d_{33}/2.5$, and has to date relegated Lamb wave resonators to oscillator, intermediate frequency filter and filter array applications, where the massively reduced size of the resonators[23] is compelling. Recently, Lamb wave resonators based on thin membranes of single crystal lithium niobate ($LiNbO_3$) have been demonstrated[8,38,39,40,41] with K^2 as high as 19.5%[41] and FOM_{filter} as large as 420[41]. This technology is very promising for realizing multiple frequency filters on a single chip for RF band selection in multi-band radios. A review of common materials used in Lamb wave resonators is presented in Table 1.

Because of the lower FOM_{filter}, a stacked crystal implementation, such as that shown in Figure 15, is much more commonly utilized in Lamb wave resonators when compared to BAW resonators. A stacked crystal resonator is also more easily realized, by simply grounding the bottom electrode and transducing the acoustic wave from the top electrodes. It is straight forward, in fact, to realize the resonator configurations in Figure 13, Figure 14, and Figure 15 all on the same wafer by simply altering the electrode geometries via CAD design.

2.2.3 Electrostatic MEMS Resonators

RF MEMS resonators driven by electrostatic[42], rather than piezoelectric, forces are commercially available for timing applications[43] and are being researched for narrowband filtering[44,45,46,47]. Because of the low FOM_{filter}[48], electrostatic resonators are almost exclusively transduced using a stacked crystal configuration, such as that schematically depicted in both cross-sectional and top down views in Figure 16. A DC bias, V_b, is applied between the conductive resonator body and the electrodes used to transduce the device. When the RF input voltage at the Port 1 electrode, $v_i << V_b$, the input signal produces a force on the resonator, F

$$F = \frac{V_b \varepsilon W t}{g^2} v_i = \frac{V_b C_S}{g} v_i, \quad (18)$$

where *W* is the width and *t* the thickness of the resonator, *g* is the electrode-to-resonator gap spacing and ε is the dielectric constant of the material in the gap, which is typically[48], but not exclusively[49], vacuum. C_S is the shunt capacitance between the resonator body and the electrode. At series resonance the force produces a mechanical displacement at the edge of the resonator, *x*,

$$x = \frac{FQ}{k}, \quad (19)$$

where *k* is the effective stiffness at the edge of the resonator body and *Q* is the resonator quality factor. The resonator displacement produces a time varying capacitance between the resonator body and the Port 2 electrode (assuming the Port 1 and Port 2 electrodes are of equal area) resulting in an output current, i_o, at Port 2 of

$$|i_o| = \frac{V_b \varepsilon W t}{g^2} 2\pi f_s x = \left(\frac{2\pi f_s Q}{k}\right)\left(\frac{V_b \varepsilon W t}{g^2}\right)^2 v_i = \left(\frac{2\pi f_s Q}{k}\right)\left(\frac{V_b C_S}{g}\right)^2 v_i. \quad (20)$$

The impedance seen through the resonator at series resonance, $2R_X$, in Figure 5 is then equal to

$$2R_X = \frac{v_i}{i_o} = \frac{k}{2\pi f_s Q}\left(\frac{g^2}{V_b \varepsilon W t}\right)^2 = \frac{k}{2\pi f_s Q}\left(\frac{g}{V_b C_S}\right)^2. \quad (21)$$

The stacked crystal model is valid here for acoustic modes and electrode configurations where, when the resonator body is expanding into and narrowing the gap between the resonator and Port 1, the resonator body is contracting and increasing the gap between the resonator and Port 2. This creates a time varying Port 1 to resonator body capacitance that is 180 degrees out of phase with the Port 2 to resonator body capacitance. In this case a positive input voltage, v_i, at Port 1 produces a positive output current at Port 2.

In the case where the expansion and contraction of the resonator body into the electrode to resonator gap are in phase at Port 1 and Port 2, i.e. the time varying Port 1 to resonator body and Port 2 to resonator body capacitors are in phase, a positive input voltage at Port 1 will produce a negative output current at Port 2. To capture this phase inversion through the resonator requires the addition of an inverting transformer between the motional arm of the resonator and Port 2 in Figure 5[48].

For a fundamental symmetric Lamb wave (S0) resonance, also referred to as the first extensional mode[48], the electromechanical coupling can be shown to be[50]

$$K^2 = \frac{{V_b}^2 \varepsilon}{\pi^2 f_s g^3 \sqrt{\mathrm{E}\rho}}. \qquad (22)$$

There are several valuable insights about electrostatic transduction that can be taken from equations 21 and 22. First, electrostatic resonators fundamentally transduce displacement, as opposed to piezoelectric resonators that transduce strain. As the stiffness of acoustic resonators increases and the displacement amplitude decreases at higher resonant frequencies, the motional impedance is seen to increase with frequency and more importantly, the electromechanical coupling is seen to decrease with operating frequency. Second, the acoustic impedance of a material, Z_A, is

$$Z_A = \sqrt{\mathrm{E}\rho}\,, \qquad (23)$$

and for a resonator, Z_R, is

$$Z_R = \sqrt{kM}. \qquad (24)$$

To maximize the electromechanical coupling, it is best to work in low acoustic impedance materials and to utilize modes, such as flexural or shear modes, with lower modulus/stiffness and thus lower acoustic impedance. Third, the electromechanical coupling is dependent on the square of the bias voltage, V_b^2, and the electrode-to-resonator gap to the third power, g^3. This has driven much of the research in

electrostatic resonators to novel methods of fabricating very small gaps[48,51], though this decreases the maximum bias voltage and the resonator power handling. Finally, the dependence of the motional impedance and electromechanical coupling on the dielectric constant between the resonator and electrodes has led to filling of the gap with high-*k* dielectrics such as silicon nitride (SiN)[49,52] and hafnium oxide (HfO_2)[53]. This approach is commonly referred to as electrostriction or internal dielectric transduction. One of the main challenges with this approach is maintaining the very high Q factor generally associated with electrostatic air gap resonators, while having the points of maximum resonator displacement mechanically anchored to the electrodes via the high-*k* dielectric.

The most commonly used electrostatic resonator materials are surface micromachined polycrystalline silicon[44,45,48] and bulk micromachined single crystal silicon (Si)[54,55,56,57]. Extremely high quality factors have been achieved in both materials, in particular for shear mode single crystal Si resonators operating in the range of 1-10 MHz[54,55]. Polycrystalline silicon germanium (SiGe)[58,59], with its low deposition temperature, is utilized to form surface micromachined electrostatic resonators integrated monolithically over CMOS electronics. Electrostatic resonators formed in polycrystalline diamond[42] have reported very high f_sQ product, which is the oscillator figure of merit, $FOM_{oscillator}$. Table 1 summarizes commonly used electrostatic resonator and dielectric materials.

The strengths of electrostatic MEMS resonators are the high quality factors and low aging[57] associated with a resonator body formed solely from low loss, single crystal semiconductor materials. By contrast, piezoelectric resonators generally require metal electrodes attached to the resonator body. For RF MEMS devices, the metals used in piezoelectric resonators constitute a large enough portion of the total resonator volume to significantly decrease the Q and can lead to aging induced by metal fatigue or work hardening.

The disadvantages of electrostatic MEMS resonators are directly linked to both the poor electromechanical coupling and the nonlinear electrostatic actuation. The nonlinear electrostatic actuation, where the force on the resonator is proportional to the square of the input voltage, limits the linear input range and input power handling for electrostatically transduced devices. The poor K^2 and FOM_{filter} of electrostatic resonators leads to large insertion loss. The combined effects of large insertion loss and small input signal levels results in significantly degraded output power handling when compared to piezoelectric resonators. For these reasons, piezoelectric resonators are almost exclusively utilized in filters.

For oscillators the fundamental phase noise limit, L_{osc}, is given by Lesson's equation[60]

$$L_{osc}(\Delta f) = \frac{2KTF}{P_{res}}\left(\frac{f_s}{2Q\Delta f}\right)^2, \qquad (25)$$

where K is Boltzmann's constant, T is temperature, F is the noise factor of the amplifier, P_{res} is the power in the resonator and Δf is the frequency offset from the carrier. In oscillators, the higher P_{res} and lower transmission loss (which results in lower amplifier noise factor) of piezoelectric resonators[61,62] results in close to carrier oscillator phase noise on par with electrostatic resonators[63], despite the much higher Q of the electrostatic devices. Examples of both electrostatic[56,64,65,66] and piezoelectric[13,67,68,69,70] micromechanical oscillators can be found in the literature. An excellent review of electrostatic microresonators can be found in Nguyen[42].

3 ELECTROMAGNETIC PASSIVES

The trend towards miniaturization and integration of RF electronics has provided incredible new capability, but this miniaturization has consequences of increased loss due to smaller metal cross-sections and substrate losses. As a result, it is difficult to realize functions requiring high-performance passive components such as filters and matching networks in traditional integrated circuit technologies. To address the need for miniature high performance RF functions, many approaches have been developed to eliminate or reduce substrate loss and increase the metal cross-section for capacitors, transmission lines, inductors, and antennas.

3.1 Micromachined Interconnects and Transmission Lines

To introduce the RF MEMS and micromachining methods and devices used to improve the performance of RF passive components, this section will introduce the loss mechanisms in an RF on-chip transmission line and describe RF MEMS-based mitigation approaches. The loss mechanisms that apply to on-chip transmission lines also apply to other monolithic passive devices such as inductors and capacitors.

A lumped element model of a transmission line section is shown in Figure 17[71]. The impedance and wave velocity along the transmission line is determined by the inductance and capacitance, while the signal loss is determined by the resistive elements. Generally, there are three sources of loss in a transmission line: metal losses (R_{series}), substrate losses ($R_{substrate}$, R_{shunt}), and radiation losses. Metal losses typically dominate the signal loss on good insulating substrates, and can be improved with high-conductivity metals and larger metal cross-sections. Substrate losses are due to finite substrate resistivity and dielectric losses, and can be improved by selecting high-resistivity substrates, or removing the substrate completely. The approximately 10 Ω-cm substrate that is commonly used in electronics is quite lossy, and substrate resistivity of >1 kΩ-cm is generally required for a transmission line to be

limited by metal loss. Radiation loss is only significant at high frequencies, and is usually mitigated with high permittivity substrates and covers.

Other considerations for RF transmission lines include dispersion, crosstalk, and power handling. Dispersion is the change of impedance and propagation velocity over frequency, and can be significant for broadband circuits. Crosstalk is unintended electrical or magnetic coupling between neighboring conductors, and can cause significant interference for circuits containing high-power and low-power signals on the same die. Power handling can be limited by either current-carrying metal cross-section or by voltage breakdown of the transmission line.

Micromachining can be used to improve the performance of transmission lines by maximizing the metal cross-section to reduce metal losses, reducing exposure to semiconductors or lossy dielectrics to reduce dielectric losses, increasing dielectric uniformity to reduce dispersion, using lower dielectric constant materials to allow for larger metal cross-sections for a given impedance, and shielding the transmission line to prevent crosstalk and radiation losses. Some examples of common transmission line cross-sections and the modifications allowed with MEMS processing are shown in Figure 18.

Micromachined transmission lines and waveguides have been realized using a variety of approaches, including planar structures using metal on silicon, high-aspect ratio multi-layer electroplated structures, and metal-coated silicon or photoresist structures. Planar structures using metal on silicon provides an additional transmission line capability with lower loss for planar active or microwave circuits. Multi-layer metal approaches allow the use of high-conductivity materials and air dielectrics for low-loss, low-dispersion transmission lines with relatively high aspect ratios. Metal-coating of high-aspect structures enables relatively complex structures with high aspect ratios and low losses.

Planar transmission line structures may be realized in the interconnect process of integrated circuits, but thin metal thickness and coupling to the underlying substrate causes these types of lines to have relatively high loss[72]. As a result, micromachining is used either to remove the substrate from underneath the transmission line, to elevate the transmission line above the substrate, or to allow the use of thicker metals than otherwise available. Replacing the substrate with air lowers the parasitic capacitance of the transmission line and reduces the coupling to the substrate. This approach has been used in full-custom approaches[73,74], or as a post-processing step for silicon integrated circuits[75]. The lower loss and higher impedance of these types of transmission lines have been used to realize filters and other components at frequencies up to 100 GHz[76].

Multi-layer electroplating has been used to demonstrate low-loss, low-dispersion on-wafer coaxial and waveguide structures. One specific example is an electroplated nickel process that has been used to realize rectangular coaxial lines, couplers, and resonators demonstrating a Q of 156 at 60 GHz, high isolation, and low dispersion[77]. More recently, a copper-based process has been used to demonstrate feed and combining networks to feed antennas at frequencies greater than 100 GHz[78]. This technology also includes the capability for integration of active microwave monolithic integrated circuits[79]. Thick electroplating has also been used to realize low-loss, high-aspect ratio coplanar waveguides on quartz[80] and 3 THz rectangular waveguides[81].

Starting in the 1990's, micromachined stripline structures have been extensively explored because of the precision and performance advantages possible relative to traditional microwave multi-layer wiring environments and planar circuits. Stripline technology has three main advantages over planar microstrip or coplanar topologies: first, the air dielectric allows for larger metal cross-section and lower loss for a targeted impedance; second, the uniform dielectric lowers dispersion; and third, the enclosed environment reduces crosstalk and radiation losses[82]. Disadvantages relative to traditional on-

wafer planar technologies are a longer wavelength due to low dielectric constant of the air and the thickness of the overall structure makes on-chip integration difficult. Generally, the micromachined versions of these stripline structures are realized by bonding and selective etching of silicon wafers, leaving metal transmission lines supported on a thin dielectric membrane[83]. The air gap between layers in this type of structure are typically defined by the thickness of the starting wafers, and are on the order of 0.5 mm. Because of the high Q achievable with this approach, this technology is frequently used to demonstrate low-loss filters[84,85]. Variations on this approach include inverted microstrip[86] and a coplanar waveguide RF MEMS packaging technology[87].

3.2 Capacitors

Capacitors are used in RF circuits for impedance matching, in resonant tank and filter circuits, and as DC blocks. Important performance attributes for RF capacitors include capacitance density, the Q, and the self-resonant frequency. The capacitance density is determined by the thickness and permittivity of the capacitor dielectric, the Q is determined by any resistive losses in the device, and the self-resonant frequency is determined by any parasitic inductance within the device. Micromachined capacitors suffer from the same performance limitations and loss mechanisms as transmission lines, and the approaches for improving the device performance are similar as those described for transmission lines.

On-chip and miniature capacitors are generally formed using parallel metal plates or by edge coupling such as in interdigital capacitors. Metal-insulator-metal (MIM) capacitors are formed by two parallel plates with an intervening dielectric, and are frequently used in RF and microwave integrated circuits due to high capacitance density and good quality factor. In most cases, the dielectric material has a sufficiently low loss tangent that the capacitor is metal loss limited. Therefore, reducing the metal loss in this type of capacitor requires increasing the metal thickness or area. Edge-coupled capacitors

use the fringing field of two adjacent conductors in the same plane, and can be used where a lower capacitance density is desired, or where an interlayer dielectric is not available. These devices are often metal-loss-limited, except in cases where the fields couple into a lossy substrate.

Micromachining provides the opportunity to utilize air as the dielectric in a parallel plate capacitor (often referred to as a "metal-air-metal", or MAM, capacitor), which allows for a larger metal area to achieve a design capacitance. This lowers the series resistance (R_s) and increases the Q of the device for a given capacitance, which for a series R-C circuit is:

$$Q = \frac{|Im(Z)|}{|Re(Z)|} = \frac{1}{\omega C R_S}. \qquad (26)$$

Almost all microscale capacitors are limited by the series resistance, so this increased Q provides for lower circuit loss, especially in filter applications. These types of devices are generally fabricated by depositing a lower electrode, depositing a sacrificial layer, depositing the upper electrode on top of the sacrificial layer, and removing the sacrificial layer through etching. Two examples of the performance advantages attained with these devices include: improving the Q of lumped element filters[88,89] and reducing the size of loaded transmission line filters[90].

Similar to transmission lines, the loss and Q of a gap or interdigitated capacitor can be influenced by any loss in the substrate, and micromachining can be used to remove the substrate from underneath these devices.[83]

3.3 Inductors

On-chip and miniature inductors are difficult to implement, because both the inductance and Q of planar spiral inductors tend to scale with size[91]. Additionally, the magnetic field from these devices can couple deeply into the substrate, generating additional eddy currents and losses. Attempting to overcome these limitations with physically larger inductors will also increase the inter-turn and shunt

capacitance, lowering the self-resonant frequency of the device. Micromachining can be used to overcome some of these tradeoffs by allowing thicker metals than otherwise available, or allowing for the removal of the substrate underneath the device[92].

4 TUNABLE COMPONENTS

With the ability to create suspended structures, micromachining can be used to create tunable and switchable devices with movable parts. If these movable parts are fabricated from low-loss materials such as metals and high-quality dielectrics, these tunable passive components can have performance similar to that of fixed devices of the same size, and much better performance than competing tunable devices such as varactor diodes or metal-oxide-semiconductor capacitors and switching devices such as FET switches, PIN diodes, and macroscale mechanical switches.

4.1 Actuation Approaches

To provide real-time tuning, force must be applied to move the tunable part of the device and cause a change in impedance. For macro-scale devices, this actuation is typically performed using electromagnetic actuators, but this approach does not scale well to microscale devices.[93] Instead, the most common techniques used to apply force to MEMS devices are electrostatic, thermal, or piezoelectric actuation. Important attributes and parameters for these four actuation techniques are compared in Table 2. Because of its low actuation power, simplicity, and versatility, electrostatic actuation is the most common actuation approach for tunable and switched RF MEMS components. However, the "snap-in instability" typically limits the tuning range to less than 1/3 of the original gap, except in cases with specialized control algorithms.[94] Piezoelectric actuation provides good tuning and low static power consumption, but requires specific piezoelectric materials, which can present integration challenges. Thermal actuation provides low voltage actuation with a nearly linear response, but consumes static power due to the current draw required to produce the desired heating.

In addition to the static power consumed while holding state, during switching all approaches have dynamic power consumption due to charging and discharging of the device capacitance through the bias line resistance. The power consumed scales with the frequency and the square of the voltage,

and with frequent switching operations the dynamic power will dominate for devices with negligible static drive current such as electrostatic and piezoelectric actuators.

4.2 Tunable Capacitors

With a broad range of structures possible, tunable or switched capacitors are the most common RF MEMS tunable and switched components. The high-Q and low loss of these capacitors provide performance advantages for MEMS tuned voltage-controlled oscillators, tunable filters, switching networks, and matching networks. A tunable capacitor and capacitive switch are similar, but in a tunable capacitor the capacitance is varied continuously as a function of the actuation signal, while a capacitive switch is intended to operate between two states, with a distinct difference in capacitance between the two states. In many cases, more values of capacitance are achieved by arranging individual capacitive switches into parallel or series banks, and individual capacitors are addressed to achieve incremental tuning.

To calculate the displacement and capacitance of a MEMS device as a function of actuation force, the device properties are often simplified into a single spring constant, which is the ratio of the force applied to a specific area of the structure to the displacement at a specified location on the same structure. The device spring constant depends upon the geometry of the switch supports and actuation structure. One example is the displacement of the tip of a rectangular cantilever beam in response to a force acting on the tip of the beam. In this case, the spring constant is given by:

$$k = \frac{Ew}{4}\left(\frac{t}{L}\right)^3, \qquad (27)$$

Where E is the Young's modulus of the cantilever material, w is the width of the cantilever, t is the thickness of the cantilever in the bending direction, and L is the length of the cantilever. While this result is specific to an end-loaded cantilever, the same trends apply to most springs with rectangular

cross-sections: the stiffness increases linearly with width, as the cube of thickness, and as the inverse of the length cubed. Often the actuator is the same width as the bridge electrode, and in these cases the actuation force also scales with the bridge width, so that the actuation properties are approximately independent of bridge width. Spring constants for specific structures and cross-sections can be derived from formulas provided in reference books such as Roark's Formulas for Stress and Strain[95], or derived using finite element modeling.

The most common tunable capacitor designs utilize two parallel plates, with the capacitance tuned by varying the distance between the two plates. In the simplest case, the RF capacitor plates also serve as the electrostatic actuation electrodes. The electrostatically-actuated tunable parallel-plate capacitor can be considered as a fixed plate with a movable plate supported by a spring, as shown in Figure 19. At small displacements, the attractive electrostatic force is equal to the spring force due to the displacement from equilibrium:

$$F_e = -\frac{\varepsilon_0 A V^2}{2g^2} = k(g_0 - g), \qquad (28)$$

where A is the electrode area, k is the spring constant, ε_0 is the permittivity of free space, V is the voltage applied between the two plates, g_0 is the initial gap, and g is the distance between the plates. Note that this static solution does not include damping effects, but that damping may be important to prevent ringing. While the mechanical response of the structure is usually too slow to respond to the RF signal, the capacitor may move or even self-actuate in response to the signal envelope or RMS value, which may limit its linearity and power handling.[96]

The gap vs. voltage solution for this electrostatic actuator is shown as the dotted line in Figure 20(a). However, gap distances of less than 2/3 of the initial gap are unstable because the nonlinear attractive force increases faster than the spring restoring force, and the gap rapidly closes as the upper

plate is attracted into the lower plate as shown by the solid line in Figure 20(a). The voltage at which this occurs is referred to as the "pull-in voltage" or "snap-in voltage", and corresponds to the actuation voltage when the gap is 2/3 of the original gap:

$$V_{pi} = \sqrt{\frac{8kg_0{}^3}{27\varepsilon_0 A}}. \qquad (29)$$

The capacitance as a function of voltage is plotted in Figure 20(b), and shows that the maximum stable tunable capacitance is $1.5C_{up}$, where C_{up} is the capacitance when the plates are at their initial position. However, tuning ranges this large are rarely obtained in practice, because it is difficult to control the capacitor near pull-in, the pull-in voltage may be reduced by tensile stress or non-linearities in the bridge spring, and the tuning range is reduced by fixed parasitic capacitance.

One strategy for increasing the tuning range of an electrostatically actuated capacitor is using separate actuation and RF gaps, with the actuation gap larger than the RF gap[97]. Another strategy is to use a three plate capacitor in which the movable plate is placed between a fixed RF electrode and fixed actuation electrode, with the gap between the actuation electrode and the movable electrode larger than the gap between the movable electrode and the RF electrode.[94] In both cases, the larger gap provides a larger actuation range prior to pull-in, which results in a larger relative change in the smaller gap.

Tunable capacitors may also be implemented using comb-drive electrostatic actuators, with either lateral[98] or angular[99] actuation. These types of actuators may provide more linear tuning and a larger tuning range, up to 31:1[99]. However, the long lengths of the fingers and support structures may add parasitic inductance and capacitance to the structure, limiting the frequency to a few GHz. These devices may be fabricated using thick metal or silicon micromachining processes, with the low stress gradient possible in silicon providing the ability to fabricate larger devices, but these devices must be

coated with metal in order to obtain good Q. Also, in some cases substrate loss may degrade the device performance; this substrate loss may be mitigated by fabricating on a low loss glass substrate[100], or by transferring the device to such a substrate after fabrication[101].

In addition to the electrostatic approaches described above, many tunable capacitors have also been realized using thermal[102] and piezoelectric[103,104] actuation. Both approaches provide the potential for using relatively low voltages to obtain precise positioning without the snap-in instability present with electrostatic actuation. For tunable capacitors, the primary disadvantage of thermal actuation is the power consumption as current must be supplied to maintain temperature and hold a position, and the primary disadvantage of piezoelectric actuation is the added fabrication complexity required by the piezoelectric material.

Some specific examples of continuously tunable parallel-plate capacitors and applications include a voltage controlled oscillator (VCO) using a MEMS capacitor with a tuning range of 1.4:1[105], tunable filters with variable capacitance[98], distributed time delays[106], and reflection phase shifters[107].

A tunable capacitor becomes a capacitive switch when a standoff or dielectric layer is added to the device to prevent contact between the two electrodes and fix the downstate capacitance to a known value. In this manner, a higher capacitance ratio can be achieved, but without intermediate values available. More details on capacitive switches will be provided in the capacitive switch section of this article.

4.3 Tunable Inductors

Tunable inductors provide an additional tunable reactive component to complement tunable capacitors in filters and matching networks. However, these devices are difficult to realize using MEMS approaches due to the large dimensional changes required to change the magnetic coupling by varying the dimensions or orientation of a loop or trace. When needed, tunable inductors are most frequently

realized in one of two ways: by changing the magnetic field coupling between adjacent current loops[108,109,110], or by switching segments of inductors into and out of a circuit using switches[111,112,113]. Other approaches include fabricating a MEMS device in which the actual loop area changes[114]. In practice, the maturity of MEMS tunable capacitors and the difficulty of realizing miniature inductors means that the tunable inductor function is performed using tunable capacitors and impedance transformers[115].

5 RF MEMS SWITCHES

Of the RF MEMS devices explored to date, capacitive and metal contacting switches offer some of the greatest potential and advantages over traditional incumbent devices such as transistors, PIN diodes, and macroscale relays[116,117]. A basic summary of the advantage is that MEMS technology has allowed the low loss and high isolation of a mechanical relay with the small size and weight of a solid-state technology.

5.1 RF MEMS Switch Advantages

The specific technology advantages of RF MEMS switches are:

- **Low Loss:** The signal carrying paths in RF MEMS switches are comprised of low resistivity metal films such as gold or aluminum and low loss dielectrics such as silicon nitride and silicon dioxide, and the signal loss in a good MEMS switch is similar to that of a transmission line with a similar structure. This is in contrast to semiconductor switches, where the signal must travel through a semiconductor material with relatively high resistivity and inherent contact resistances.

- **High Linearity:** The change in impedance of an RF MEMS switch is achieved with a mechanically moving structure. This type of device has excellent linearity because the mechanical response has a very low cutoff frequency (typically kHz), and because the majority of the impedance change is achieved by making and breaking a mechanical contact. Typically, the linearity of these devices is determined by the linearity of the underlying substrate or metal junctions, and is consistent with a transmission line made from the same materials.

- **Near-zero actuation power:** A typical RF MEMS switch is actuated electrostatically, which requires negligible static drive current, and therefore very low actuation power, to hold state. Aside from reduced system power consumption, this also means that excellent actuation pad

isolation can be achieved using high-value resistors instead of the more complex biasing and choke networks required for devices requiring drive current for actuation.[118]

- **Size consistent with integrated circuit technology:** RF MEMS metal contact switches offer mechanical switching performance in an integrated circuit form factor. As typical mechanical switches are generally "macro-sized", this attribute represents either a substantial decrease in size, weight, and power relative to existing mechanical switches, or a substantial improvement in the performance available in a die-scale technology. Additionally, the small size translates into shorter electrical length, which allows the device to be used at higher frequencies, especially in a shunt configuration.

- **Z_{on}/Z_{off} ratio:** This advantage applies to both types of RF MEMS switches, but especially to metal contact switches. The impedance ratio is a key performance attribute for a switching technology, and often determines the bandwidth of switches and switching networks. As reconfigurable systems move towards higher complexity, RF MEMS switches will offer more switching paths to higher frequency than any other technology. In most switches with a resistive channel, the off-state isolation is limited by off-state capacitance and the on-state loss is limited by the on-state resistance, with the most common figures of merit being the $(R_{on}C_{off})^{-1}$ product or the cutoff frequency of $(2\pi R_{on}C_{off})^{-1}$. However, some switching technologies such as phase change or memristor resistive switches have a non-negligible off-state conductance, and the off-state resistance may dominate the isolation, especially at lower frequencies[119,120]. In either case, because the on-state impedance is dominated by a contact resistance, RF MEMS switches break the traditional trade-off seen in FET switches, in which the on/off ratio is fixed and the only way to achieve lower on-state impedance is to sacrifice off-state capacitance by increasing gate width.

- **Broadband operation:** The simple structures possible with RF MEMS can produce devices with small parasitic capacitance and inductance. These smaller parasitic elements can easily be absorbed into the transmission line or other circuit impedances to realize broadband operation, with RF MEMS switches reported beyond 100 GHz. Additionally, metal contact switches provide broadband performance down to DC frequencies.

5.2 Capacitive RF MEMS Switches

Capacitive RF MEMS switches are switched capacitors with two capacitance values, and are used in cases where high-Q devices are required either as switches or for loading transmission lines or other structures.[121] The best capacitive switches have capacitance (and therefore impedance) ratios of >300:1, but capacitive switches with ratios as low as 10:1 can be useful for impedance tuning.[122] Cross-sections of typical capacitive switches in the up- and down- states are shown in Figure 21 for a switch with a dielectric coating the bottom electrode (a) or standoffs to maintain an airgap in the downstate (b). The switch with the intervening dielectric will have a higher downstate capacitance than one with just an airgap, but the dielectric may be susceptible to charging.

Neglecting fringing fields and assuming that the beam is in intimate contact in the downstate, the parallel plate equation can be used to calculate the capacitance of the switch in the up- and down-state as well as the impedance ratio:

$$C_{up} = \frac{\varepsilon_r \varepsilon_0 A}{\varepsilon_r g + d} \qquad C_{down} = \frac{\varepsilon_r \varepsilon_0 A}{d} \qquad \frac{C_{down}}{C_{up}} = \frac{Z_{off}}{Z_{on}} = \frac{\varepsilon_r g}{d} + 1, \tag{30}$$

where A is the overlap area of the top and bottom electrodes, d is the distance between the two electrodes in the downstate, g is the distance that the switch travels between the upstate and downstate, ε_0 is the permittivity of free space, and ε_r is the relative dielectric constant of the material between the electrodes when the switch is in the downstate (dielectric materials such as SiO_2 or Si_3N_4

for the dielectric switch or air in the case of the standoff-based switch). Maximizing the on/off impedance ratio of the switch requires a large ratio between the up-state and down-state gap and a high-k dielectric material[123]. However, the influence of a high-k dielectric material may be reduced by surface roughness, which lowers the down-state capacitance relative to a switch fabricated in intimate contact[124].

The electrostatically actuated switch follows the same position vs. voltage relationship as the tunable capacitor described in Section 4.2, except that the maximum capacitance is now determined by the thickness of the dielectric layer or standoff gap. Additionally, the higher electrostatic force in the downstate causes the re-opening voltage to be lower than the original pull-in voltage, so that the C-V curve demonstrates the hysteresis shown in the calculated curve in Figure 22. The figure also shows that, in the absence of charging, the C-V curve is symmetric for the positive and negative voltage.

Capacitive switches can be used in both a series and a shunt configuration, with equivalent circuit diagrams shown in Figure 23. The shunt configuration is most commonly used, with the transmission of an ideal capacitive shunt RF MEMS switch with capacitance C at frequency f in a system with characteristic impedance of Z_0 and no additional series or shunt matching inductance given by:

$$S_{21} = \frac{1}{1 - j\pi f C Z_0} , \qquad (31)$$

Thus, if the ratio between the up-state and down-state capacitance is fixed, there is a trade-off between the insertion loss in the up-state and the isolation in the down-state for an unmatched switch. However, the up-state insertion loss may be improved by adding a small series inductance (L_{series}) to the device, such that the combination of the up-state capacitance and series inductance matches the characteristic impedance of the circuit and the only switch losses are due to series resistance (R_{series}). Additionally, the down-state isolation may be improved at a given frequency with the addition of an inductance in the

shunt path (L_{shunt}), such that the series resonance of C_{shunt} and L_{shunt} is at the desired frequency, and the isolation is determined by the parasitic resistance (R_{shunt}) in the shunt path. In practice, L_{shunt} may be adjusted by changing the length of the switch bridge or bridge anchor[125].

5.3 Metal Contacting RF MEMS Switches

Metal contact RF MEMS switches offer an ideal resistive contact in the on-state and an ideal capacitive impedance in the off-state, making these devices ideal broadband RF switches. Because the devices have a very low $R_{on}C_{off}$ product, they allow for broader bandwidth operation than other switching technologies, and also allow for more complex multiple-throw switching networks than other technologies.

There have been hundreds of metal contacting switches reported, with a wide variation of actuation approaches and structures. Metal contact switches can use lateral motion within the substrate plane to make contact at the edges of two traces[126], or use vertical motion to make contact between the upper surface of one electrode and the bottom surface of another electrode. Actuation approaches include electrostatic, thermal, piezoelectric, and magnetic, with electrostatic actuation used most frequently for vertical switches due to the simple compact actuator. Thermal actuation is most commonly used for lateral switching due to the larger size of the actuator. Piezoelectric actuation offers the ability to apply force to both make and break a contact, but is less commonly used, probably due to increased materials integration complexity[127]. Magnetic actuation provides the possibility of latching operation, but has only found limited use due to material and design complexity and low actuator force density[128]. Because the vertical, electrostatically actuated, switch has become the most common metal contacting RF MEMS switch structure, the following discussion will focus on this device type.

Electrostatically actuated RF MEMS switches generally fall into one of the three designs shown in Figure 24. The first design, shown in Figure 24(a), is a cantilever that is anchored to the RF input on

one end and supports a metal contact on the free end. The switch is operated by applying a voltage on an actuation pad underneath the beam, which deflects the beam towards the substrate through electrostatic actuation. The switch is closed when the upper beam makes contact with the lower contact pad (labeled RF_{OUT}). After contact is made, the spring constant of the switch increases, and a gap is maintained between the beam and the actuation pad in normal operation. Additional force may be applied to the contact by increasing the actuation voltage, but excessive voltage or force will cause the beam to pull in and short to the actuation electrode. This design has the advantage of relatively simple fabrication, minimal dielectric charging, and the ability to adjust the contact force. Disadvantages include the potential for actuation electrode short circuits and limited isolation due to a single contact. Many electroplated gold switches, including the Radant switch[129] and some UCSD switches[130] are a variant of this design.

The second metal contact switch category is a cantilever where the beam is intended to collapse at the actuation pad, which is coated in a dielectric or has standoffs to prevent short circuits, as shown in Figure 24(b). This type of switch allows for a much higher contact force for a given pull-in voltage because after the switch has been pulled in by electrostatic actuation, the contact force is applied by beam bending rather than with an electrostatic force. However, it can be susceptible to dielectric charging at the actuation electrode, and the restoring is typically substantially lower than the contacting force. Examples of this type of switch include the early HRL switch[131] and the Intel switch[132].

The third general switch category is shown in Figure 24(c), and consists of two contacts in series connected by a rigid plate that is suspended by springs. Similar to the cantilever design, the switch body is pulled down by an electrostatic force between the actuation electrode and the switch body, and the contact force may be increased by further increasing the actuation voltage (up to the point where the plate collapses into the actuation electrode). In this case, the upper actuation electrode and switch

body are separate structures from the switch beams, allowing the actuator and beams to be optimized independently. Additionally, the two contact gaps in series increases the isolation of the switch beyond that of a switch with a single gap. Disadvantages of this switch design include increased contact loss due to the series combination of two contact resistances, the potential for actuation electrode short circuits, reduced contact and restoring force per contact, and potentially complex higher-order mechanical modes that limit the switch's mechanical response speed. Examples of this type of switch include the Rockwell (Teledyne) switch[133], the Omron switch[134], some Sandia switches[135], and some recent UCSD switches[136].

Regardless of the mechanical structure of the switch, appropriate contact metallurgy is essential for low resistance, high reliability operation of a switch[137]. The contact must achieve low resistance (~1 Ω), low adhesion force, and not be susceptible to oxidation, tarnishing, or contamination. The resistance of a pure metallic contact asperity is given by:

$$R_c = \sqrt{\frac{\rho^2 \eta \pi H}{4F}} \qquad (32)$$

which is a function of an empirical coefficient (η~1), metal resistivity (ρ), hardness (H), and the contacting force (F)[138]. Because there is inevitably a contamination layer at the contact surface, this equation will underestimate the resistance of a contact, but it illustrates the important parameters for achieving low contact resistance. However, resistance must be traded off against robustness, so the contact metal cannot be too soft. For instance, while gold is an ideal contact metal because it has low resistivity, does not oxidize, and is a relatively soft metal, the softness of the gold also causes high adhesion forces and is prone to stuck shut failures[139]. As a result, gold was used for many early low-loss demonstrations, but cannot achieve the required reliability. More recent reliability work focuses on hardened gold or transition-metal based contacts, and research continues, with a recent overview provided by Toler[137].

The contact and restoring forces are critical parameters for successful switch operation. For a design such as the one shown in Figure 24(c), assuming that the switch is not closed prior to electrostatic snap-in, the pull-in voltage is determined by the initial gap and spring constant as described earlier for tunable capacitors:

$$V_{pi} = \sqrt{\frac{8kg_0{}^3}{27\varepsilon_0 A}} \qquad (33)$$

Where *k* is the spring constant, g_o is the initial gap, ε_o is the permittivity of free space, and *A* is the area of the actuation electrode. After the switch is closed, the contact force is found by subtracting the spring force from the electrostatic force at the applied voltage:

$$F_c = \frac{\varepsilon_0 A V^2}{2d^2} - k(g_0 - d) \qquad (34)$$

And the restoring force can be found as:

$$F_r = k(g_0 - d) \qquad (35)$$

Where *d* is the contact height that maintains the air gap during actuation. This equation shows that the best approach to maximizing contact force is maximizing the applied voltage and minimizing the gap in the closed state because the contact force increases with the square of these parameters. The force increases linearly with the actuation area, so increasing the area of the switch body is not as effective for increasing contact force. In the ideal case, the initial gap and the downstate gap can be optimized so that the restoring force is similar to the contact force to ensure adequate force for re-opening the contact.

A circuit model for a metal contacting switch of the type shown in Figure 24(c) is shown in Figure 25 for the open (a) and closed (b) state. In most switches, the switch body capacitance and inductance and the influence of the actuation path is negligible, so that the off-state isolation is dominated by the

combination of the contact and substrate capacitances (C_{off} = 0.5$C_{contact}$ + $C_{substrate}$) and the on-state insertion loss is dominated by the contact and body resistance ($R_{on} = 2R_{contact} + R_{body}$):

$$S_{21closed} = \frac{1}{1+\frac{R_{on}}{2Z_0}}. \qquad S_{21open} = \frac{1}{1+\frac{1}{j4\pi f C_{off} Z_0}} \tag{36}$$

In order for the actuation path to have minimal influence on the switch operation, the actuation line must be isolated from the RF path. This is usually achieved using bias resistor (R_{bias}) that is significantly larger than the characteristic impedance of the switch. Typical values are >10 kΩ in a 50 Ω system, and often both the connection to the bias line and the actuation pad are realized with a high resistivity film[118].

Because of the reliability challenges associated with the contact, the maturity of metal contact switches has lagged that of capacitive switches. Recent advances have demonstrated that optimized contact metals, mechanical design that optimizes impact dynamics, high contact and restoring forces, and clean hermetic packaging are required for production of reliable metal contact switch and switch products[140]. As of 2013, the only metal contact switch available through mass commercial channels is a high-force switch with a bandwidth of about 8 GHz[141]. However, recent advances provide promise for future opportunities in metal contact switches and switch-based circuits, but advances at higher frequencies may be limited by a lack of market demand.

6 RF MEMS RELIABILITY

6.1 General Reliability Challenges

Because RF MEMS devices are microfabricated, the reliability of the technology is often compared to electronic devices, which have lifetimes measured in decades of time and trillions of operating cycles. However, the failure mechanisms and failure modes of MEMS differ from electronic devices, so not all of the established principles of microelectronic reliability apply to MEMS technologies[142]. As a result, RF MEMS reliability has been an area of concern, with significant research advances and new understanding gained in the past decade.

The small size and low forces of RF MEMS devices makes them more susceptible to degradation due to small amounts of contamination or adhesion when compared to larger structures. Different devices are degraded differently, but the two most common contamination-related failures are undesired changes in electrical properties due to mass loading or contaminants and failure due to adhesion. Additionally, the relatively high stresses and large deflections in the devices makes them susceptible to fatigue for metal springs, which causes a change in contacting and restoring force as well as actuation voltages[143].

Because switches are most sensitive to these reliability challenges, most RF MEMS reliability work has focused on specific failure mechanisms for RF MEMS capacitive and metal contacting switches. The most common figure of merit used for MEMS switches has been the number of cycles before 50% of the switches fail, but in many cases other parameters may be equally or even more relevant. For example, for circuits with large numbers of switches, the circuit will fail when the first switch fails, and in other cases, switches may be sensitive to being held in an open or closed position. Also, switches can be cycled under three main conditions: hot switching (with signal power incident during the entire switching event), cold switching (with signal power gated off during opening and closing), and

mechanical cycling (with no signal power other than an occasional low-level test signal). The different types of cycling, and different power levels, can produce different results for a given switch design.

RF MEMS switch reliability has advanced, with mean cycle lifetimes exceeding 10^9 cycles[144]. Obtaining the understanding required to achieve this improvement has required an iterative process of testing large quantities of switches to failure under different operating conditions, followed by failure analysis of failed switches, and application of the learning to future generations of switches. Future improvements will require continued focus on this testing and evaluation of stabilizing switch technologies.

6.2 Capacitive Switch Reliability

A brief summary of capacitive switch failure modes appears in Table 3. For a capacitive switch, the switch failing to open or close represents a fatal device failure. The predominant failure mode is a switch stuck in the down-state, which occurs when the spring restoring force is exceeded by the force holding the switch down, even in the absence of applied bias. The most common cause of this adhesion is a dramatic change in actuation voltage caused by charge trapping[145]. The amount of trapped charge may be reduced by eliminating dielectrics in high-field regions[122], using reduced actuation voltage (charging is an exponential function of voltage)[146], and using bipolar or intelligent actuation signals to minimize the net DC voltage across the switch[147]. Both charging and stuck-closed failures may also be due to contaminants on the surface that increase the adhesion force, so minimizing contaminants during operation is essential. In all cases, increasing the restoring force will increase the amount of adhesion force that can be tolerated, but at the expense of higher actuation voltage.

More subtle capacitive switch failure modes include changes in actuation and release voltage and changes in upstate and downstate capacitance. Shifts in actuation and release voltage may be caused by changes in temperature, dielectric charging, or by changes in spring constant due to fatigue or

wear. Sensitivity due to changes in temperature may be mitigated with appropriate designs for both capacitive[148] and metal contact switches[130,149], with good performance demonstrated down to cryogenic temperatures[150]. Charging will be polarity-dependent, while fatigue will be the same for both polarities, so the cause of these actuation voltage changes can be determined by testing with a bipolar ramped actuation waveform[151]. Various studies have explored the nature, location, permanence, and frequency dependence of charge trapping in capacitive switches[152].

With these reliability issues understood, several highly reliable RF MEMS capacitive switch technologies have been developed with excellent cycling and hold-down lifetimes[153]. These reliability results have been achieved through a combination of advances in the understanding of capacitive switch design (including techniques to limit charging and reduce stress), advances in the MEMS switch materials (especially dielectrics that are less sensitive to charging and metals less sensitive to fatigue), and investments in manufacturing and evaluation infrastructure.

6.3 Metal Contact Switch Reliability

As shown in Table 4, metal contact switches have many of the same reliability issues of capacitive switches, with the added challenge of an electrical contact. A MEMS contact presents a more significant reliability challenge than macro-scale contacts because of the low contacting and separation forces available in micro-scale devices. In macro-scale contact devices, the contacting force is sufficient to break through any thin contamination layers on the surface and provide a low contact resistance. Additionally, scrubbing of the two contact surfaces also helps break through any contamination, oxidation, or tarnish. By contrast, the RF MEMS contact closure is usually normal to the contact surface, and maximum forces are generally less than 1 mN per contact point. While 1 mN is sufficient to make a low resistance contact with two clean metal surfaces, it may be insufficient to break through some surface contamination.

To minimize the impact of surface contamination, the switch and package must be made of low outgassing materials such as metals and inorganic dielectrics. All contaminants on the surface of the switch die and package must be cleaned off prior to packaging, and the switch must be packaged in a clean hermetic volume that excludes all environmental moisture and contaminants. Some contamination will always be present, prompting investigation of metallurgy that is less susceptible to surface contamination and "friction polymers".[154]

In addition to increasing contact resistance, the relatively low restoring force of MEMS switches results in failures due to adhesion at the switch contact, usually due to fusion of the contact metals. These failures can be mitigated with high restoring forces, using hard metals that are less susceptible to fusion, and keeping the current through the contacts low enough to prevent softening due to heating.

Electric field breakdown, especially during opening and closing of the switch contact, may also damage the contact. Electrical breakdown across the contact gap may be caused by hot switching, electrostatic discharge, or feedthrough of the high voltage actuation signal onto the contacts[155]. These types of failures can be prevented through handling and operating practices that prevent high voltages across the contacts during operation.

The contact may also be damaged by the high velocity impact that is inherent with electrostatic actuation. This damage may result in increased contact adhesion and changes in contact resistance over the life of the switch. This damage may be minimized by designing electrostatic actuators so that the switch does not exhibit the pull-in instability, by using shaped drive waveforms to minimize the contact closing velocity[156], or by using linear actuation with piezoelectric or thermal actuators.

Another potential failure of electrostatically actuated switches is leakage current or breakdown in air-gap actuators.[157] While the Paschen curve shows that breakdown voltage increases at very low gaps, it only considers avalanche breakdown and neglects other effects such as field emission that are

dominant with small gaps and high fields.[158] These discharges may cause increased actuation current or damage to the actuation electrode or switch structure. To prevent this damage, the actuators must be designed to minimize breakdown at the required actuation voltages.

7 RF MEMS PACKAGING

7.1 Packaging Considerations

RF MEMS devices, especially switches, present unique packaging challenges beyond those presented by typical microelectronic technologies and devices. As a result, packaging is critical to the success of an RF MEMS technology. In addition to the typical requirements of small size and mechanical robustness at low cost, specific packaging challenges presented by RF MEMS devices are:

- Low loss and large bandwidth are significant advantages of RF MEMS devices, and these advantages are lost if the package does not have electrical performance similar to or better than the intrinsic device. As a result, an RF MEMS package must be carefully designed using low loss materials, with particular attention to minimizing parasitic resistance, capacitance, and inductance.
- RF MEMS devices must be protected from environmental contamination as well as handling damage, but the free-standing nature of the devices must be preserved. As a result, packages must contain voids for the RF MEMS devices, which excludes common low-cost approaches such as using bare die or plastic injection molding. In addition, the packaging voids must be hermetic to protect the MEMS device from external contamination or moisture, and the interior of the package must be free of any contamination that may foul switch contacts or mass load resonators.
- Freestanding MEMS devices are delicate, and can be easily damaged using standard packaging approaches after release. Because die singulation generates particles and uses high pressure water, MEMS devices that will be packaged individually using conventional approaches must be singulated prior to final release, and then released individually. After release, the individual die must be assembled without touching the top surface, and then lidded to provide a hermetic

environment. This die handling increases cost and lowers yield, making this approach impractical for large quantities of devices.

7.2 Packaging Approaches

RF MEMS devices have been packaged using numerous approaches, which can be broken down into four categories as shown in Figure 26: traditional assembly into glasswall or ceramic packages (a), chip-scale packaging by bonding lids individually onto MEMS die and accessing the interior using through-substrate vias (b1) or with a lateral underpass beneath the seal ring (b2), wafer-scale bonding of a lid wafer onto a device wafer followed by singulation (c), and local encapsulation of the MEMS devices using capping layers (d). These approaches are listed in order of suitability for mass production, but also in order of increasing investment required to develop the approach.

Chip-in-package assembly of MEMS devices into traditional glasswall or ceramic packages leverages traditional microelectronics packaging infrastructure[159]. After singulation and release, individual die are attached to the package well, the signal pads are wirebonded to the package leads, the package and devices are cleaned prior to lid sealing, and the package lid is attached using a solder or epoxy seal. The advantage of this approach is a relatively small initial investment because it requires no modification to the MEMS die and can be performed using common equipment and packages. However, it also requires the largest amount of die handling, results in a large package for a given die size, and offers the poorest performance because of the wirebonding and package parasitic capacitance and inductance. Therefore, this type of packaging is suitable for prototyping and evaluation, but is impractical for realizing large volumes of packaged RF MEMS devices or broadband (>10 GHz) MEMS devices.

Chip-scale packaging of individual die requires specifically designed MEMS device and lidding components[160]. After the MEMS devices are singulated and released individually, they are cleaned, and

a lid is attached to each die. In the most common approach, signals are brought out of the package using through-substrate via holes, realizing a broadband surface-mount package with a footprint only slightly larger than the MEMS device area[161]. In cases where via holes are not available, the signal traces may pass underneath the sealring to a bondpad on the top of the device die but outside of the hermetic volume, which can also provide broadband performance if the capacitance between the trace and sealring is managed appropriately[162]. The advantages of this approach are a small die size and good electrical performance, but it requires individual handling of specifically designed die and careful alignment of the lid to the die. Also, the bonding tolerances often limit minimum dimensions of the parts and seal rings as well as the performance of underpass feedthroughs. This approach provides miniature high-performance packaged MEMS devices, but at the cost of additional investment and process development beyond the chip-in-package approach.

Wafer-scale bonding is probably the most commonly used method for obtaining large quantities of packaged MEMS devices.[129,163] This approach is similar to the chip-scale approach, but instead of releasing the devices after dicing, all of the RF MEMS devices on an entire wafer are released prior to singulation. The entire device wafer is cleaned and then bonded to a matching lid wafer. Bonding is performed using a variety of bonding materials, including metal-to-metal compression, metal eutectic, glass frit, or organic films. This approach has the advantage of small package size, the ability to package a large number of devices at once, and eliminating handling and release of individual MEMS die. While developing a successful wafer-level bonded package requires substantial investment in tooling and process development, the approach provides excellent yield and reproducibility with a minimum of parts handling.

Encapsulation uses MEMS processing steps to build a cap over the RF MEMS device, which allows a very small form factor.[164,165,166] A dielectric film is often used to prevent any parasitic loading or

additional capacitance on the RF structure, and because of the tight tolerances achievable with modern lithography, the addition of the dielectric cap often requires no real estate beyond that of the MEMS device and associated circuitry. With this approach, RF MEMS devices can be encapsulated and protected from environmental contaminants in mass quantities without adding any additional thickness or volume to the device die. This approach is most frequently used in mass production for integrating MEMS devices with electronics.

8 FUTURE OUTLOOK

8.1 Commercialization

RF MEMS technology is transitioning from a research topic to a commercial technology, but the substantial investment and effort to mature a new technology requires a large market pull and volume. Recently, the wireless handset market has provided sufficient incentive to mature capacitive switch technologies for antenna impedance tuning[167,168]. Also, the test and measurement equipment market has been the driver for a reliable commercially available metal contacting switch[141].

In addition to the pervasive use of SAW and BAW resonators in modern RF systems, RF MEMS resonators are commercially available for low-cost and miniature timing applications[169,170,171]. As contour-mode devices mature and become more prevalent, it is likely that resonators will find additional commercialization as RF filters and oscillator references.

8.2 Integration

With the ongoing miniaturization and integration of electronic technologies, a key enabler for RF MEMS technologies is the ability to integrate them with other technologies such as active transistors for addressing and signal processing[172].

High-quality electromagnetic passives have been demonstrated using MEMS-like approaches in the back end of CMOS electronics, providing higher Q than achievable with the standard interconnect[173]. Acoustic passive devices can be used to demonstrate high-quality switched filter banks[25] and integrated oscillators[174].

Metal contacting switches have been integrated with active microelectronics to achieve high-performance circuits such as tunable and switched amplifiers[175]. Additionally, integration has been used to achieve small packaged metal contact switches with integrated driver circuits targeting low-cost

wireless applications[176]. This type of integration, with the signal conditioning and addressing circuitry included in the switch die, is essential for incorporating RF MEMS technologies into future systems.

The integration of capacitive switches into the CMOS interconnect layers has enabled the successful insertion of RF MEMS capacitive switch circuits into commercial wireless handsets[165] as well as the ability to realize high-performance microwave circuits[177].

8.3 Research Topics

While RF MEMS technologies are being commercialized, research opportunities continue to exist in reliability, performance, circuits, integration, packaging, and scaling. Some examples of ongoing research opportunities include:

- Improving the Q of switched and tunable filters through new architectures or integrated acoustic technologies[178,179].
- Continuing advances in microscale contact phenomena, especially in the areas of hot switching and high power handling.
- Scaling of both metal contacting[180] and capacitive[181] RF MEMS devices to smaller scales to address emerging opportunities in nanoscale switches and integration with electronics.
- Incorporation of novel materials to improve devices performance such as coupling[182] or Q[183].

9 FURTHER READING

A search of a popular database for "RF MEMS" reveals over 4,000 articles as of late 2013, indicating that there is a great breadth of available information available on the topic. While this article has provided a general introduction to the field, numerous books and review articles provide additional, more detailed, information.

While somewhat dated, Rebeiz's *RF MEMS Theory, Design, and Technology* (Wiley, 2003) provides an extensive treatment of RF MEMS switch and design fundamentals as well as an overview of the RF MEMS switch technologies available at the time. Lucyszen's more recent *Advanced RF MEMS* (Cambridge, 2010) provides an additional summary of more recent advances in the field. Varadan's *RF MEMS and Their Applications* (Wiley, 2002) provides a broader view of the RF MEMS field, and includes material on other RF MEMS technologies. Hashimoto's book *RF Bulk Acoustic Wave Filters for Communication* (Artech, 2009) provides an overview of piezoelectric bulk acoustic wave resonators and filters.

Over the years, several excellent review articles have been written covering various aspects of RF MEMS technologies, and many of these articles have been included in the references. Many of these articles were included in special issues, and cover RF MEMS devices[13,184], circuits[1,116], applications[117], testing[185], reliability[137,140,144,145], and integration[172]. While some of these articles are dated, they describe the breadth of the field and the fundamental concepts well, and also provide a snapshot of the technology at a given point in time.

GLOSSARY OF ABBREVIATIONS AND SYMBOLS

A	Electrode area
BAW	Bulk acoustic wave
BVD	Butterworth-Van Dyke resonator model
CAD	Computer aided design
$C_{contact}$	Open-state capacitance of the contacting structure of a MEMS switch
C_{down}	Capacitance of a MEMS switch in the down-state
CMOS	Complementary metal-oxide-semiconductor
C_{off}	Off-state capacitance of a device
C_s	Parallel capacitance of an acoustic resonator
$C_{substrate}$	Capacitance through a MEMS switch due to substrate coupling
C_{up}	Capacitance of a MEMS switch in the up-state
C-V	Capacitance-voltage
C_x	Motional capacitance of an acoustic resonator
d	Switch gap when closed
Δf	Frequency change
d_{ij}	Piezoelectric coefficient tensor component for mode i,j
E	Young's modulus of a material
E_{eff}	Effective Young's modulus of a structure
ε_0	Dielectric permitivitty of free space = 8.85×10^{-12} F/m
ε_{ij}	Permittivity tensor of a material
ε_r	Dielectric constant relative to free space
η	An empirical factor used in calculating contact resistance
F	Force
FBAR	Frequency bulk acoustic resonator
f_c	Resonator center frequency
F_e	Electrostatic force
FET	Field effect transistor
FOM_{filter}	Figure of merit of a resonator for filter applications
$FOM_{oscillator}$	Figure of merit for a resonator in an oscillator application
f_p	Anti-resonance frequency of an acoustic resonator
F_r	Restoring force
g	Gap between two plates in a structure
g_0	Initial gap
H	Hardness of a material
H(s)	S-domain circuit transfer function
HF	High frequency (3-30 MHz)
HfO_2	Hafnium dioxide
IF	Intermediate Frequency
i_0	Output current of a device
I-Q	Digital modulation using in-phase (I) and quadrature (Q) signals
K	Boltzmann's constant = 1.38×10^{-23} J/K

k	For switches: spring constant For resonators: effective mechanical resonator stiffness
K^2	Resonator electromechanical coupling coefficient
k_{eff}^2	Coupling coefficient approximated by series and parallel resonance frequencies
L	Length of a structure
λ	Wavelength
LFE	Lateral field excitation
L_{osc}	Fundamental phase noise limit of an oscillator
L_{series}	Series inductance of a device
L_{shunt}	Inductance between a node and ground in a network
L_x	Motional inductance of an acoustic resonator
M	Effective mass of a mechanical resonator
MAM	Metal-air-metal
MIM	Metal-insulator-metal
Mo	Molybdenum
PIN	P-type/intrinsic/N-type diode
P_{res}	RF power passing through a resonator
PZT	lead-zinc-titanate
Q	Resonator quality factor: the ratio of energy stored to energy lost
R_{bias}	Resistor in the actuation bias netork of a MEMS switch
R_{body}	Resistance of a MEMS switch body structure
$R_{contact}$	Contact resistance
RF MEMS	Radio Frequency Microelectromechanical Systems
ρ	Electrical: resistivity of a metal Mechanical: density of a mechanical material
ρ_{eff}	Effective density of a structure
RLC	Resonant circuit comprised of a resistor (R), inductor (L) and capacitor (C)
R_{ON}	On-state resistance of a device
R_s	Series resistance of a device
R_{series}	Series resistance in a network
R_{shunt}	Resistance between a node and ground in a network
$R_{substrate}$	Resistance due to substrate conductivity
R_X	Motional resistance of an acoustic resonator
S0	Fundamental symmetric Lamb wave mode
SAW	Surface acoustic wave
SHF	Super high frequency (3-30 GHz)
s_{ij}	Scattering parameter between nodes i and j
SMR	Solidly mounted resonator
SPDT	Single-Pole Double-Throw
SPnT	Single-Pole n-Throw, where n is the number of throws
t	Thickness of a structure
T	Temperature

TFE	Thickness field excitation
v	Velocity
V	Voltage
V_b	Bias voltage
VCO	Voltage-controlled-oscillator
v_i	Input voltage of a device
V_{pi}	Pull-in voltage of a MEMS devices
W	Tungsten
w	Width of a structure
y_{11}	Admittance looking into port 1 of a device
Z	Impedance
Z_0	Characteristic impedance a system (typically 50 Ω)
Z_a	Acoustic impedance of a material
Z_{Cs}	Impedance of the shunt capacitance across a resonator
Z_{off}	Off-state impedance of a device
Z_{on}	On-state impedance of a device
Z_R	Acoustic impedance of a resonator

ACKNOWLEDGMENT

The authors would like to thank our colleagues and management for their efforts and support of the RF MEMS program at Sandia National Laboratories, and would especially like the thank Chris Dyck, Janet Nguyen, and M. David Henry for careful review of the manuscript. Sandia National Laboratories is a multi-program laboratory managed and operated by Sandia Corporation, a wholly owned subsidiary of Lockheed Martin Corporation, for the U.S. Department of Energy's National Nuclear Security Administration under contract DE-AC04-94AL85000.

TABLES

FIGURE CAPTIONS

REFERENCES

[1] G. M. Rebeiz, G.-L. Tan, and J. S. Hayden, "RF MEMS Phase Shifters: Design and Applications," *IEEE Microwave Mag.*, vol. 3, no. 2, pp. 72-81, June 2002.

[2] J. A. Walraven, "Failure Mechanisms in MEMS," *Proc. International Test Conference,* pp. 828-822, 2003.

[3] T. P. Singh, "RF-MEMS Devices' Taxonomy," *Intl. J. Advances in Engineering Sciences,* vol. 3, no. 4, pp. 31-37, Oct. 2013.

[4] M. J. Madou, *Fundamentals of Microfabrication and Nanotechnology,* 3rd ed., CRC Press, 2011.

[5] C. K. Campbell, "Applications of Surface Acoustic and Shallow Bulk Acoustic Wave Devices," *Proc. of the IEEE,* vol. 77, no. 10, Oct. 1989.

[6] K. M. Lakin, "Modeling of Thin Film Resonators and Filters," *IEEE MTT-S Int. Microwave Symp. Digest,* vol.1, pp. 149-152, June 1992.

[7] *IEEE Standard on Piezoelectricity*, pp 51, 1988.

[8] S. Gong and G. Piazza, "Design and Analysis of Lithium-Niobate-Based High Electromechanical Coupling RF-MEMS Resonators for Wideband Filtering," *IEEE Trans. on Microwave Theory and Tech*., Vol. 61, No. 1, pp. 403-414, Jan. 2013.

[9] H. A. C. Tilmans, "Equivalent Circuit Representation of Electromechanical Transducers: II. Distributed Parameter Systems," *J. Micromech. Microeng.,* no. 7, pp. 285-309, 1997.

[10] K. M. Lakin and J. S. Wang, "Acoustic Bulk Wave Composite Resonators," *Applied Physics Letters,* **38** 125 (1981).

[11] K. M. Lakin, "A Review of Thin Film Resonator Technology," *IEEE Microwave Magazine,* Vol. 4, Issue 4, pp. 61-67, Dec. 2003.

[12] R. Ruby, P. Bradley, J. D. Larson and Y. Oshmyansky, "PCS 1900MHz Duplexer Using Thin Film Bulk Acoustic Resonators (FBARs)," *Electronics Letters,* Vol. 35, Issue 10, pp. 794-795, May 1999.

[13] G. Piazza, V. Felmetsger, P. Muralt, R. H. Olsson III and R. Ruby, "Piezoelectric Aluminum Nitride Thin Films for Microelectromechanical Systems," *MRS Bulletin*, Vol. 37, pp. 1051-1061, Nov. 2012.

[14] Q-X. Su, P. Kirby, E. Komuro, M. Imura, Q. Zhang and R. Whatmore, "Thin-Film Bulk Acoustic Resonators and Filters Using ZnO and Lead-Zirconium-Titanate Thin Films," *IEEE Trans. on Microwave Theory and Tech.,* vol. 49, no. 4, pp. 769-778, April 2001.

[15] N. Yamuchi, T. Shirai, T. Yoshihara, Y. Hayasaki, T. Ueda, T. Matsushima, K. Wasa, I. Kanno and H. Kotera, "High Coupling Piezoelectric Thin Films of Pb (Zr, Ti) O 3 –Based Ternary Perovskite Compounds for GHz-Range Film Bulk Acoustic Resonators," *Applied Physics Letters,* **94** 172903 (2009).

[16] S-H. Lee, K. H. Yoon and J-K. Lee, "Influence of Electrode Configurations on the Quality Factor and Piezoelectric Coupling Constant of Solidly Mounted Bulk Acoustic Wave Resonators," *J. of Applied Physics,* **92**, 4062 (2002).

[17] F. P. Stratton, D. T. Chang, D. J. Kirby, R. J. Joyce, T-Y Hsu and R. L. Kubena, "A MEMS-Based Quartz Resonator Technology for GHz Applications," *Proc. of the IEEE International Ultrasonics, Ferroelectrics and Frequency Control Joint 50th Anniversary Conf.,* pp. 27-34, 2004.

[18] R. Aigner, (2003), *MEMS in RF Filter Applications: Thin-film Bulk Acoustic Wave Technology. Sensors Update*, 12: 175–210. doi: 10.1002/seup.200390006.

[19] K-Y. Hashimoto, *Bulk Acoustic Wave Filters for Communications,* 1st ed. Artech House, 2009.

[20] G. Piazza, P. J. Stephanou, and A. P. Pisano, "Piezoelectric Aluminum Nitride Vibrating Contour-Mode MEMS Resonators," *J. of Microelectromechanical Systems,* vol. 15, no. 6, pp 1406-1418, Dec. 2006.

[21] D. J. D. Carter, J. Kang, D. White and A. E. Duwel, "Fabrication and Measurement of an IC-Compatible GHz-Range Piezoelectric Longitudinal Bar Resonator," *Proc. of the Solid-State Sensor, Actuator, and Microsystems Workshop,* pp. 254-257, June 2004.

[22] B. Kim, R. H. Olsson III and K. E. Wojciechowski, "AlN Microresonator-Based Filters with Multiple Bandwidths at Low Intermidate Frequencies," *J. of Microelecromechanical Sys*., vol. 22, no. 4, pp. 949-961, Aug. 2013.

[23] C. Zuo, N. Sinha and G. Piazza, "Very High Frequency Channel-Select MEMS Filters Based on Self-Coupled Piezoelectric AlN Contour-Mode Resonators," *Sensors and Actuator A:Physical*, 160, pp. 132-140, 2010.

[24] R. H. Olsson III, J. Nguyen, T. Pluym and V. M. Hietala, "A Method for Attenuating the Spurious Responses of Aluminum Nitride Micromechanical Filters," *J. of Microelectromechanical Sys.*, vol .PP, no. 99, pp. 1-10.

[25] E. R. Crespin, R. H. Olsson III, K. E. Wojciechowski, D. W. Branch, P. Clews, R. Hurley and J. Gutierrez, "Fully Integrated Switchable Filter Banks*", Proc. of IEEE Int. Microwave Symp.,* June 2012.

[26] M. Rinaldi, C. Zuniga, C. Zuo, and G. Piazza. "AlN Contour-Mode Resonators for Narrow-Band Filters above 3 GHz" *2009 Joint Meeting of the European Frequency and Time Forum and the IEEE International Frequency Control Symposium (EFTF-IFCS 2009)* pp. 70-74, 2009

[27] M. Rinaldi, C. Zuniga, C. Zuo and G, Piazza, "Super-High-Frequency Two-Port AlN Contour-Mode Resonators for RF Applications," *IEEE Trans. on Ultrasonics, Ferrolectrics, and Frequency Cntrl.,* vol. 57, no. 1, pp. 38-45, Jan. 2010.

[28] M. Rinaldi, C. Zuniga and G. Piazza, "5-10 GHz AlN Contour-Mode Nanoelectromechanical Resonators," *IEEE Int. Conf. on Microelectromechanical Sys.,* pp. 916-919, Jan. 2009.

[29] G. Wingqvist, L. Arapan, V. Yantchev and I. Katardjiev, "A Micromachined Thermally Compensated Thin Film Lamb Wave Resonator for Frequency Control and Sensing Applications," *J. Micromech. Microeng.* **19** (2009) 035018 (9pp).

[30] I. E. Kuznetsova, B. D. Zaitsev, S. G. Joshi, and I. A. Borodina, "Investigation of Acoustic Waves in Thin Plates of Lithium Niobate and Lithium Tantalate," *IEEE Trans. on Ultrasonics, Ferrolectrics and Frequency Cntrl.,* Vol. 48, No. 1, pp. 322-328, Jan. 2001.

[31] G. Piazza, R. Abdolvand, G. K. Ho and F. Ayazi, "Voltage-Tunable Piezoelectrically-Transduced Single-Crystal Silicon Micromechanical Resonators," *Sensors and Actuators A,* 111, pp. 71-78, 2004.

[32] J. S. Pulskamp, R. G. Polcawich, R. Q. Rudy, S. S. Bedair, R. M. Proie, T. Ivanov and G. L. Smith, "Piezoelectric PZT MEMS Technologies for Small-Scale Robotics and RF Applications," *MRS Bulletin*, vol. 37, pp. 1062-1070, Nov. 2012.

[33] G. K. Ho, R. Abdolvand, A. Sivapurapu, S. Humad and F. Ayazi, "Piezoelectric-on-Silicon Lateral Bulk Acoustic Wave Micromechanical Resonators," *J. of Microelectromechanical Systems,* vol. 17, no. 2, pp. 512-520, April 2008.

[34] H. Fatemi, H. Zeng, J. Carlisle and R. Abdolvand; "High-Frequency Thin-Film AlN-on-Diamond Lateral–Extensional Resonators," *J. of Microelectromechanical Sys.*, vol.22, no.3, pp.678-686, June 2013.

[35] S. Gong, N-K. Kuo and G. Piazza, "GHz High-Q Lateral Overmoded Bulk Acoustic-Wave Resonators Using Epitaxial SiC Thin Film," *J. of Microelectromechanical Sys.*, vol.21, no.2, pp.253-255, April 2012.

[36] N-K. Kuo, S. Gong, J. Hartman, J. Kelliher, W. Miller, J. Parke, S. V. Krishaswamy, J. D. Adam, and G. Piazza, "Micromachined Sapphire GHz Lateral Overtone Bulk Acoustic Resonators Transduced by Aluminum Nitride," *IEEE Conf. on Microelectromechanical Sys.,* pp. 27-30, Jan. 2012.

[37] L-W. Hung and C. T.-C. Nguyen, "Capacitive-Piezo Transducers for Higher-Q Contour Mode AlN Resonators at 1.2 GHz," *Tech, Digest of the Solid-State Sensor, Actuator and Microsystems Workshop,* pp. 463-466, June 2010.

[38] R. R. Wang, S. A. Bhave, and K. Bhattacharjee, "Thin-film High k_t^2Q, Multi-Frequency Lithium Niobate Resonators," *26th IEEE International Conference on Micro Electro Mechanical Systems (MEMS 2013)*, pp. 165-168. Jan. 2013.

[39] R. H. Olsson III, K. Hattar, S. J. Homeijer, M. Wiwi, M. Eichenfield, D. W. Branch, M. S. Baker, J. Nguyen, B. Clark, T. Bauer and T. A. Friedmann, "A High Electromechanical Coupling Coefficient SH0 Lamb Wave Lithium Niobate Micromechanical Resonator and a Method for Fabrication," *Sensors and Actuators A:* 209 pp. 183-190, 2014.

[40] S. Gong and G. Piazza, "Figure of Merit Enhancement of Laterally Vibrating Lithium Niobate MEMS Resonators," *IEEE Trans. on Electron Dev.,* vol. 60, no. 11, pp. 3888-3894, Nov. 2013.

[41] R. H. Olsson III, K. Hattar, M. S. Baker, M. Wiwi, J. Nguyen, C. Padilla, S. J. Homeijer, J. R. Wendt and T. A. Friedmann, "Lamb Wave Micromechanical Resonators Formed in Thin Plates of Lithium Niobate," *Tech, Digest of the Solid-State Sensor, Actuator and Microsystems Workshop,* June 2014, In-Press.

[42] C. Nguyen, "MEMS Technology for Timing and Frequency Control," *IEEE Trans. Ultrasonics, Ferroelectrics and Frequency Control*, Vol. 54, No. 2, pp. 251-270, Feb. 2007.

[43] M. Lutz, A. Partridge, P. Gupta, N. Buchan, E. Klaassen, J. McDonald and K. Peterson, "MEMS Oscillators for High Volume Commercial Applications," *Proc. of the Solid-State Sensors, Actuators and Microsystems Conference (Transducers),* pp. 49-52, 2007.

[44] F. D. Bannon III, J. R. Clark, and C. Nguyen, "High-Q HF Microelectromechanical Filters," *IEEE J. Solid-State Circuits*, vol. 35, no. 4, pp. 512-526, April 2000.

[45] M. U. Demirci and C. Nguyen, "Mechanically Corner-Coupled Square Microresonator Array for Reduced Series Motional Resistance," *J. Microelectromechanical Systems*, vol. 15, no. 6, pp. 1419-1436, Dec. 2006.

[46] S. Pourkamali and F. Ayazi, “Electrically Coupled MEMS Bandpass Filters; Part I: With Coupling Element,” *Sensors and Actuators A*, pp. 307-316, Aug. 2005.
[47] S. Pourkamali and F. Ayazi, “Electrically Coupled MEMS Bandpass Filters; Part II: Without Coupling Element,” Sensors and Actuators A, pp. 317-325, Aug. 2005.
[48] J. R. Clark, W. Hsu, M. A. Abdelmoneum, and C. Nguyen, "High-Q UHF Micromechanical Radial-Contour Mode Disk Resonators," *J. Microelectromechanical Systems*, vol. 14, no. 6, pp. 1298-1310, Dec. 2005.
[49] D. Weinstein and S. A. Bhave, "Internal Dielectric Transduction in Bulk-Mode Resonators," *IEEE Journal of Microelectromechanical Systems,* vol. 18, No. 6, pp. 1401-1408, Dec. 2009.
[50] R. H. Olsson III, “Microresonator Filters and Oscillators: Technology and Applications,” *IEEE International Electron Devices Meeting Tutorial Presentation,* Dec. 2011.
[51] S. Pourkamali, Z. Hao and F. Ayazi, “VHF Single Crystal Silicon Capacitive Elliptic Bulk-Mode Disk Resonators-PartII: Implementation and Characterization,” *IEEE Journal of Microelectromechanical Systems,* vol. 13, no. 6, pp. 1054-1062, Dec. 2004.
[52] M. Ziaei-Moayyed, D. Elata, E. P. Quevy and R. T. Howe, “Differential Internal Dielectric Transduction of a Lame’-Mode Resonator,” *J. Micromech. Microeng,* **20** (2010) 115036 (15pp).
[53] H. Chandrahalim, D. Weinstein, L. F. Cheow and S. A. Bhave, "High-K Dielectrically Transduced MEMS Thickness Shear Mode Resonators and Tunable Channel-Select RF Filters," *Sensors and Actuators A: Physical* 136(2) pp. 527-539, 2007.
[54] J. E-Y. Lee, J. Yan and A. A. Seshia, “Study of Lateral Mode SOI-MEMS Resonators for Reduced Anchor Loss,” *J. of Micromech. Microeng.* **21** (2011) 045010 (10pp).
[55] L. Khine and M. Palaniapan, “High-Q Bulk-Mode SOI Square Resonators with Straight-Beam Anchors,” *J. of Micromech. Microeng.* **19** (2009) 015017 (10pp).
[56] V. Kaajakari, T. Mattila, A. Oja, J. Kiihamäki and Heikki Seppä, “Square-Extensional Mode Single-Crystal Silicon Micromechanical Resonator for Low-Phase-Noise Oscillator Applications,” *IEEE Electron Device Letters,* vol. 25, no. 4, pp. 173-175, April 2004.
[57] B. Kim, R. N. Candler, M. A. Hopcroft, M. Agarwal, W-T. Park, and T. W. Kenny, "Frequency Stability of Wafer-Scale Film Encapsulated Silicon Based MEMS Resonators," *Sensors and Actuators A: Physical*, vol. 136, No. 1, pp. 125-131, 2007.
[58] A. E. Franke, J. M. Heck, T.-J. King, and R. T. Howe, “Polycrystalline silicon germanium films for integrated microsystems,” *IEEE/ASME Journal of Micro-electromechanical Systems*, **12**, pp. 160-171, 2003.
[59] G. K. Fedder, R. T. Howe, T.-J. King Liu, and E. P. Quévy, “Technologies for Co-Fabricating MEMS and Electronics,” *Proceedings of the IEEE*, 96, pp. 306-322, 2008.
[60] D. B. Lesson, “A Simple Model of Feedback Oscillator Noise Spectrum,” *Proc. of the IEEE,* pp. 329-330, Feb. 1966.
[61] M. Rinaldi and G. Piazza, “Effects of Volume and Frequency Scaling in AlN Contour Mode NEMS Resonators on Oscillator Phase Noise,” *Joint Conference of the IEEE Frequency Cntrl. Symp. and the European Frequency and Time Forum,* pp. 1-5, May 2011.
[62] C. D. Nordquist and R. H. Olsson III, “Power Handling and Intermodulation Distortion of Contour-Mode AlN MEMS Resonators and Filters,” *IEEE International Microwave Symposium*, 978-1-61284-757-3/11, June 2011.
[63] J. T. M. van Beek and R. Puers, “A Review of MEMS Oscillators for Frequency Reference and Timing Applications,” *J. of Micromech. Microeng.,* vol. 22, no. 1, pp. 1-35, 2012.
[64] T. L. Naing, T. O. Rocheleau, E. Alon and C. T.-C. Nguyen, “A 78 Microwatt GSM Phase Noise-Compliant Pierce Oscillator Referenced to a 61-MHz Wine-Glass Disk Resonator,” *Proc. of the 2013 Joint UFFC, EFTF and PFM Symp.,* pp. 562-565, July 2013.
[65] H. M. Lavasani, A. K. Samarao, G. Casinovi and F. Ayazi, “A 145 MHz Low Phase-Noise Capacitive Micromechanical Oscillator,” *IEEE Int. Electron Device Meeting,* pp. 1-4, Dec. 2008.
[66] J. E.-Y. Lee, B. Bahreyni, Y. Zhu and A. A. Seshia, “A Single-Crystal-Silicon Bulk-Acoustic-Mode Microresonator Oscillator,” *IEEE Electron Device Lett.,* vol. 29, no. 7, July 2008.
[67] R. Ruby, M. Small, F. Bi, D. Lee, L. Callaghan, R. Parker, and S. Ortiz, "Positioning FBAR Technology in the Frequency and Timing Domain," *IEEE Trans. on Ultrasonics, Ferroelectrics and Frequency Control*, vol.59, no.3, pp. 334,345, March 2012.

[68] R. L. Kubena, D. J. Kirby, Y-K. Yong, D. T. Chang, F. P. Stratton, H. D. Nguyen, R. J. Joyce, R. Perahia, H. P. Moyer and R. G. Nagele, "UHF Quartz MEMS Oscillators for Dynamics-Based System Enhancements," *Joint Conference of the European Frequency and Time Forum & the IEEE International Frequency Control Symposium (EFTF/IFC)*, pp. 1-8, July 2013.

[69] M. Rinaldi, C. Zuo, J. Van der Spiegel and G. Piazza, "Reconfigurable CMOS Oscillator Based on Multifrequency AlN Contour-Mode MEMS Resonators," *IEEE Trans. on Electron Devices*, vol.58, no.5, pp.1281-1286, May 2011.

[70] R. Abdolvand, H. Mirilavasani, G.K. Ho, and F. Ayazi, "Thin-Film Piezoelectric-on-Silicon Resonators for High-Frequency Reference Oscillator Applications," *IEEE Transactions on Ultrasonics, Ferroelectrics, and Frequency Control*, Vol. 55, Issue 12, pp. 2596-2606, Dec. 2008.

[71] K. C. Gupta, *Microstrip Lines and Slotlines,* 2nd ed., Artech House, 1996.

[72] T. H. Lee and S. S. Wong, "CMOS RF Integrated Circuits at 5 GHz and Beyond," *Proc. IEEE,* vol. 88, no. 10, pp. 1560-1571, Oct. 2000.

[73] M. Sterner, N. Roxhed, G. Stemme, and J. Oberhammer, "Electrochemically Assisted Maskless Selective Removal of Metal Layers for Three-Dimensional Micromachined SOI RF MEMS Transmission Lines and Devices," *J. Microelectromech. Sys.,* vol. 20, no. 4, pp. 899-908, Aug. 2011.

[74] C.-P. Lin and C. F. Jou, "New CMOS-Compatible Micromachined Embedded Coplanar Waveguide, ", *IEEE Trans. Microwave Theory and Techniques,* vol. 58, no. 9, pp. 2511-2516, Sept. 2010.

[75] V. Milanovic, M. Gaitan, E. D. Bowen, and M. E. Zaghoul, "Micromachined Microwave Transmission Lines in CMOS Technology," *IEEE Trans. Microwave Theory and Techniques,* vol. 45, no. 5, pp. 630-635, May 1997.

[76] K. J. Herrick, T. A. Schwarz, and L. P. B. Katehi, "Si-Micromachined Coplanar Waveguides for Use in High-Frequency Circuits, , *IEEE Trans. Microwave Theory and Techniques,* vol. 46, no. 6, pp. 762-768, June 1998.

[77] J. R. Reid, E. D. Marsh, R. T. Webster, "Micromachined Rectangular-Coaxial Transmission Lines," *IEEE Trans. Microwave Theory and Techniques,* vol. 54, no. 8, pp. 3433-3442, Aug. 2006.

[78] L. Ranzani, D. Kuester, K. J. Vanhille, A. Boryssenko, E. Grossman, and Z. Popovic, "G-Band Micro-Fabricated Frequency-Steered Arrays With 2°/GHz Beam Steering," *IEEE Trans. Terahertz Science and Technology,* vol. 3, no. 5, pp. 566-573, Sept. 2013.

[79] N. Ehsan, E. Cullens, K. Vanhille, D. Frey, S. Rondineau, R. Actis, S. Jessup, R. Lender Jr., A. Immorlica, D. Nair, D. Filipovic, and Z. Popovic, "Micro-coaxial lines for Active Hybrid-Monolithic Circuits, *IEEE MTT-S Intl. Microwave Symp. Dig.,* pp. 465-468, Boston, MA, June 2009.

[80] M. A. Forman, "Low-Loss LIGA-Fabricated Coplanar Waveguide and Filter," *Proc. Asia-Pacific Microwave Conf.,* pp. 1905-1907, Dec. 2006.

[81] C. D. Nordquist, M. C. Wanke, A. M. Rowen, C. L. Arrington, A. D. Grine, and C. T. Fuller, "Properties of Surface Metal Micromachined Rectangular Waveguide Operating Near 3 THz," *IEEE J. Selected Topics in Quantum Electronics,* vol. 17, no. 1, pp. 130-137, Jan. 2011.

[82] H. Cheng, J. F. Whitaker, T. M. Weller, and L. P. B. Katehi, "Terahertz-bandwidth characterization of coplanar waveguide via time-domain electro-optic sampling," , *IEEE MTT-S Intl. Microwave Symp. Dig.,* pp. 477-480, May 1994.

[83] C.-Y. Chi, and G. M. Rebeiz, "Planar Microwave and Millimeter-Wave Lumped Elements and Coupled-Line Filters Using Micro-Machining Techniques, *IEEE Trans. Microwave Theory and Techniques,* vol. 43, no. 4, pp. 730-728, April 1995.

[84] C.-Y. Chi and G. M. Rebeiz, "Conductor-loss limited stripline resonator and filters," *IEEE Trans. Microwave Theory and Techniques,* vol. 44, no. 4, pp. 626-630, April 1996.

[85] G. M. Rebeiz, L. P. B. Katehi, T. M. Weller, C.-Y. Chi, S. V. Robertson, "Micromachined Membrane Filters for Microwave and Millimeter-wave Applications," *Intl. J. Microwave and Millimeter-wave Computer-Aided Engineering,* vol. 7, no. 2, pp. 149-166, March 1997.

[86] S. Lucyszyn, K. Miyaguchi, H. W. Jiang, I. D. Roberton, G. Fisher, and A. Lord, and J.-Y. Choi, "Micromachined RF-Coupled Inverted-Microstrip Millimeter-Wave Filters," *J. Microelectromechanical Syst.,* vol. 17, no. 3, pp. 767-776, June 2008.

[87] J. Muldavin, C. Bozler, S. Rabe, and C. Keast, "Wide-Band Low-Loss MEMS Packaging Technology," *IEEE MTT-S Intl. Microwave Symp. Dig.*, Long Beach, CA, June 2005.

[88] H. Leblond, D. Baillargeat, P. Blondy, "Integrated RF Devices in Suspended Technology," *IEEE Intl Conf on Electronics, Circuits, and Systems,* pp. 475-477, Dec. 2006.
[89] K. Entesari, T. Vaha-Heikkila, and G. M. Rebeiz, "Miniaturized Differential Filters for C- and Ku-Band Applications," *Proc. European Microwave Conference,* pp. 227-230, 2003.
[90] H.-K. Kim, J.-H. Park, Y.-K. Kim, and Y. Kwon, "Compact Low-Loss Monolithic CPW Filters Using Air-Gap Overlay Structures," *IEEE Microwave and Wireless Component Letters,* vol. 8, no. 6, pp. 422-432, Nov. 1998.
[91] J. N. Burghartz, "Spiral Inductors on Silicon – Status and Trends," *Int. J. RF Microwave Comput Aided Eng.,* vol. 11, no. 5, pp. 322-329, Sept. 2001.
[92] P. J. Bell, N. D. Hoivik, R. A. Saravanan, N. Ehsan, V. M. Bright, and Z. Popovic, "Flip-Chip-Assembed Air-Suspended Inductors," *IEEE Trans. Microwave Theory and Techniques,* vol. 30, no. 11, pp. 148-154, Feb. 2007.
[93] W. S. N. Trimmer, "Microrobots and Micromechanical Systems," *Sensors and Actuators,* vol. 19, no. 3, pp. 267-287, Sept. 1989.
[94] A. Dec and K. Suyama, "Micromachined Electro-Mechanically Tunable Capacitors and Their Applications to RF IC's," *IEEE Trans. Microwave Theory and Techniques,* vol. 46, no. 12, pp. 2587-2596, Dec. 1998.
[95] W. Young and R. Budnyas, *Roark's Formulas for Stress Strain, 8th ed.,* McGraw-Hill, 2001.
[96] J. R. Reid, L. A. Starman, and R. T. Webster, "RF Actuation of Capacitive MEMS Switches," , *IEEE MTT-S Intl. Microwave Symp. Dig.,* pp. 1919-1922, June 2003.
[97] J. Zou, J. E. Schutt-Aine, "Development of a Wide-Tuning-Range Two-Parallel-Plate Tunable Capacitor for Integrated Wireless Communication Systems," *Int. J. RF Microwave Computer Aided Eng.,* vol. 11, no. 5, pp. 322-329, Sept. 2001.
[98] R. L. Borwick, P. A. Stupar, J. F. DeNatale, R. Anderson, and R. Erlandson, "Variable MEMS Capacitors Implemented Into RF Filter Systems, " *IEEE Trans. Microwave Theory and Techniques,* vol. 51, no. 1, pp. 315-319, Jan. 2003.
[99] H. D. Nguyen, D. Hah, P. R. Patterson, R. Chao, W. Piyawattanametha, E. K. Lau, and Min C. Wu, "Angular Vertical Comb-Driven Tunable Capacitor With High-Tuning Capabilities, *J. Microelectromechanical Syst.,* vol. 13, no. 3, pp. 406-413, June 2004.
[100] D. T. McCormick, N. C. Tien, N. MacDonald, R. Matthews, and A. Hibbs, "Ultra-Wide Tuning Range Silicon MEMS Capacitors on Glass with Tera-Ohm Isolation and Low Parasitics," *Solid-State Sensors, Actuators, and Microsystems Digest – TRANSDUCERS -05,* pp. 1075-1079, June 2005.
[101] K. F. Harsh, W. Zhang, V. M. Bright, and Y. C. Lee, "Flip-Chip Assembly for Si-Based RF MEMS," *Proc. Intl. Conf. on Microelectromechanical Sys.,* pp. 273-278, Jan. 1999.
[102] Z. Feng, W. Zhang, B. Su, K. F. Harsh, K. C. Gupta, V. Bright, and Y. C. Lee, "Design and Modeling of RF MEMS Tunable Capacitors Using Electro-Thermal Actuators, *IEEE MTT-S Intl. Microwave Symp. Dig.,* pp. 1507-1510, June 1999.
[103] T. Kawakubo, T. Nagano, M. Nishigaki, K. Abe, and K. Itaya, "RF-MEMS Tunable Capacitor With 3 V Operation Using Folded Beam Piezoelectric Bimorph Actuator," *J. Microelectromechanical Syst.,* vol. 15, no. 6, pp. 1759-1755, Dec. 2006.
[104] J. Y. Park, Y. J. Yee, H. J. Nam, J. U. Bu, "Micromachined RF MEMS Tunable Capacitors Using Piezoelectric Actuators," *IEEE MTT-S Int. Microwave Symp. Dig.,* pp. 2111-2114, June 2001.
[105] A. Dec and K. Suyama, "A 1.9-GHz CMOS VCO with Micromachined Electromechanically Tunable Capacitors," *IEEE J. Solid State Circuits,* vol. 35, no. 8, pp. 1231-1237, Aug. 2000.
[106] N. S. Barker and G. M. Rebeiz, "Distributed MEMS True-Time Delay Phase Shifters and Wide-Band Switches," *IEEE Trans. Microwave Theory and Techniques,* vol. 46, no. 11, pp. 1881-1890, Nov. 1998.
[107] S. Lee, J.-H. Park, H.-T. Kim, J.-M. Kim, Y.-K. Kim, and Y. Kwon, "Low-Loss Analog and Digital Reflection-Tyle MEMS Phase Shifters With 1:3 Bandwidth," *IEEE Trans. Microwave Theory and Techniques,* vol. 52, no. 1, pp. 211-219, Jan. 2004.
[108] V. M. Lubecke, B. Barber, E. Chan, D. Lopez, M. E. Gross, and G. Gammel, "Self-Assembling MEMS Variable and Fixed RF Inductors, *IEEE Trans. Microwave Theory and Techniques,* vol. 49, no. 11, pp. 2093-2098, Nov. 2001.
[109] I. Zine-El-Abidine, M. Okoniewski, and J. G. McRory, "Tunable Radio Frequency MEMS Inductors with Thermal Bimorph Actuators", *J. Micromech. Microeng.* Vol. 15, no. 11, pp. 2063-2068, Nov. 2005

[110] J.-I. Kim and D. Peroulis, "Tunable MEMS Spiral Inductors with Optimized RF Performance and Integrated Large-Displacement Electrothermal Actuators," *IEEE Trans. Microwave Theory and Techniques,* vol. 57, no. 9, pp. 2276-2285, Sep. 2009.
[111] M. Rais-Zadeh, P. A. Kohl, and F. Ayazi, "MEMS Switched Tunable Inductors," *J. Microelectromechanical Syst.,* vol. 17, no. 1, pp. 78-84, Feb. 2008.
[112] A. Shirane, Y. Mizuochi, S. Amakawa, N. Ishihara, and K. Masu, "A Study of Digitally Controllable Radio Frequency Micro Electro Mechanical Systems Inductor," *Japanese Journal of Applied Physics,* vol. 50, no 5 pt. 2, pp. 05EE01, May 2011.
[113] S. Zhou, X.-Q. Sun, and W. N. Carr, "A Monolithic Variable Inductor Network Using Microrelays with Combined Thermal and Electrostatic Actuation," *J. Micromech. Microeng.* Vol. 9, no. 1, pp. 45-50, March 1999.
[114] I. Zine-El-Abidine and M. Okoniewski, "A Tunable Radio Frequency MEMS Inductor Using MetalMUMPs," *J. Micromech. Microeng.* Vol. 17, no. 11, pp. 2280-2287, Nov. 2007
[115] J. A. G. Malherbe, *Microwave Transmission Line Filters,* Artech House, 1979.
[116] G. M. Rebeiz and J. B. Muldavin, "RF MEMS Switches and Switch circuits," *IEEE Microwave Mag*., vol. 2, no. 4, pp. 59–71, Dec. 2001.
[117] E. R. Brown, "RF-MEMS Switches for Reconfigurable Integrated Circuits," *IEEE Trans. Microwave Theory and Techniques,* vol. 46, no. 11-2, pp. 1868-1880, Nov. 1998.
[118] D. A. Goins, R. D. Nelson, and J. S. McKillop, "Design of a 20 GHz Low Loss Ohmic Contact RF MEMS Switch," *IEEE MTT-S Int. Microwave Symp. Dig.,* pp. 371-374, June 2007.
[119] A. Vena, E. Perret, S. Tedjini, C. Vallee, P. Gonon, and C. Mannequin, "A Fully Passive RF Switch Based on Nanometric Conductive Bridge," *IEEE MTT-S Int. Microwave Symp. Dig.,* pp. 6258428, June 2012.
[120] H. Lo, E. Chua, J. C. Huang, C. C. Tan, C.-Y. Wen, R. Zhao, L. Shi, C. T. Chong, J. Paramesh, T. E. Shlesinger, and J. A. Bain, "Three-Terminal Prove Reconfigurable Phase-Change Material Switches," *IEEE Trans. Electron Dev.,* vol. 57, no. 1, pp. 312-320, Jan. 2010.
[121] C. L. Goldsmith, Z. Yao, S. Eshelman, and D. Denniston, "Performance of Low-Loss RF MEMS Capacitive Switches," *IEEE Microwave Guided Wave Letters,* vol. 8, no. 8, pp. 269-271, Aug. 1998.
[122] P. Blondy, A. Cruntenau, C. Champeaux, A. Catherinot, P. Tristant, O. Vendier, J. L. Cazaux, and L. Marchand, "Dielectric Less Capacitive MEMS Switches," *IEEE MTT-S Int. Microwave Symp. Dig.,* pp. 573-576, June 2004.
[123] J. Y. Park, G. H. Kim, K. W. Chung, and J. U. Bu, "Monolithically Integrated Micromachined RF MEMS Capacitive Switches", *Sensors and Actuators A,* vol. 89, no. 1-2, pp. 88-94, Mar. 2001.
[124] A. B. Yu, A. Q. Liu, Q. X. Zhang, A. Alphones, L. Zhu, and A. P. Shacklock, "Improvement of Isolation for MEMS Capacitive Switch Via Membrane Planarization," *Sensors and Actuators A,* vol. 119, no. 1, pp. 206-213, Mar. 2005.
[125] J. B. Muldavin and G. M. Rebeiz, "High-Isolation CPW MEMS Shunt Switches (two parts: modeling and design)," *IEEE Trans. Microwave Theory and Techniques,* vol. 48, no. 6, pp. 1045-1056, Jun. 2000.
[126] R. D. Streeter, C. A. Charles, R. Wood, and R. Mahadevan, "VHF High-Power Tunable RF Bandpass Filter Using Microelectromechanical (MEM) Microrelays," *Int. J. RF Microwave Comput Aided Eng,* vol. 11, no. 5, pp. 261-275, Sept. 2001.
[127] H.-C. Lee, J.-Y. Park, and J.-U Bu, "Piezoelctrically Actuated RF MEMS DC Contact Switches With Low Voltage Operation," *IEEE Microwave and Wireless Component Letters,* vol. 15, no. 4, pp. 202-204, April 2005.
[128] M. Ruan, J. Shen, and C. B. Wheeler, "Latching Micromagnetic Relays," *IEEE J. Microelectromech. Systems,* vol. 10, no. 4 , pp. 511-517, Dec. 2001.
[129] J. Lampen, S. Majumder, R. Morrison, A. Chaudrey, and J. Maciel, "A Wafer-Capped, High-Lifetime Ohmic MEMS RF Switch," *Int J RF Microwave Comput Aided Eng,* vol.14, no. 4, pp. 338-344, June 2004.
[130] C. D. Patel and G. R. Rebeiz, "RF MEMS Metal-Contact Switches with mN-Contact and Restoring Forces and Low Process Sensitivity", *IEEE Trans. Microwave Theory Tech.,* vol. 59, no. 5, pp. 1230-1237, May 2011.
[131] D. Hyman, J. Lam, B. Warneke, A. Schmitz, T. Y. Hsu, J. Brown, J. Schaffner, A. Walston, R. Y. Loo, M. Mehregany, and J. Lee, "Surface Micromachined RF MEMs Switches on GaAs Substrates," *Int J RF Microwave Comput Aided Eng,* vol. 9, no. 4, pp. 348-361, 1999.
[132] Q. Ma, Q. Tran, T.-K. A. Chou, J. Heck, H. Bar, R. Kant, and V. Rao, "Metal Contact Reliability of RF MEMS Switches," *Proc. SPIE,* vol. 6463, pp. 646305, Jan. 2007.

[133] R. E. Mihailovich, M. Kim, J. B. Hacker, E. A. Sovero, J. Studer, J. A. Higgins, and J. F. DeNatale, "MEMS Relay for Reconfigurable RF Circuits," *IEEE Microwave Compon. Lett,* vol. 11, no. 2, pp. 53-55, Feb. 2001.
[134] T. Seki, Y. Uno, K. Narise, K. Inoue, S. Sato, F. Sato, K. Imanaka, S. Sugiyama, "Development of a Large-Force Low-Loss Metal-Contact RF MEMS Switch," *Sens. Actuators A. Phys,* vol. 132, no. 2, pp. 683-688, Nov. 2006.
[135] C. W. Dyck, T. A. Plut, C. D. Nordquist, P. S. Finnegan, F. Austin, I. Reines, and C. Goldsmith, "Fabrication and Characterization of Ohmic Contacting RF MEMS Switches," *Proc. SPIE,* vol. 5344, pp. 222-229, Jan. 2004.
[136] C. D. Patel and G. M. Rebeiz, "A High-Reliability High-Linearity High-Power RF MEMS Metal-Contact Switch for DC-40-GHz Applications, " *IEEE Trans. Microwave Theory Tech.,* vol. 60, no. 10, pp. 3096-4012, Oct. 2012.
[137] B. F. Toler, R. A. Coutu Jr, and J. W. McBride, "A Review of Micro-Contact Physics for Microelectromechanical Systems (MEMS) Metal Contact Switches," *J. Micromechanics Microengineering,* vol. 23, no. 10, pp. 103001, Oct. 2013.
[138] P. G. Slade, ed., *Electrical Contacts,* CRC Press, 1999.
[139] H. Eid, N. Joshi, N. E. McGruer, and G. G. Adams, "Adhesion of a Layered Elastic-Plastic Microsphere With a Rigid Flat Surface," *J. Tribology,* vol. 133, 031406-1, Jul. 2011.
[140] G. M. Rebeiz, C. D. Patel, S. K. Han, C.-H. Ko, and K. M. J. Ho, "The Search for a Reliable MEMS Switch," *IEEE Microwave Magzine,* vol. 14, no. 1, pp. 57-67, Jan. 2013.
[141] http://www.omron.com/ecb/products/sensor/51/2smes-01.html (accessed Nov 25, 2013)
[142] D. M. Tanner, "MEMS Reliability: Where Are We Now?, *Microelectronics Reliability,* vol. 49, pp. 937-940, 2009.
[143] H.-H. Hsu, M. Koslowski, and D. Peroulis, "An Experimental and Theoretical Investigation of Creep in Ultrafine Crystalline Nickel RF-MEMS Devices," *IEEE Trans. Microwave Theory Tech.*, vol. 59, no. 10, pp. 2655-2664, Oct. 2011.
[144] C. Goldsmith, J. Maciel, and J. McKillop, "Demonstrating Reliability," *IEEE Microwave Mag.,* vol. 8, no. 6, pp. 56-60, Dec. 2007.
[145] W. M van Spengen, "Capacitive RF MEMS Switch Dielectric Charging and Reliability: A Critical Review with Recommendations," *J. Micromech. Microeng.,* vol. 22, no. 7, pp. 074001, July 2012.
[146] C. Goldsmith, J. Ehmke, A. Malczewski, B. Pillans, S. Eshelman, Z. Yao, J. Brank, and M. Eberly, "Lifetime Characterization of Capacitive RF MEMS Switches," *IEEE MTT-S Int. Microwave Symp. Dig.,* pp. 227-230, June 2001.
[147] G. Ding, D. Molinero, W. Wang, C. Palego, S. Halder, J. C. M. Hwang, and C. L. Goldsmith, "Intelligent Bipolar Control of MEMS Capacitive Switches," *IEEE Trans. Microwave Theory Tech.*, vol. 61, no. 1, pp. 464-471, Jan. 2013.
[148] I. Reines, B. Pillans, and G. M. Rebeiz, "Thin-Film Aluminum RF MEMS Switched Capacitors With Stress Tolerance and Temperature Stability," *J. Microelectromechanical Syst.,* vol. 20, no. 1, pp. 193-203, Feb. 2011.
[149] S. Gong, T. Reck, and N. S. Barker, "A Temperature Insensitive DC-Contact RF-MEMS Switch," *Proc. European Microwave Conference,* pp. 1114-1117, 2010.
[150] S. Gong, H. Shen, and N. Scott Barker, "Study of Broadband Cryogenic DC-Contact RF MEMS Switches," *IEEE Trans. Microwave Theory Tech.*, vol. 57, no. 12, pp. 3442-3449, Dec. 2009.
[151] J. R. Reid, R. T. Webster, and L. A. Starman, "Noncontact Measurement of Charge Induced Voltage Shift in Capacitive MEM-Switches, *IEEE Microwave Comp. Lett.,* vol. 13, no. 9, pp. 367-369, Sept. 2003.
[152] J. C. M. Hwang, C. L. Goldsmith, "Reliability of MEMS Capacitive Switches," *Proc. IEEE Intl. Wireless Symp.,* pp. 6616841, Apr. 2013.
[153] S. Kim, S. Cunningham, J. Mckillop, and A. Morris, "Characterization of Dielectric Charging and Reliability in Capacitive RF MEMS Switches," *IEEE MTT-S Int. Microwave Symp. Dig.,* pp. 6B.4, June 2013.
[154] D. A. Czaplewski, C. D. Nordquist, C. W. Dyck, G. A. Patrizi, G. M. Kraus, and W. D. Cowan, "Lifetime Limitations of Ohmic, Contacting RF MEMS Switches with Au, Pt, and Ir Contact Materials Due to Accumulation of Friction Polymer on the Contacts," *J. Micromech. Microeng.*, vol. 22, no. 10, pp. 105005, Oct. 2012.
[155] R. P. Hennessy, A. Basu, G. G. Adams, and N. E. McGruer, "Hot-Switched Lifetime and Damage Characteristics of MEMS Switch Contacts, *J. Micromech. Microeng.*, vol. 23, no. 5, pp. 055003, May 2013.
[156] D. A. Czaplewski, C. W. Dyck, H. Sumali, J. E. Massad, J. D. Kuppers, I. Reines, W. D. Cowan, and C. P. Tigges, "A Soft-Landing Waveform for Actuation of a Single-Pole Single-Throw Ohmic RF MEMS Switch," *J. Microelectromech Syst.,* vol. 15, no. 6, pp. 1586-1594, Dec. 2006.

[157] L. Michalas, A. Garg, A. Venkattraman, M. Koutsoureli, A. Alexeenko, D. Peroulis, and G. Papaioannou, "A Study of Field Emission Process in Electrostatically Actuated MEMS Switches," *Microelectron. Reliab.,* vol. 52, no. 9-10, pp. 2267-2271, Sep-Oct 2012.

[158] D. B. Go and D. A. Pohlman, "A Mathematical Model of the Modified Paschen's Curve for Breakdown in Microscale Gaps," *J. Appl. Phys.,* vol. 107, pp. 103303, May 2010.

[159] A. P. De Silva and H. G. Hughes, "The Package Integration of RF-MEMS Switch and Control IC for Wireless Applications," *IEEE Trans. Adv. Pkg.,* vol.26, no. 3, pp. 255-260, Aug. 2003.

[160] D. J. Hyman and R. Kuroda, "Flip-Chip Assembly of RF MEMS For Microwave Hybrid Circuitry," *Proc. Tech. Conf. Exhib. Integr. Packag. Elec. Syst. Adv. Elec. Packag.,* pp. 2053-2056, July 2005.

[161] K. Entesari and G. M. Rebeiz, "A Low-Loss Microstrip Surface-Mount K-Band Package, *Proc. 36th European Microwave Conf.,* pp. 1763-1766, Sept. 2006.

[162] B.-W. Min, G. M. Rebeiz, "A Low-loss Silicon-on-Silicon DC-110 GHZ Resonance-Free Package," *IEEE Trans. Microwave Theory Tech.*, vol. 54, no. 2, pp. 710-716, Feb. 2006.

[163] M. D. Henry, D. K. Greth, J. Nguyen, C. D. Nordquist, R. Shul, M. Wiwi, T. A. Plut, and R. H. Olsson III, "Hermetic Wafer-Level Packaging for RF MEMS: Effects on Resonator Performance," *Proc. Electron. Compon. Technol. Conf.,* pp. 362-369, Jun. 2012.

[164] K. D. Leedy, R. E. Strawser, R. Cortez, and J. L. Ebel, "Thin-Film Encapsulated RF MEMS Switches," *J. Microelectromech Syst.,* vol. 16, no. 2, pp. 304-309, Apr. 2007.

[165] A. K. Stamper, C. V. Jahnes, S. R. Dupuis, A. Gupta, Z.-X. He, R. T. Herrin, S. E. Luce, J. Maling, D. R. Miga, W. J. Murphy, E. J. White, S. J. Cunningham, D. R. DeReus, I. Vitomirov, and A. S. Morris, "Planar MEMS RF Capacitor Integration," *Int. Solid-State Sensors, Actuators, and Microsystems Conference, TRANSDUCERS'11,* pp. 1803-1806, Jun. 2011.

[166] D. I. Forehand and C. L. Goldsmith, "Wafer Level Micropackaging for RF MEMS Switches," *Proc. Tech. Conf. Exhib. Integr. Packag. Elec. Syst. Adv. Elec. Packag.,* pp. 2047-2051, July 2005.

[167] A. S. Morris III, V. Steel, "Integrated Tunable Systems for Scalable 4G Radios," *IEEE MTT-S Intl. Microwave Symp. Digest,* June 2013.

[168] P. A. Tornatta, R. Gaddi, "Aperture Tuned Antennas for 3G-4G Applications Using MEMS Digitial Variable Capacitor," *IEEE MTT-S Intl. Microwave Symp. Digest,* June 2013.

[169] M. Lutz, "Revolutionary Embedded Silicon MEMS Resonators Obsoletes Bulky External 32 kHz Crystals in the System," *DesignCon : Where ChipHeads Connect,* pp. 299-332, Jan. 2012.

[170] J. H. Kuypers, G. Zolfagharkhani, A. Gaidarzhy, F. Thalmayr, A. Sparks, D. M. Chen, R. Rebel, B. Newman, M. Asmani, D. Badillo, and K. J. Schoepf, "Wafer-Level Chip Scale MEMS Oscillator for Wireless Applications," *Proc. IEEE Int. Freq. Control Symp.,* pp. 340-344, May 2012.

[171] http://www.idt.com/products/clocks-timing/crystals-oscillators-and-frequency-control-products-fcp/mems-oscillators (accessed Nov 28 2013).

[172] R. R. Mansour, "RF MEMS-CMOS Device Integration: An Overview of the Potential for RF Researchers," *IEEE Microwave Mag.,* vol. 14, no. 1, pp. 39-56, Jan. 2013.

[173] J. Reinke, G. K. Fedder, and T. Mukherjee, "CMOS-MEMS 3-bit Digital Capacitors With Tuning Ratios Greater Than 60:1," *IEEE Trans. Microwave Theory Tech.,* vol. 59, no. 5, pp. 1238-1248, May 2011.

[174] K. E. Wojciechowski, R. H. Olsson, T. A. Hill, M. R. Tuck and E. Roherty-Osmun, "Single-Chip Precision Oscillators Based on Multi-Frequency, High-Q Aluminum Nitride MEMS Resonators," *IEEE International Solid-State Sensors, Actuators and Microsystems Conference*, pp. 2126-2130, June, 2009.

[175] J. B. Hacker, M. Kim, R. E. Mihailovich, and J. F. DeNatale, "Monolithic GaAs PHEMT MMICs Integrated with RF MEMS Switches," *Compound Semiconductor Integrated Circuit Symp. Digest,* pp. 229-232, Oct. 2004

[176] J. Costa, T. Ivanov, M. Carroll, J. Hammond, E. Glass, J. Jorgenson, D. Denning, D. Kerr, J. Reed, Q. Ren, S. Crist, T. Mercier, S. Kim, T. Mckay, P. Gorisse, and J. Gering, "Silicon RFCMOS SOI Technology with Above-IC MEMS Integration for Front End Wireless Applications," *Proc. IEEE Bipolar/BiCMOS Circuit Tech. Mtg.,* pp. 204-207, Oct. 2008.

[177] O. Auciello, A. V. Sumant, C. Goldsmith, S. O'Brien, S. Sampath, C. Gudeman, W. Wang, J. C. M. Hwang, J. Swonger, J. A. Carlisle, S. Balachandran, and D. C. Mancini, "Fundamentals and Technology for Monolithically

Integrated RF MEMS Switches with Ultra-Nanocrystalline Diamond Dielectric/CMOS Devices," *Proc. SPIE Micro- and Nanotechnology Sensors, Systems, and Apps II,* vol. 7679, p. 76791, 2010.

[178] A. Tazzoli, M. Rinaldi, C. Zuo, N. Sinha, J. Van Der Spiegel, and G. Piazza, "Aluminum Nitride Reconfigurable RF-MEMS Front-Ends," *Proc. Int. Conf. ASIC,* pp. 1046-1049, Oct. 2011.

[179] C. D. Nordquist, R H. Olsson III, S. M. Scott, D. W. Branch, T. Pluym, and V. Yarberry, "On/Off Micro-electromechanical Switching of AlN Piezoelectric Resonators," *Proc. IEEE MTT-S International Microwave Symposium*, June 2013.

[180] R. Stefanini, M. Chatras, P. Blondy, and G. M. Rebeiz, "Miniature MEMS Switches for RF Applications," *J. Microelectromech Syst.,* vol. 20, no. 6, pp. 1324-1325, Dec. 2011.

[181] B. Lakshiminarayanan, D. Mercier, and G. M. Rebeiz, "High Reliability Miniature RF-MEMS Switched Capacitors," *IEEE Trans. Microwave Theory Tech.,* vol. 56, no. 4, pp. 971-981, Apr. 2008.

[182] S. Gong and G. Piazza, "Multi-Frequency Wideband RF Filters Using High Electromechanical Coupling Laterally Virbrating Lithium Niobate MEMS Resonators," *Proc. IEEE Int. Conf. Micro Electro Mech. Syst. MEMS,* pp. 785-788, Jan. 2013.

[183] T. L. Naing, T. Beyazoglu, L. Wu, M. Akgul, Z. Ren, R. O. Rocheleau, C. T.-C. Nguyen, "2.97-GHz CVD Diamond Ring Resonator with Q>40,000," *Proc. IEEE Int. Freq. Control Symp.,* pp. 565-570, May 2012.

[184] J. J. Yao, "RF MEMS From a Device Perspective," *J. Micromech. Microengineering,* vol. 10, no. 4, pp. R9-R38, Dec. 2000.

[185] J. L. Ebel, D. J. Hyman, and H. S. Newman, "RF MEMS Testing – Beyond the S-parameters," *IEEE Microwave Mag.,* vol. 8, no. 6, pp. 76-88, Dec. 2007.

	Material	Comments
Piezoelectric Materials		
	Aluminum Nitride (AlN)[12,13,19,20,22]	Most Commonly Used Piezoelectric Material, Doping Can be Used to Increase K^2, Can be Deposited as a Thin Film
	Zinc Oxide (ZnO)[10,14.32]	Similar Properties to AlN Except Higher Dielectric Losses, Can be Deposited as a Thin Film
	Lead Zirconate Titanate (PZT)[14,15,32]	Very High Piezoelectric and Dielectric Constants, Higher Coupling Coefficient than AlN, High Acoustic Damping, Can be Deposited as a Thin Film
	Lithium Niobate ($LiNbO_3$)[8,38,39,40,41]	High K^2 and high Q, Requires Single Crystal for High Performance
	Quartz[5,17]	Low Temperature Coefficient of Frequency (TCF) and Low Acoustic Damping, Requires Single Crystal
Capacitive Resonator Materials	Single Crystal Silicon (Si)[54,55,56,57]	High-Q Material Commonly Used in Bulk Micromachining of Resonators
	Poly Crystalline Si (Poly Si)[44,45,48]	High-Q Material Used in Surface Micromachining of Resonators
	Poly Crystalline Silicon Germanium (SiGe)[58,59]	Low Deposition Temperature Alternative to Poly Si for Post-CMOS Resonator Integration
	Polycrystalline Diamond (PCD)[42]	High Velocity and High-Q Material
Metals	Molybdenum (Mo)[16]	Commonly Used BAW Electrode Material
	Tungsten (W)[16]	BAW Electrode Material Used to Maximize K^2
	Aluminum (Al)[16]	Commonly Used in Lamb Wave Piezoelectric Resonators
Thermal Compensation Materials	Silicon Dioxide (SiO_2)[29]	Positive TCF Allows for Thermal Compensation of Negative TCF Materials
Electrostrictive Materials	Silicon Nitride (SiN)[35,52]	Historical Electrostrictive Material
	Hafnium Oxide (HfO_2)[53]	High Dielectric Constant Leads to Improved Transduction is Electrostrictive Devices

Table 1

	Electrostatic	Thermal	Piezoelectric	Electromagnetic
Force Scaling	AV^2d^{-1}	$I^2LW^{-1}t^{-1}$	AVd^{-1}	ILt (constant I)
Actuation Voltage	20 V – 200 V	3 V – 10 V	5 V – 200 V	12 V – 36 V
Static Actuation Current	<1 pA	10 mA – 100 mA	<1 pA	100 mA – 500 mA
Static Power	<1 nW	10 mW – 1 W	<1 nW	0 W (latching)
Dynamic Power	fCV^2	fCV^2	fCV^2	fCV^2
Response Time	1 -100 µsec	0.5 -10 msec	1 -100 µsec	0.5 -10 msec
Actuation Direction	In-plane or out-of-plane	Typically in-plane	Typically out-of-plane	Typically rotation
Other Comments		High temperature	Requires specialized piezoelectric materials	Requires specialized magnetic materials. Constant current assumed.

A = area I = current t = thickness
V = voltage W = width C = capacitance
d = distance L = length f = frequency

Table 2

Failure Mode	Cause	Mitigation Approaches
Adhesion	Dielectric Charging	• Reduce Actuation Voltage[144,146] • Bipolar Actuation Signals[144,157] • Eliminate dielectric materials in high-field regions[122,145] • Clean, low-moisture packaging[144,145]
	Surface adhesion	• Reduce contacting area[153] • Eliminate contamination[142,144,145]
Changing Up-State Capacitance	Fatigue in Spring	• Reduce stress in spring[143] • Brittle spring materials[142]
Changing Down-State Capacitance	Surface contamination or damage	• Clean packaging[142,144,145]

Table 3

Failure Mode	Cause	Mitigation Approaches
Adhesion	Dielectric Charging	• Reduce Actuation Voltage[145,157] • Eliminate dielectric materials in high-field regions[123,145]
	Contact fusion	• Use hard contact metals[137,156] • Reduce impact velocity[137,156] • Increase restoring force[130]
Open Contact	Contact destruction due to ESD or Hot Switching	• Ensure zero-voltage switching[155,157] • ESD handling precautions
Increased Resistance	Contact Contamination	• Clean packaging[142,145] • Low reactivity metals[154] • Increase contact force[130]
Increased Resistance	Contact Damage	• Hard contact metals[137,155] • Reduce impact velocity[156]
Increased Gate Current	Leakage current across actuation gap	• Sufficient acutation gap[157] • Reduce actuation voltage[157]
Actuation Voltage Shift	Change in spring constant due to fatigue	• Design low stress in spring[143] • Use brittle spring material[142]

Table 4

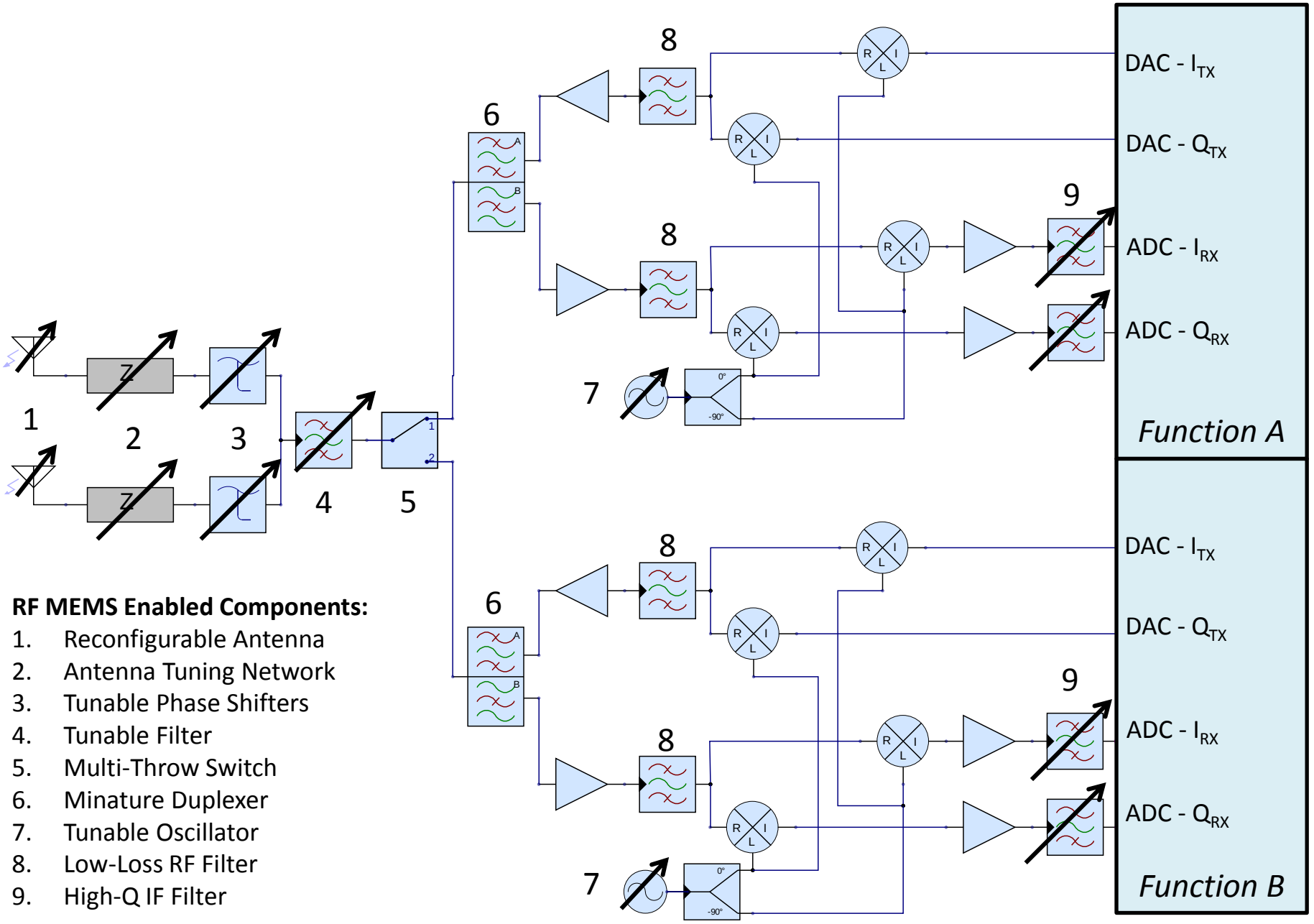

RF MEMS Enabled Components:

1. Reconfigurable Antenna
2. Antenna Tuning Network
3. Tunable Phase Shifters
4. Tunable Filter
5. Multi-Throw Switch
6. Minature Duplexer
7. Tunable Oscillator
8. Low-Loss RF Filter
9. High-Q IF Filter

Figure 1

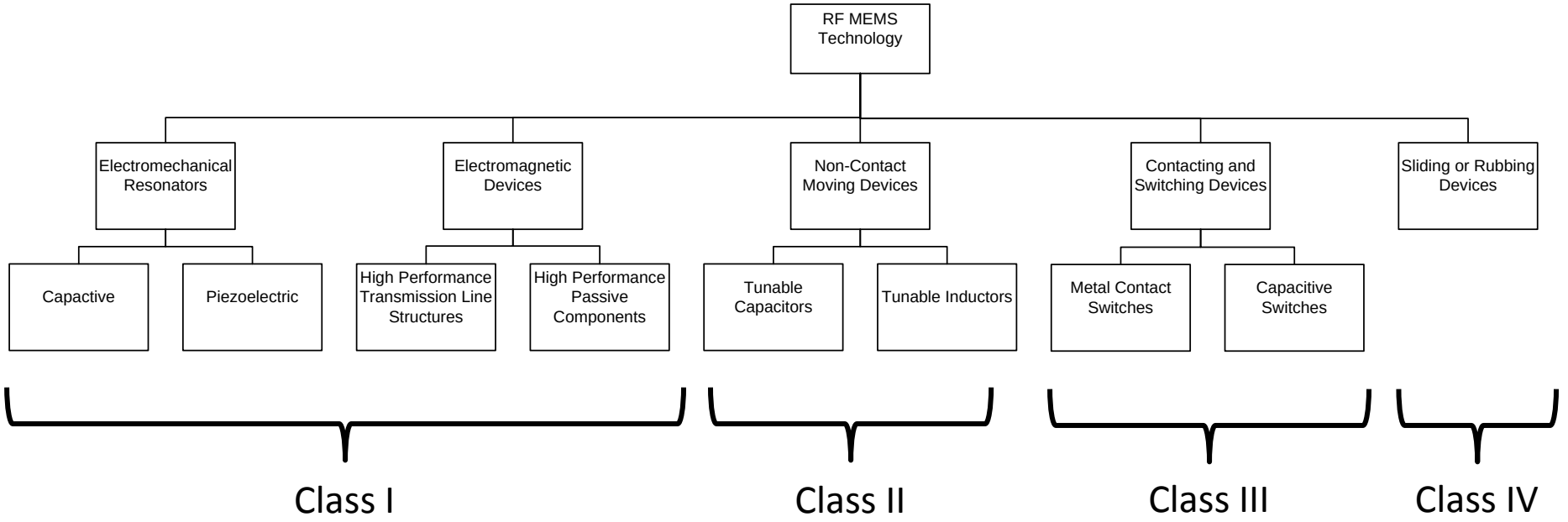
RF MEMS Technology
Electromechanical Resonators
Electromagnetic Devices
Non-Contact Moving Devices
Contacting and Switching Devices
Sliding or Rubbing Devices
Capactive
Piezoelectric
High Performance Transmission Line Structures
High Performance Passive Components
Tunable Capacitors
Tunable Inductors
Metal Contact Switches
Capacitive Switches
Class I
Class II
Class III
Class IV

Figure 2

1. Deposit sacrificial film onto a device substrate

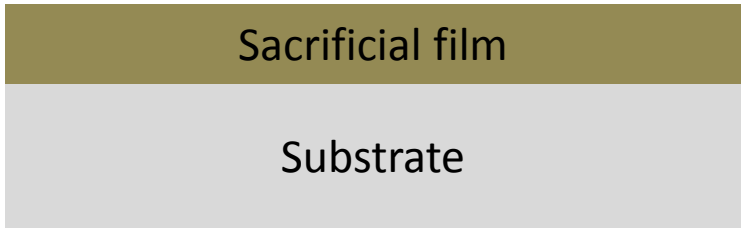

2. Etch openings into sacrificial layer to define device anchors.

3. Deposit and pattern device mechancial layer.

4. Remove sacrificial layer to create free-standing structure.

Figure 3

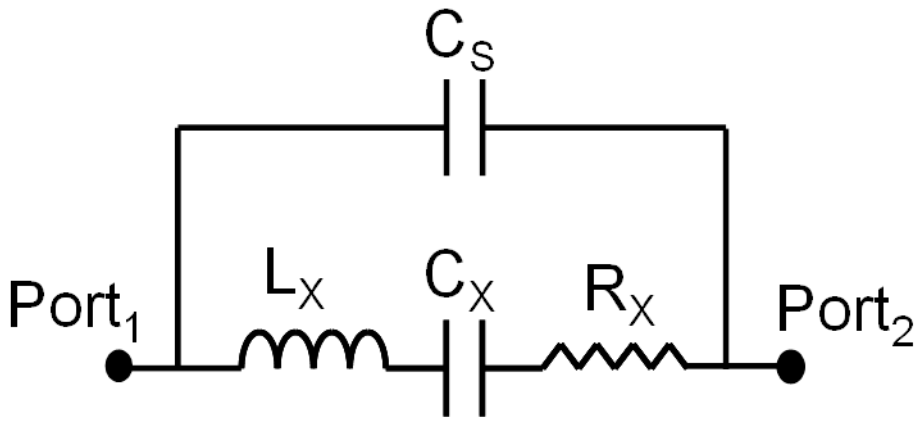

Figure 4

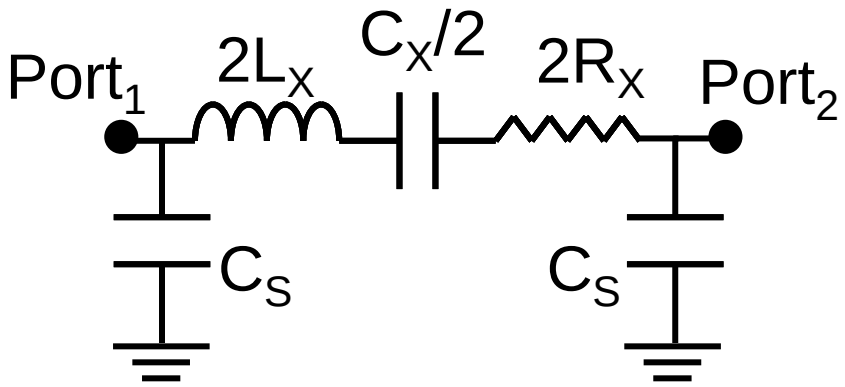

Figure 5

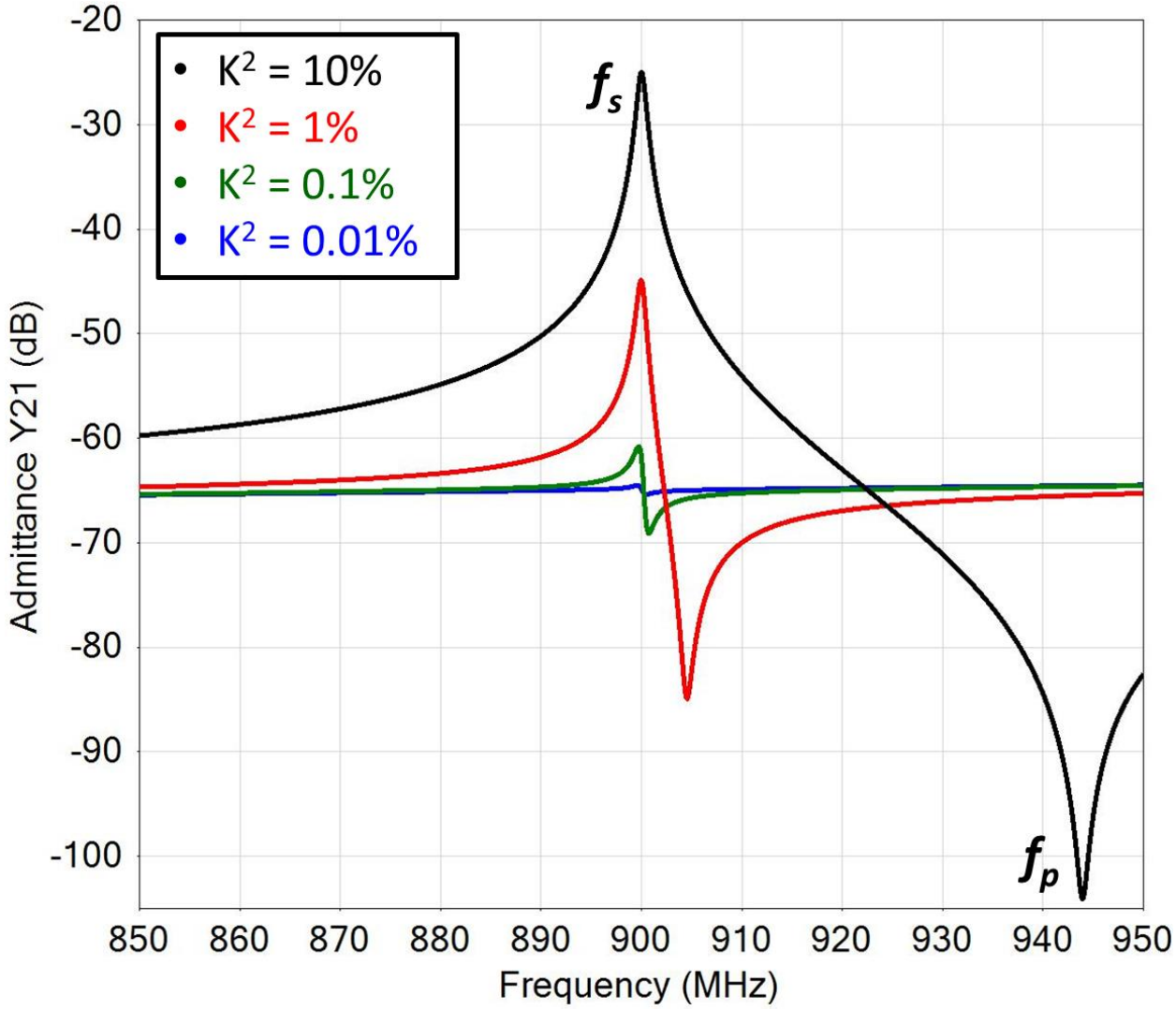
-20
-30
-40
-50
-60
-70
-80
-90
-100
Admittance Y21 (dB)
850
860
870
880
890
900
910
920
930
940
950
Frequency (MHz)
K² = 10%
K² = 1%
K² = 0.1%
K² = 0.01%
fs
fp

Figure 6

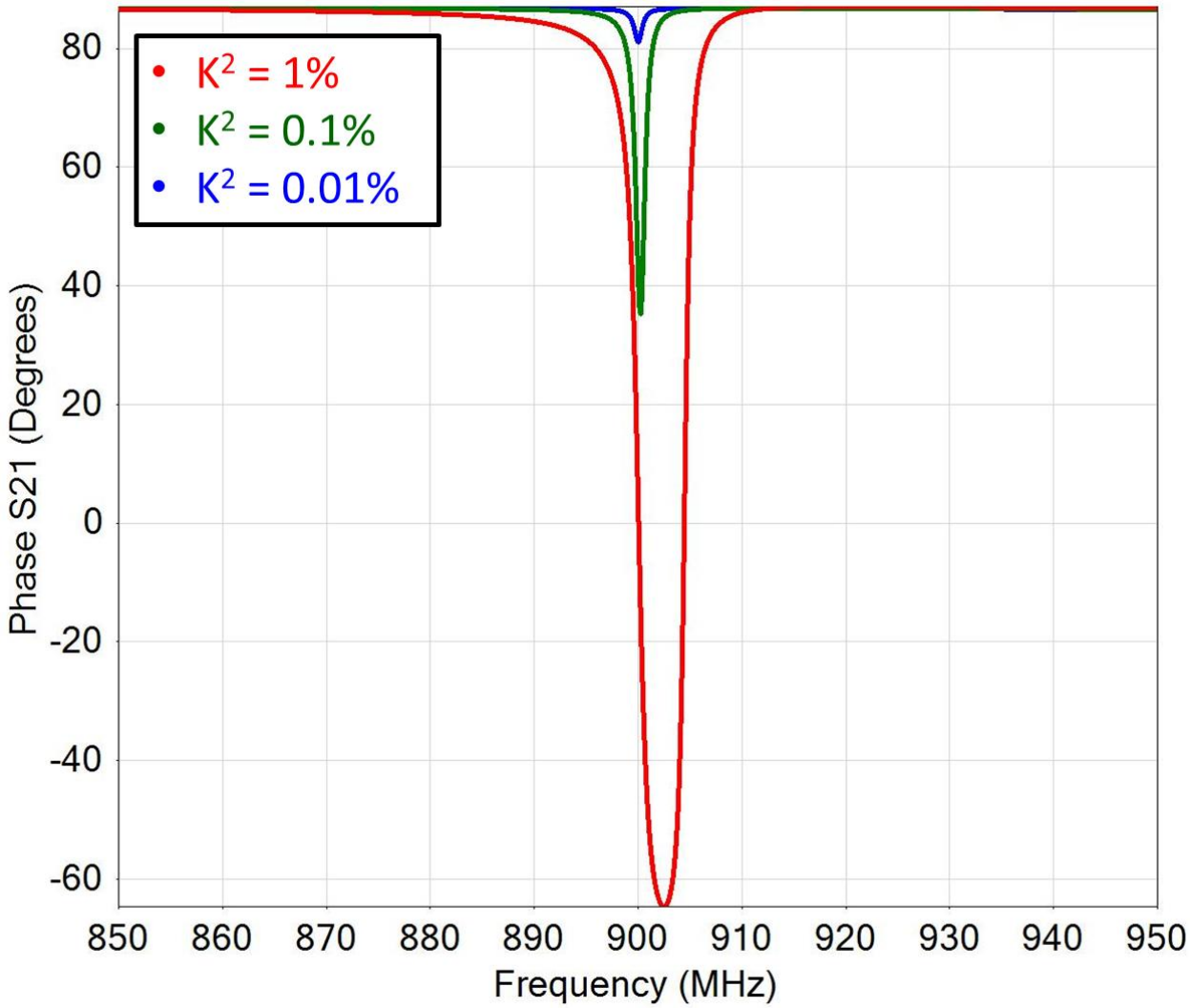
K² = 1%
K² = 0.1%
K² = 0.01%
Phase S21 (Degrees)
80
60
40
20
0
-20
-40
-60
850
860
870
880
890
900
910
920
930
940
950
Frequency (MHz)

Figure 7

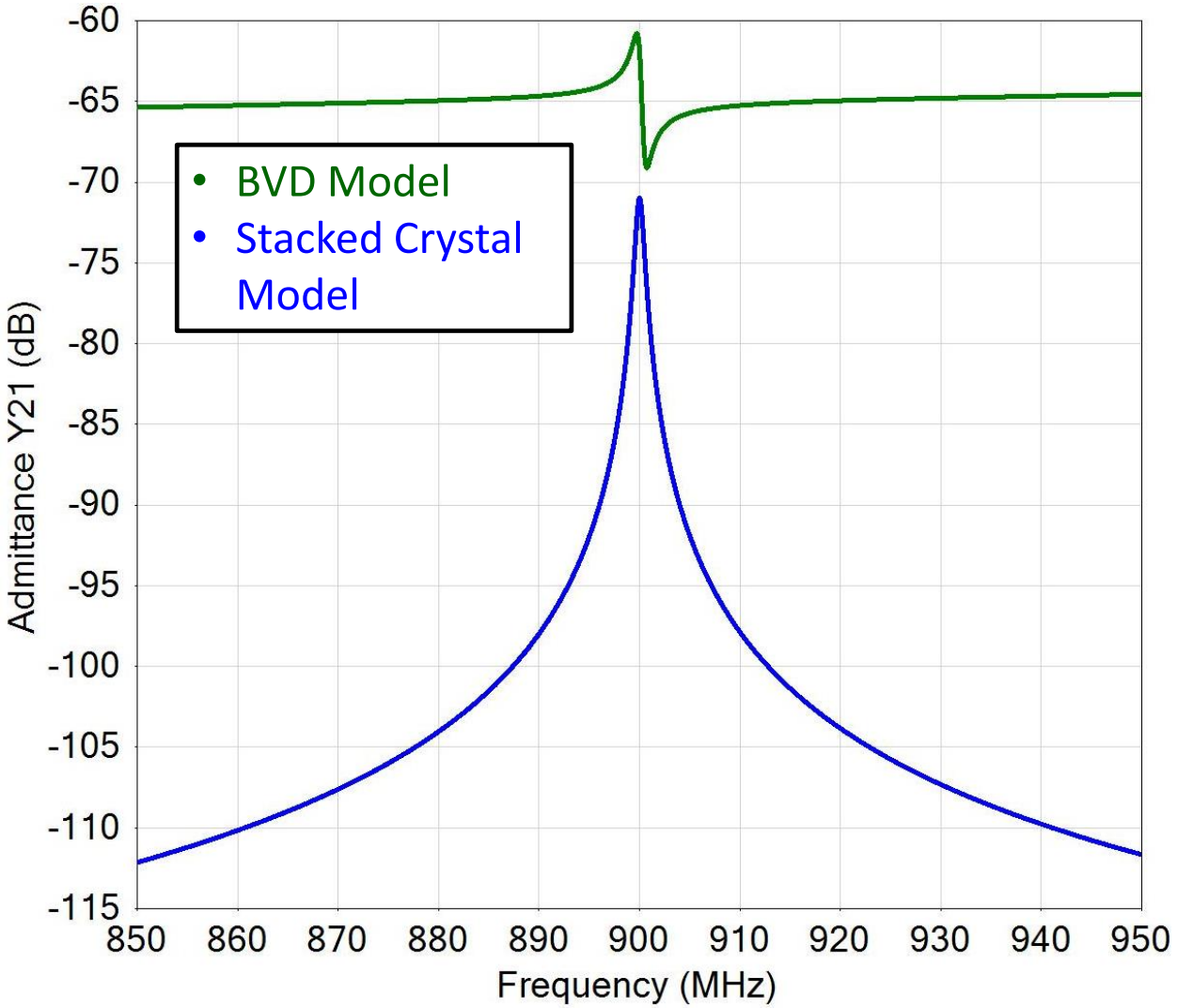
-60
-65
-70
-75
-80
-85
-90
-95
-100
-105
-110
-115
Admittance Y21 (dB)
850
860
870
880
890
900
910
920
930
940
950
Frequency (MHz)
• BVD Model
• Stacked Crystal Model

Figure 8

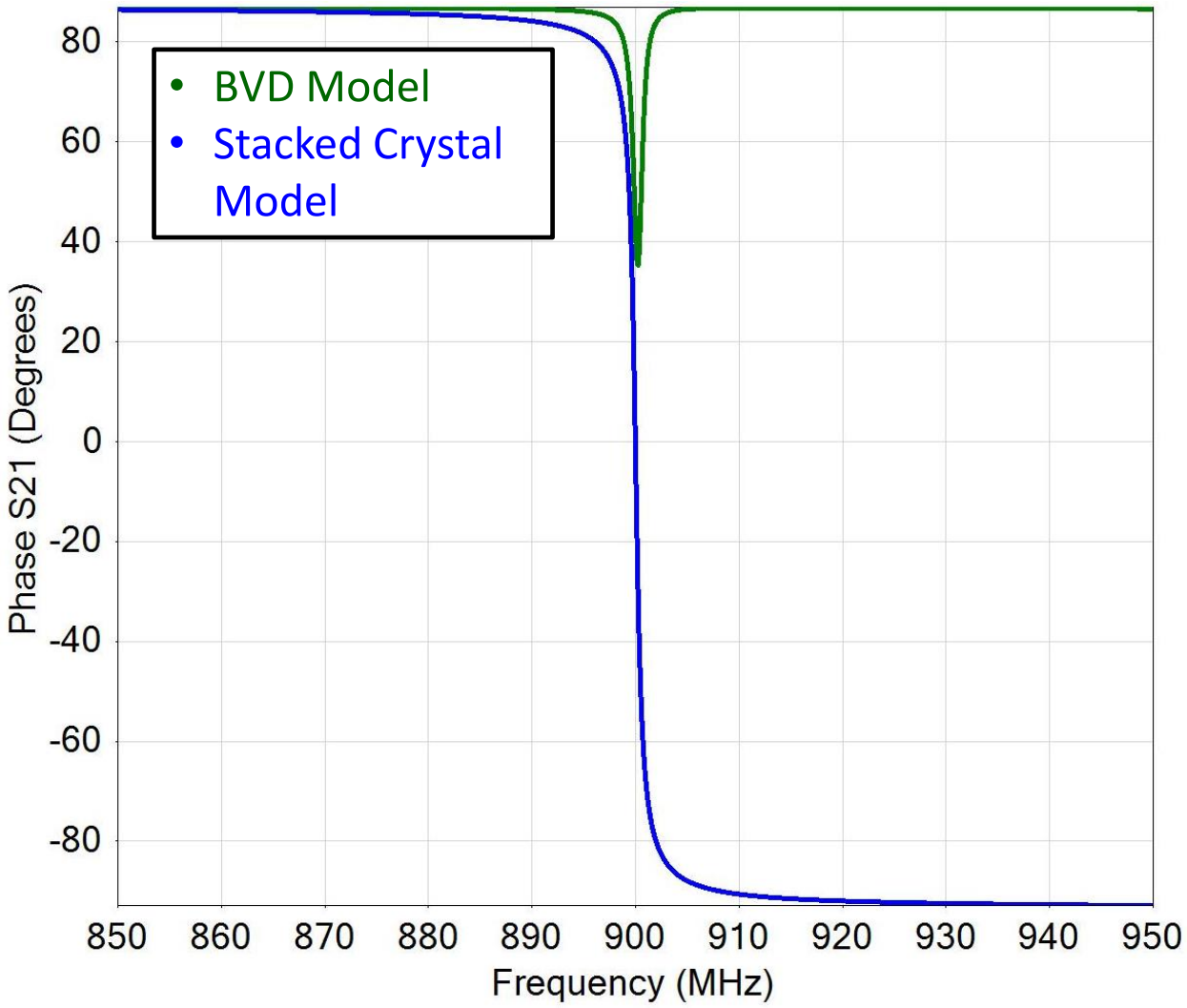
BVD Model
Stacked Crystal Model
Phase S21 (Degrees)
80
60
40
20
0
-20
-40
-60
-80
850
860
870
880
890
900
910
920
930
940
950
Frequency (MHz)

Figure 9

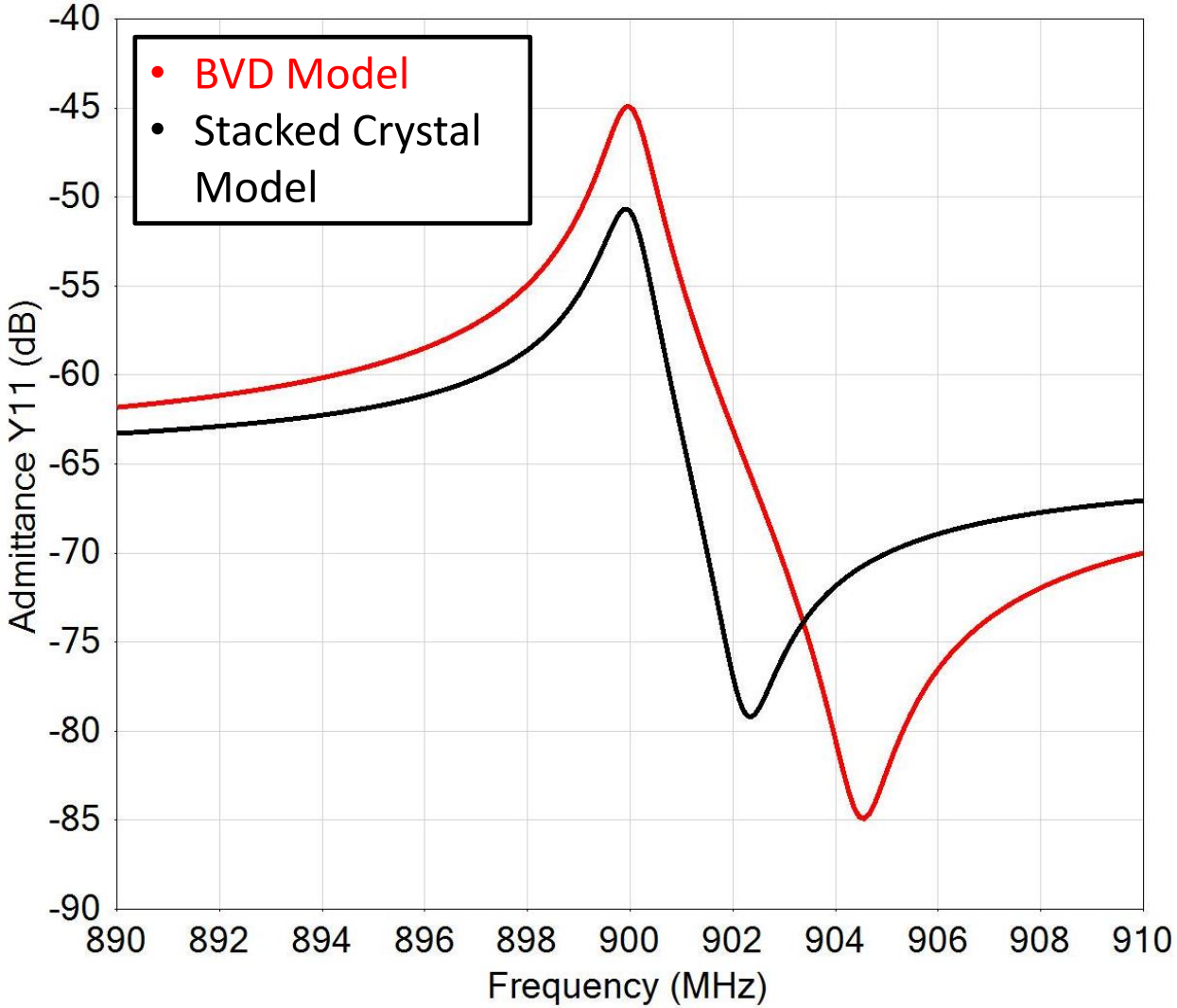
BVD Model
Stacked Crystal Model
Admittance Y11 (dB)
-40
-45
-50
-55
-60
-65
-70
-75
-80
-85
-90
890
892
894
896
898
900
902
904
906
908
910
Frequency (MHz)

Figure 10

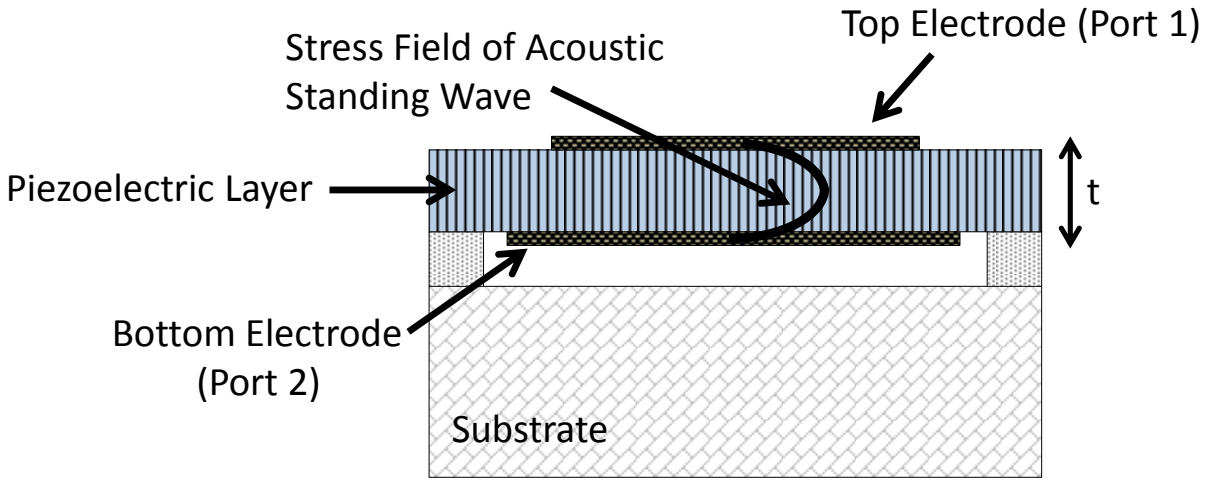
Top Electrode (Port 1)
Stress Field of Acoustic
Standing Wave
Piezoelectric Layer
t
Bottom Electrode
(Port 2)
Substrate

Figure 11

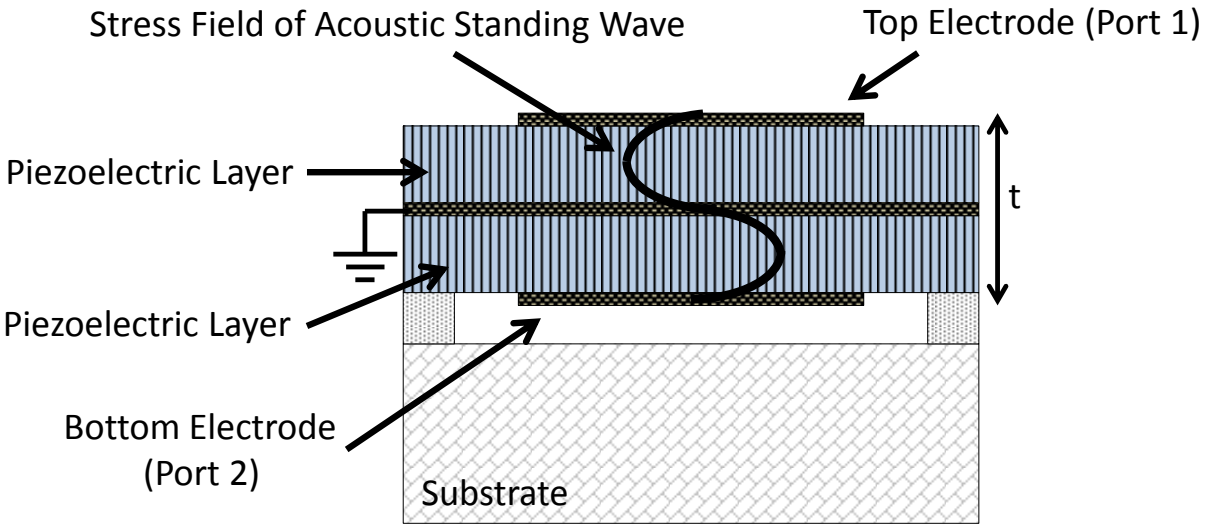
Stress Field of Acoustic Standing Wave
Top Electrode (Port 1)
Piezoelectric Layer
t
Piezoelectric Layer
Bottom Electrode
(Port 2)
Substrate

Figure 12

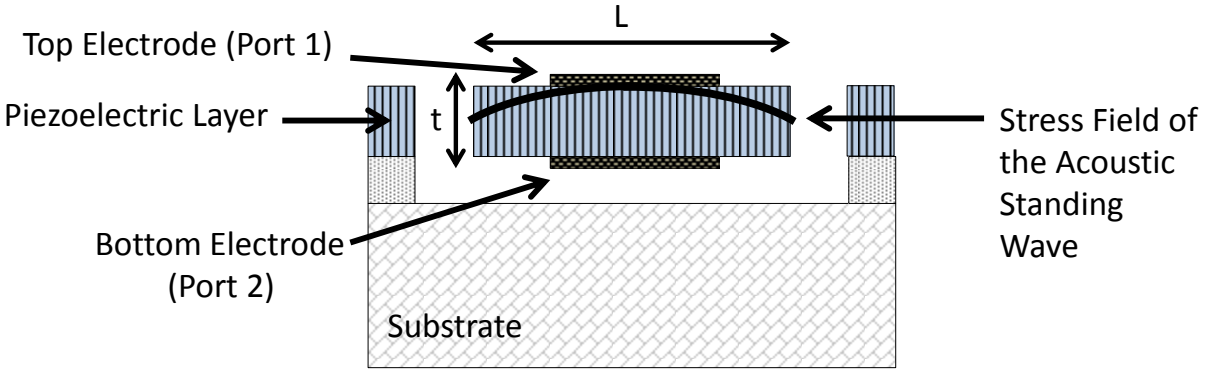
L
Top Electrode (Port 1)
Piezoelectric Layer
t
Stress Field of the Acoustic Standing Wave
Bottom Electrode (Port 2)
Substrate

Figure 13

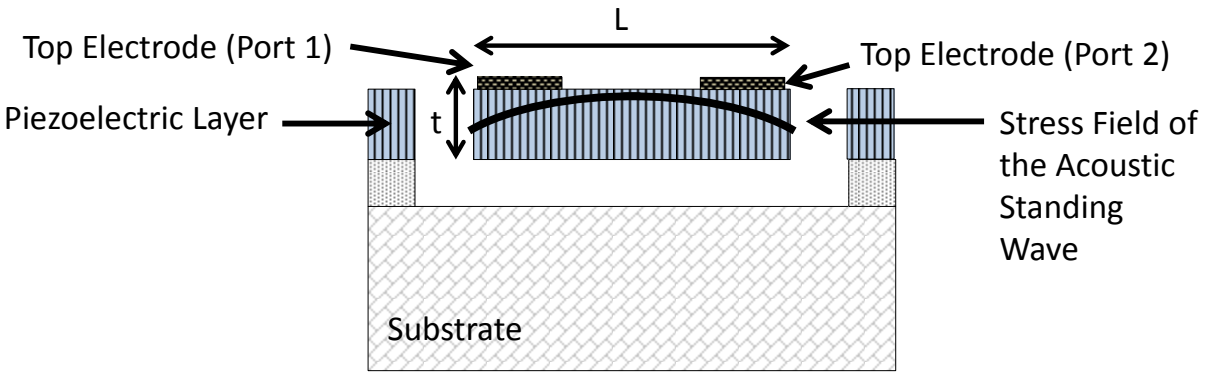
L
Top Electrode (Port 1)
Top Electrode (Port 2)
Piezoelectric Layer
t
Stress Field of the Acoustic Standing Wave
Substrate

Figure 14

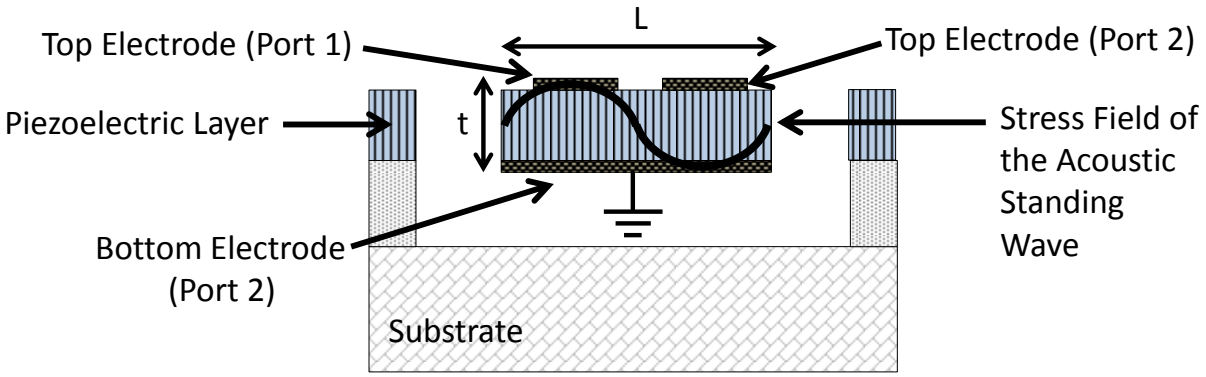
L
Top Electrode (Port 1)
Top Electrode (Port 2)
Piezoelectric Layer
t
Stress Field of the Acoustic Standing Wave
Bottom Electrode (Port 2)
Substrate

Figure 15

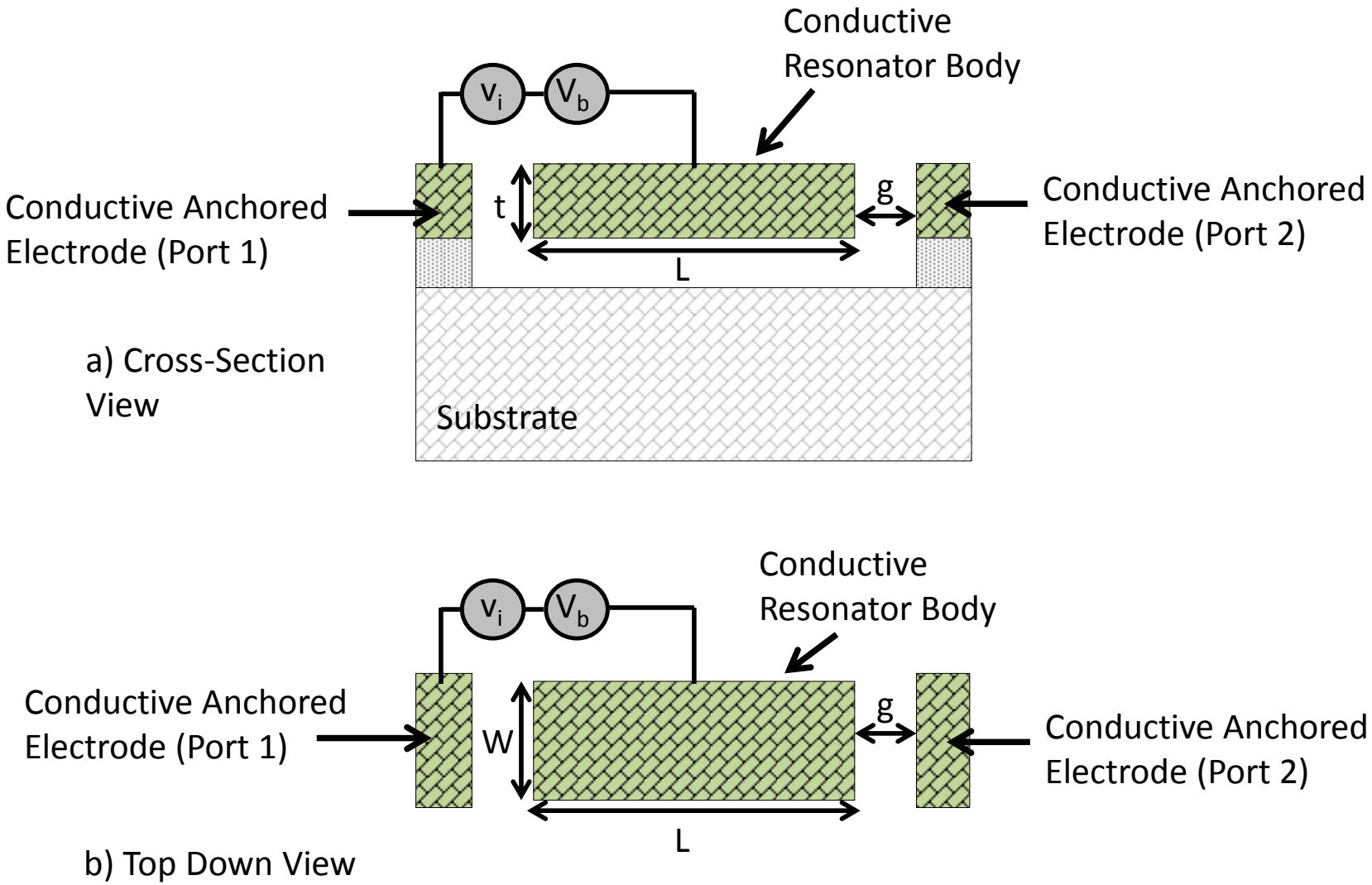
Conductive
Resonator Body
V_i
V_b
Conductive Anchored
Electrode (Port 1)
t
g
Conductive Anchored
Electrode (Port 2)
L
a) Cross-Section
View
Substrate
Conductive
Resonator Body
V_i
V_b
Conductive Anchored
Electrode (Port 1)
W
g
Conductive Anchored
Electrode (Port 2)
L
b) Top Down View

Figure 16

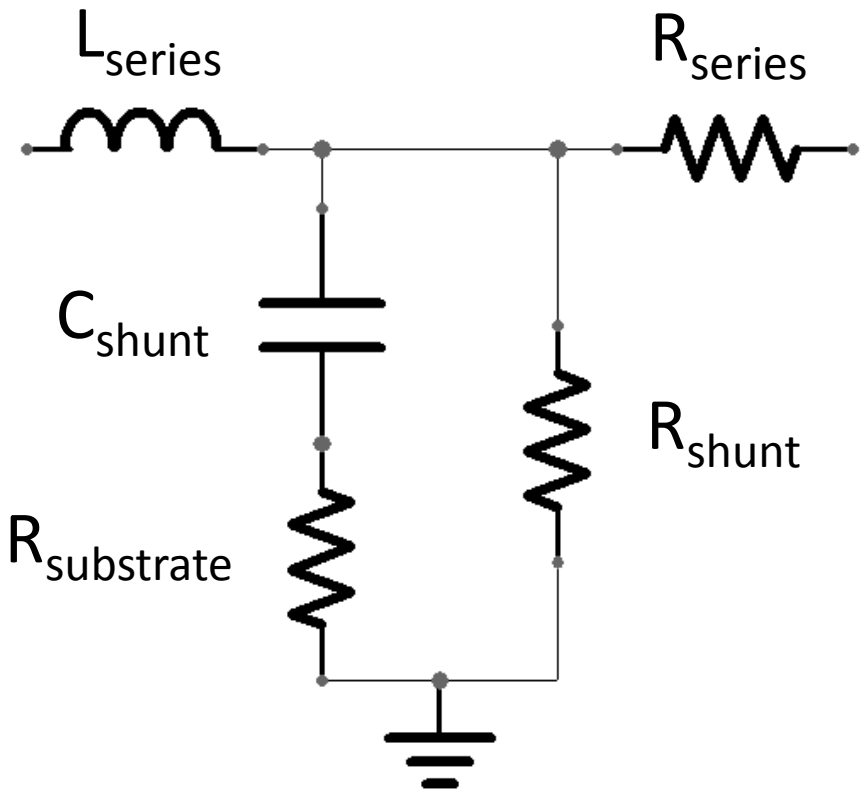

Figure 17

Cross-Sections of Commonly Used Transmission Lines

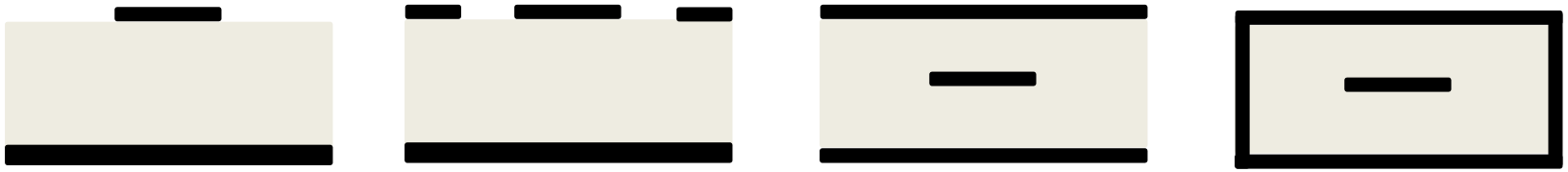

Microstrip | Grounded Coplanar | Stripline | Rectangular Coaxial

Examples of Micromachined Transmission Line Structures

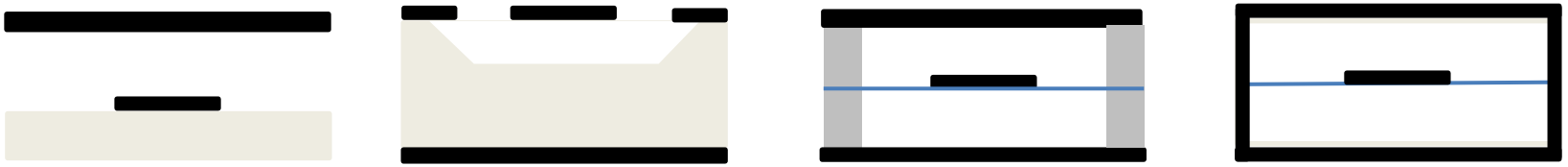

Inverted Microstrip | Coplanar with Silicon Removed | Stripline with Air Dielectric | Coaxial Line with Air Dielectric

Figure 18

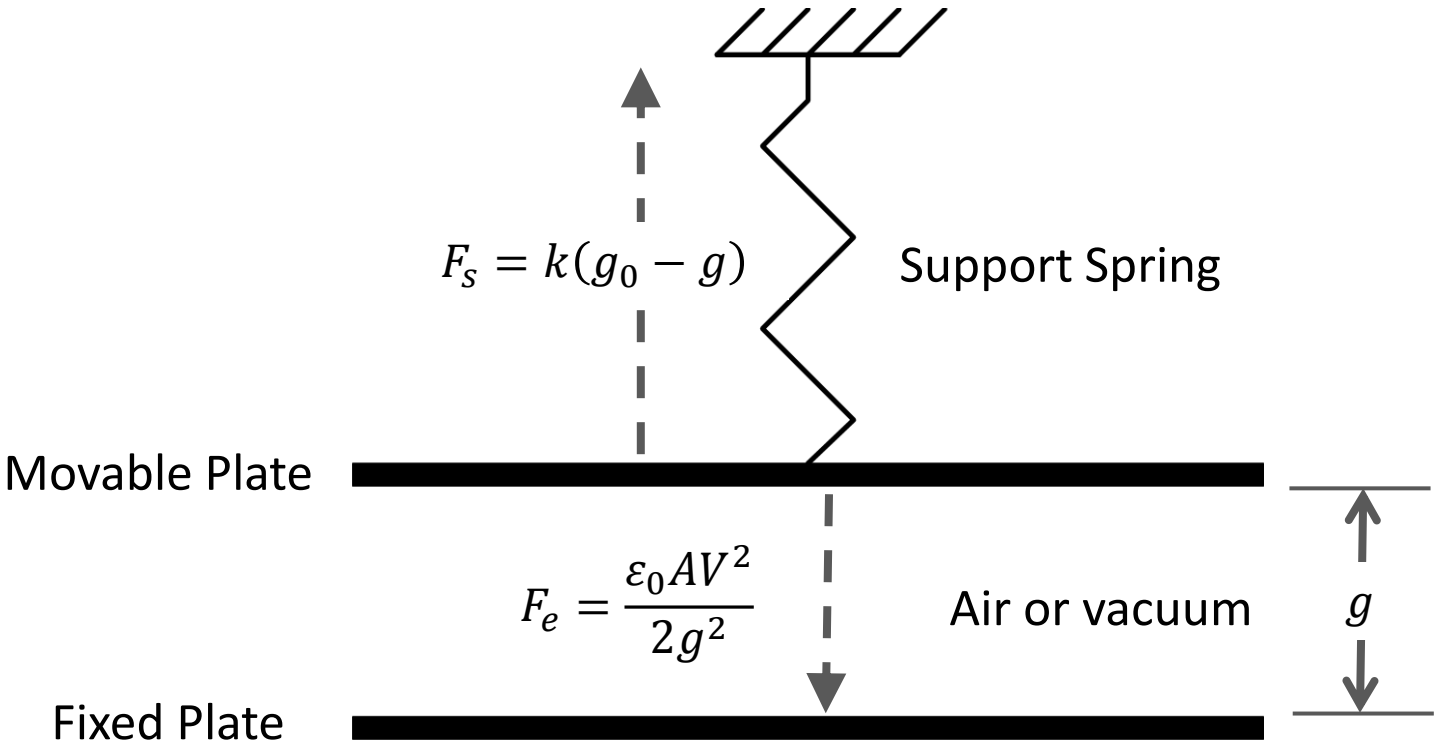

A: actuation electrode area
g: gap
F_s: spring force

V: voltage
g_o: intial gap
F_e: electrostatic force

Figure 19

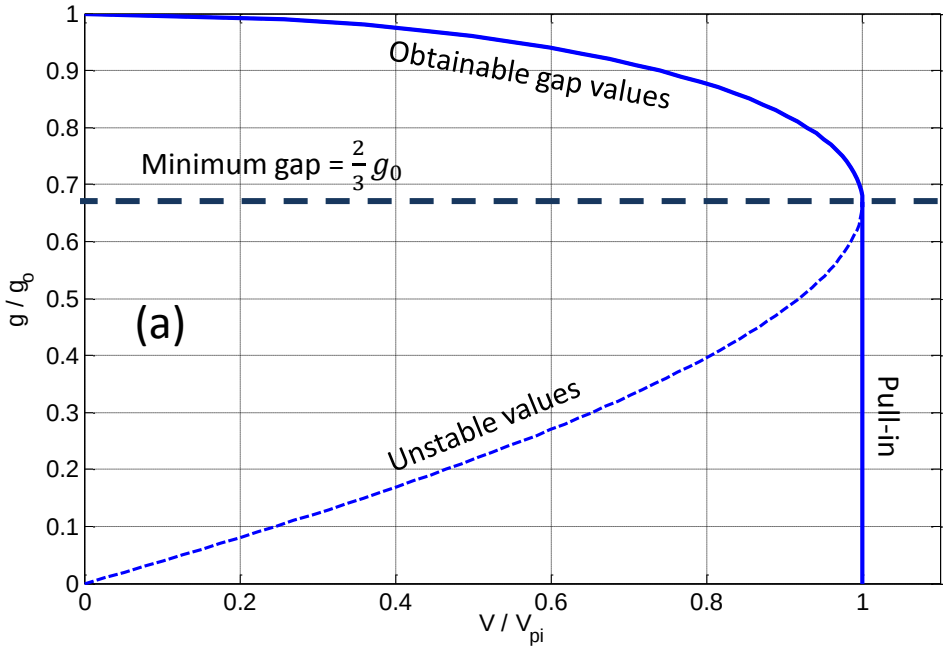
Obtainable gap values
Minimum gap = $\frac{2}{3}g_0$
(a)
Unstable values
Pull-in
g / g0
V / Vpi
0
0.1
0.2
0.3
0.4
0.5
0.6
0.7
0.8
0.9
1
0.2
0.4
0.6
0.8

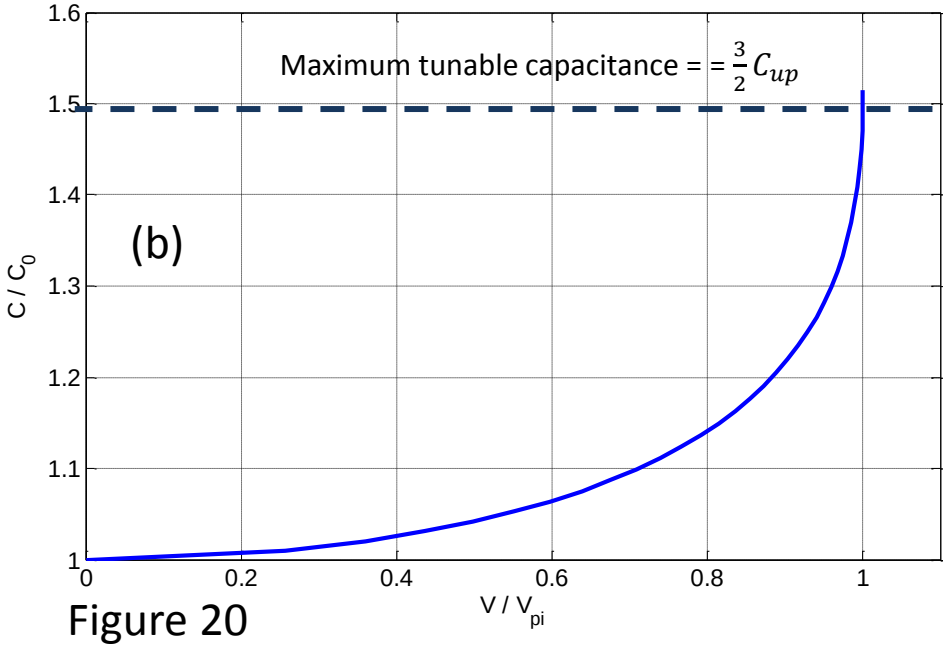
Maximum tunable capacitance = = $\frac{3}{2}C_{up}$
(b)
C / C0
V / Vpi
1
1.1
1.2
1.3
1.4
1.5
1.6
0.2
0.4
0.6
0.8

Figure 20

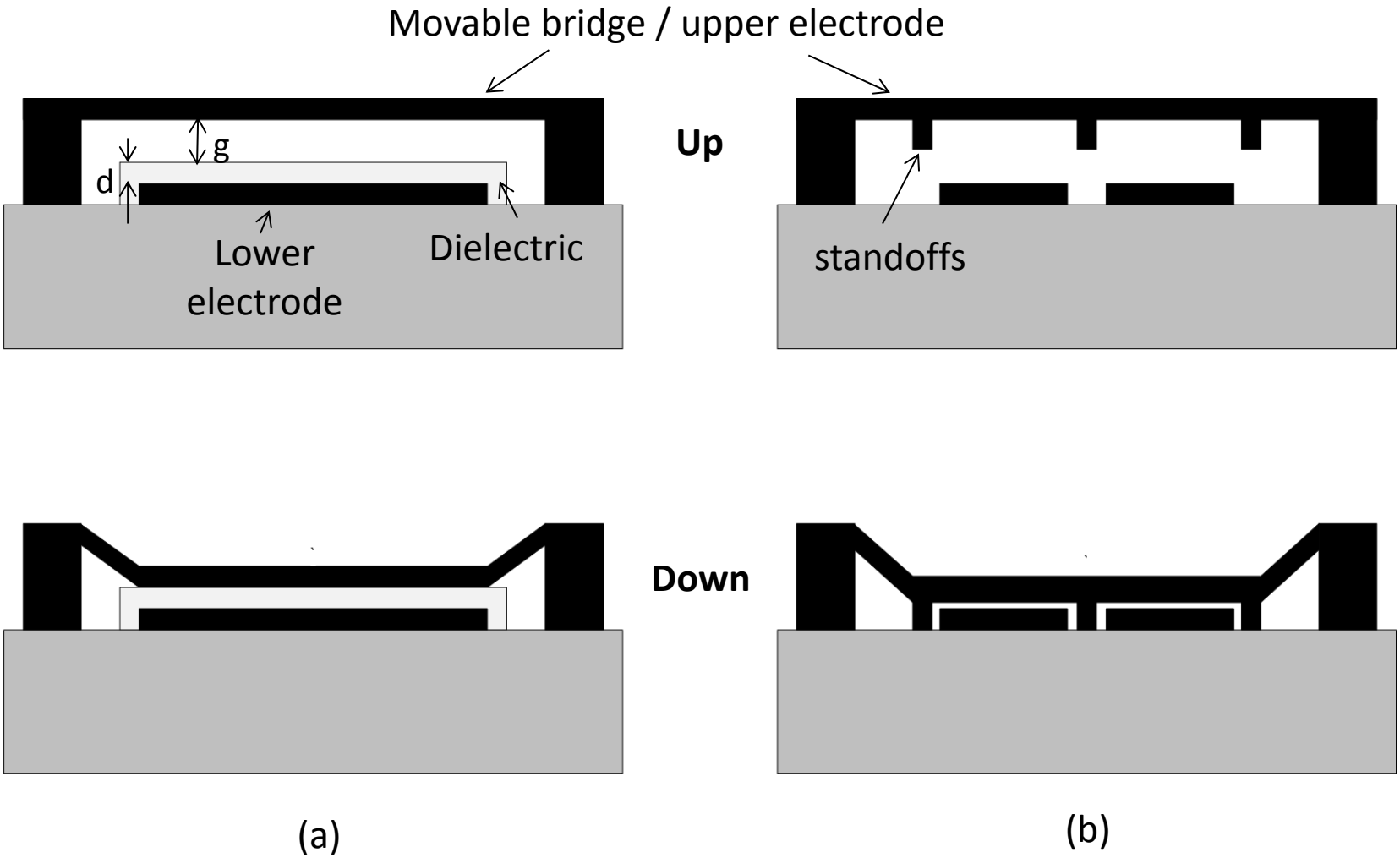
Movable bridge / upper electrode
g
d
Lower electrode
Dielectric
Up
standoffs
Down
(a)
(b)

Figure 21

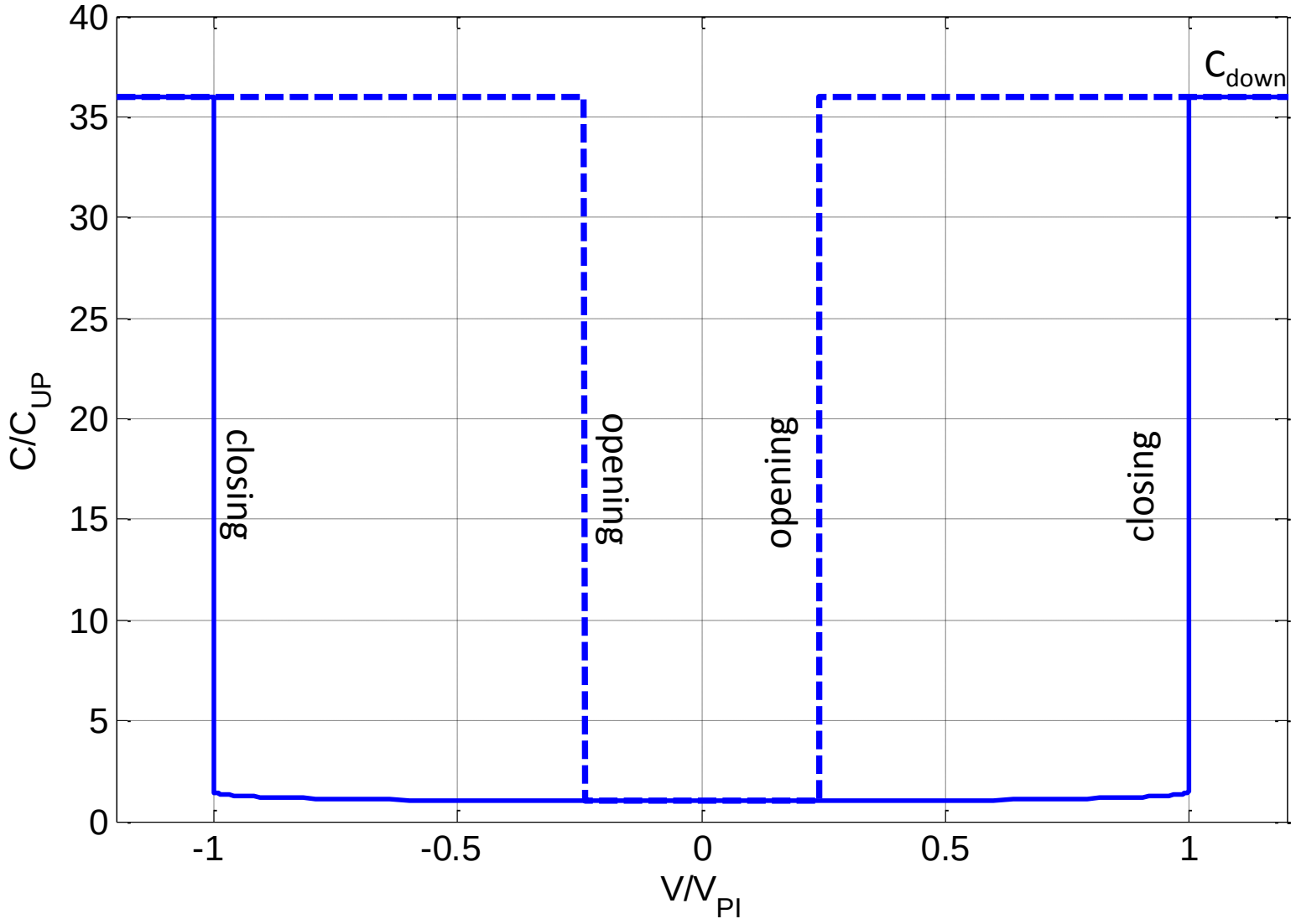
40
35
30
25
20
15
10
5
0
C/C_UP
-1
-0.5
0
0.5
1
V/V_PI
C_down
closing
opening
opening
closing

Figure 22

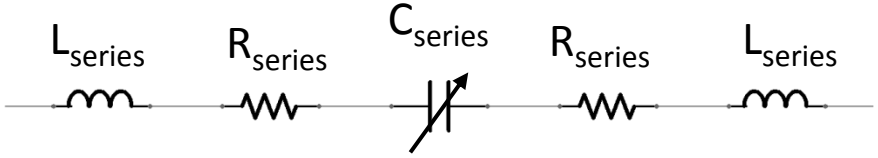

(a) series capacitive switch

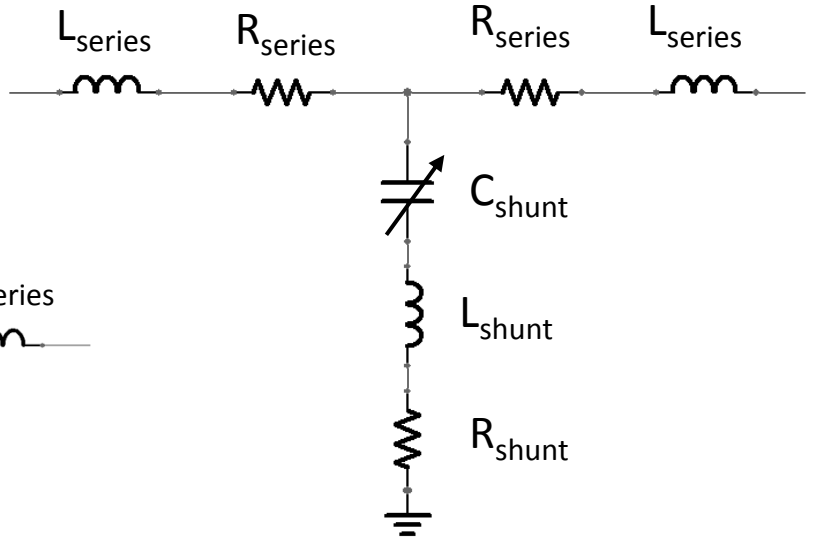

(b) shunt capacitive switch

Figure 23

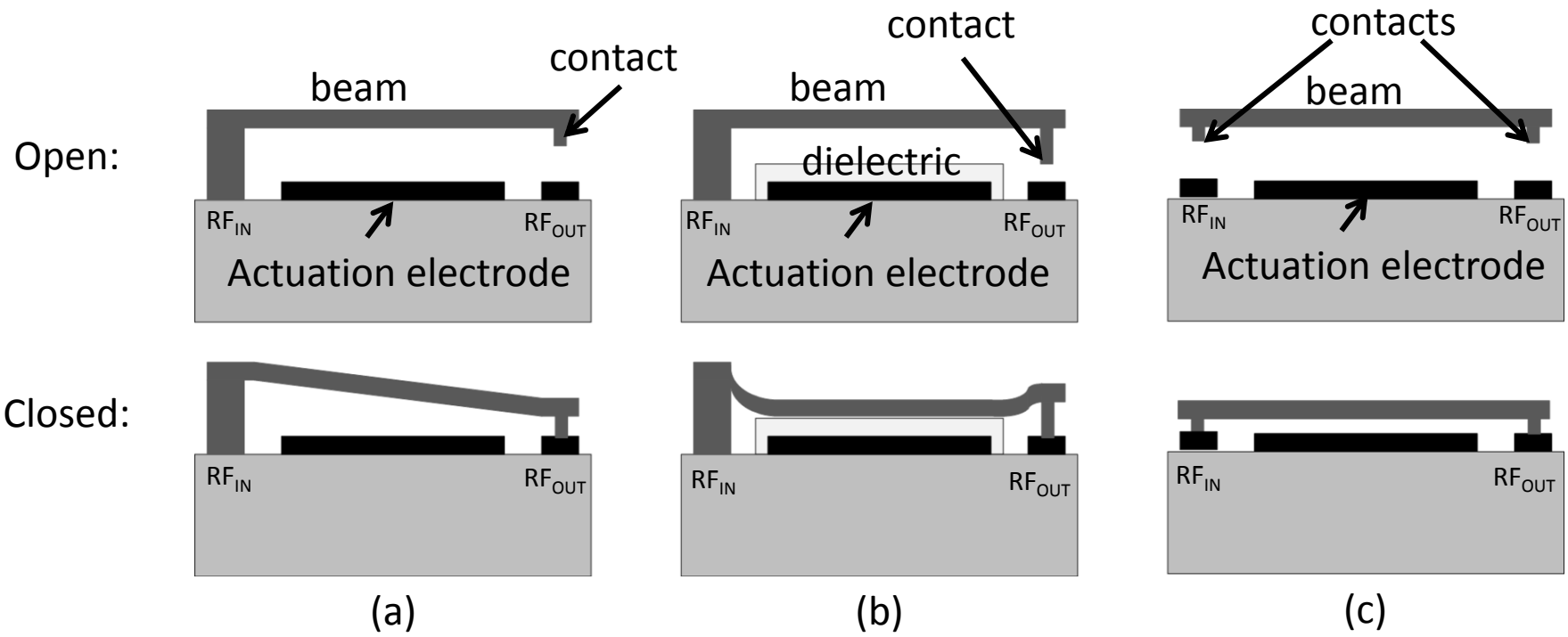
Open:
Closed:
beam
contact
beam
contact
dielectric
beam
contacts
RF_IN
RF_OUT
Actuation electrode
(a)
(b)
(c)

Figure 24

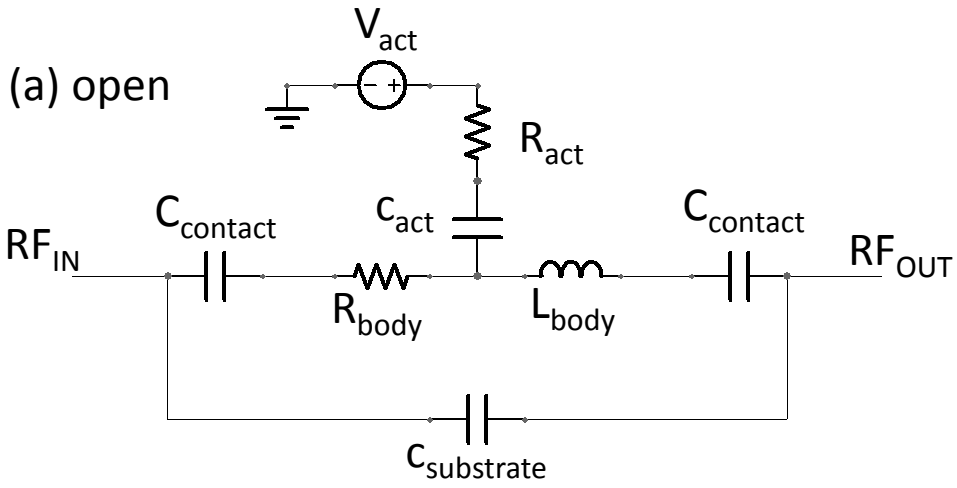
(a) open
V_{act}
R_{act}
$C_{contact}$
c_{act}
$C_{contact}$
RF_{IN}
RF_{OUT}
R_{body}
L_{body}
$c_{substrate}$

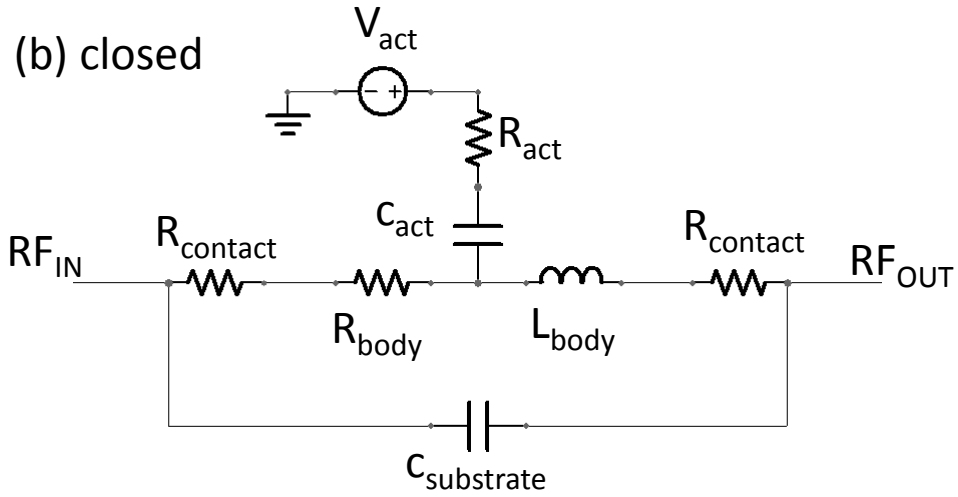
(b) closed
V_{act}
R_{act}
c_{act}
$R_{contact}$
$R_{contact}$
RF_{IN}
RF_{OUT}
R_{body}
L_{body}
$c_{substrate}$

Figure 25

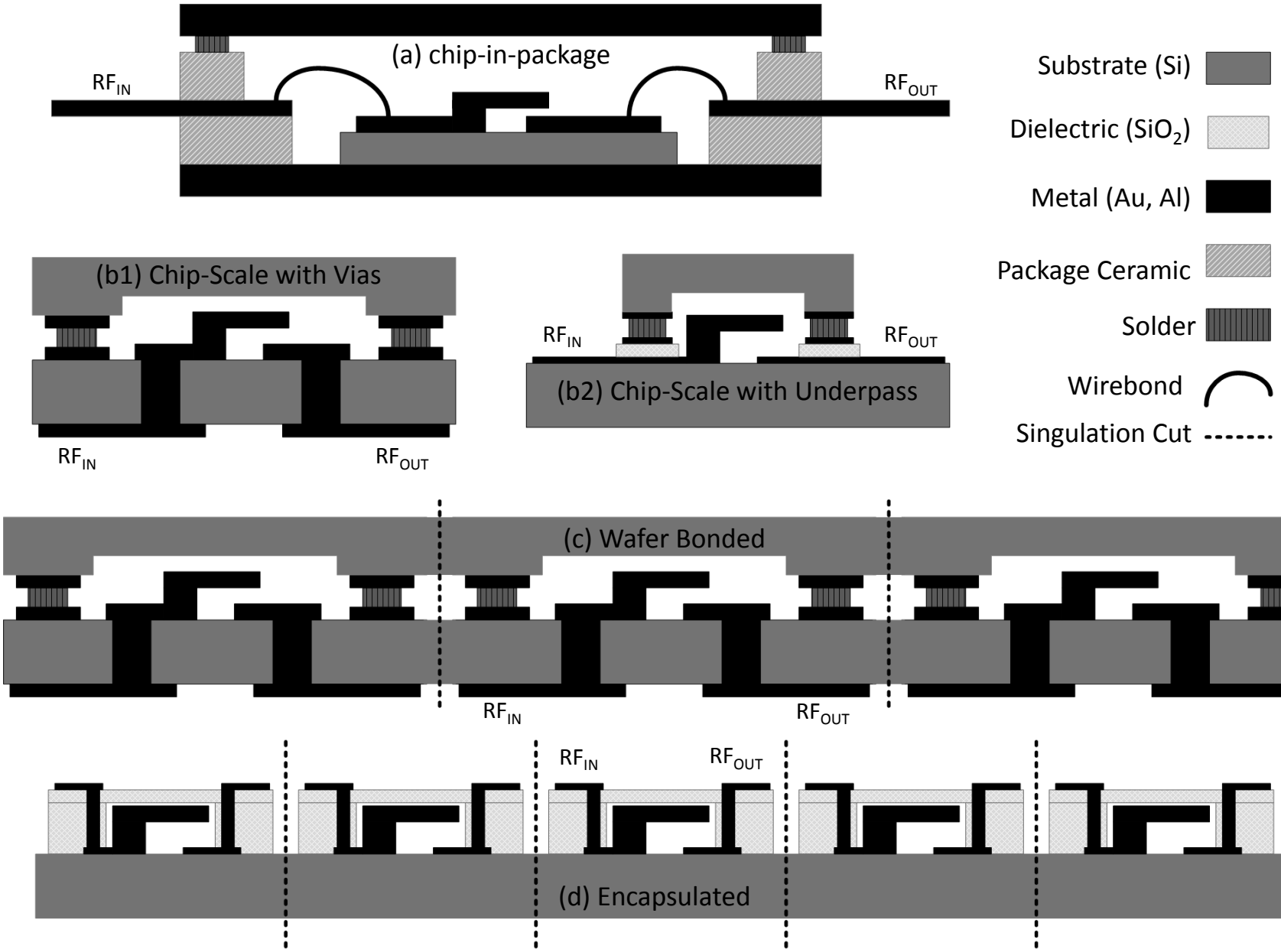
(a) chip-in-package
RF_IN
RF_OUT
(b1) Chip-Scale with Vias
RF_IN
RF_OUT
RF_IN
RF_OUT
(b2) Chip-Scale with Underpass
Substrate (Si)
Dielectric (SiO2)
Metal (Au, Al)
Package Ceramic
Solder
Wirebond
Singulation Cut
(c) Wafer Bonded
RF_IN
RF_OUT
RF_IN
RF_OUT
(d) Encapsulated

Figure 26